Colour and Technology in Historic Decorated Glazes and Glasses

Glòria Molina i Giralt

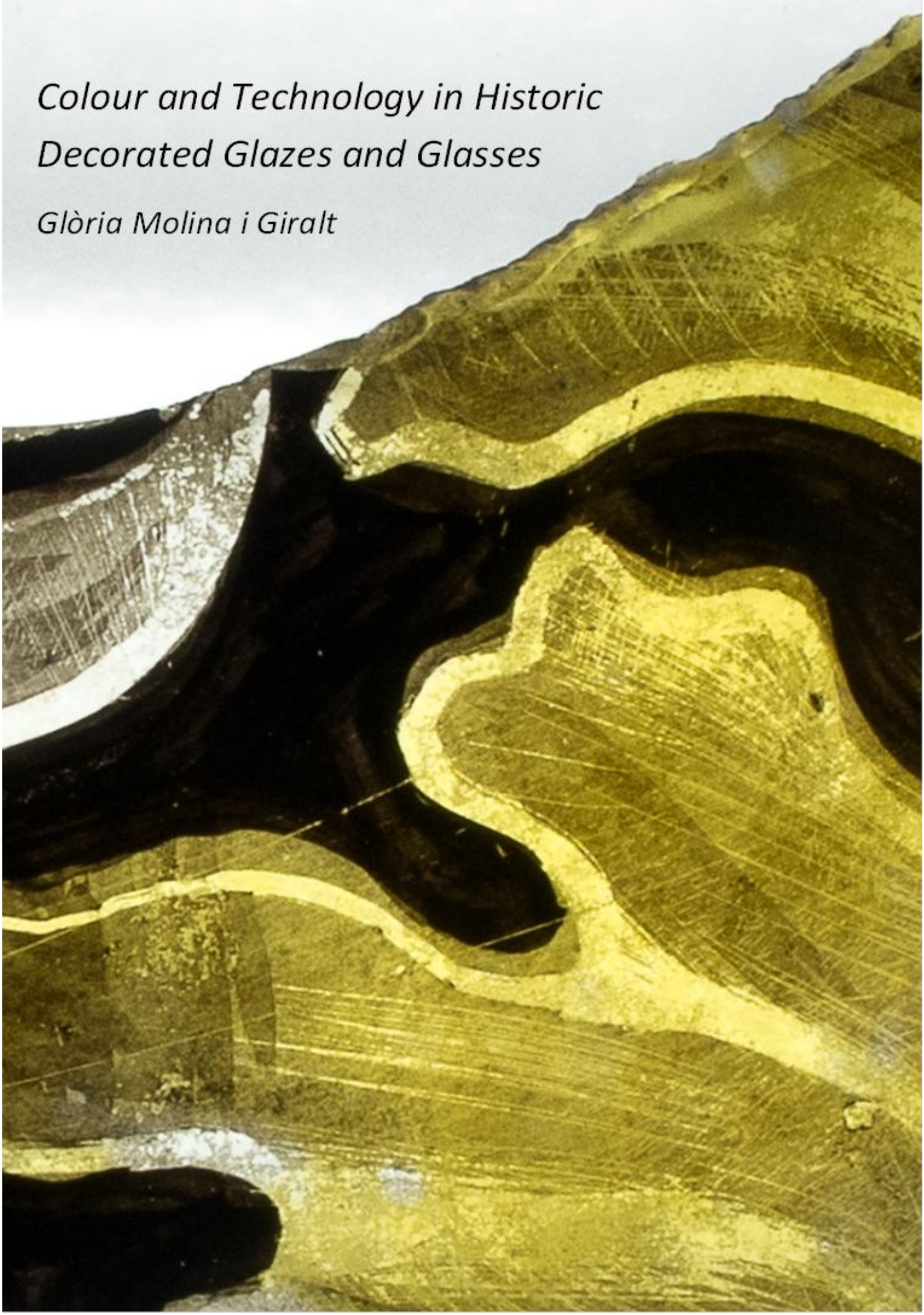

Departament de Física i Enginyeria Nuclear
Programa de Doctorat en Física Aplicada I Computacional

Colour and Technology in historic decorated glazes and glasses

Glòria Molina Giralt

Directores: Trinitat Pradell i Cara
Judit Molera i Marimon

Barcelona, Febrer 2014
Tesi presentada per obtenir el Títol de Doctora per la Universitat Politècnica de Catalunya
1 Volum

Pels meus pares

I pel meu amor, Xavi

Abstract

Historical decorated glass and glazed ceramics are studied with the object to determine the technology of production and to relate it with the optical properties (colour, shine, opacity). Four different case of study are investigated: production technology and replication of lead antimonate yellow glass from New Kingdom Egypt and the Roman Empire, technology of production of polychrome lustre, analyses of Syrian lustre pottery (12^{th}–14^{th} centuries AD) and study of color and dichroism of silver stained glasses. These different coloured glazes or glasses have in common to be produced by the presence of micro or nanoparticles embedded into the glaze which give their special optical effect. Chemical and microstructural analyses are performed using a selection of complementary Microscopic and Spectroscopic techniques that are the most adequate for the analyses of each decoration. Physical optical properties are also modeled and measured by means of UV-Vis spectroscopy. The composition and structure of the different phases formed during the processing of the decorations in historical times is obtained with the object to learn about their stability and processing conditions and to relate them to their optical properties.

Key words: Glass, Pigment, Metallic nanoparticles, Optical properties, Glaze, Lustre, Technology, Nanostructure, Historic objects

Acknowledgements

The study is funded by CICYT grant MAT2010-20129-C02 and Generalitat de Catalunya Grants 2009SGR01225 and 2009SGR01251. And CRG projects 16-01770 and 16-01742 at BM16, European Synchrotron Radiation Facility (ESRF) in Grenoble.

Professor Ian Freestone (University College London) is thanked for providing the Roman glass sample; the *Victoria Museum of Egyptian Antiquities* (Uppsala) and the *Nationalmuseet* (Copenhagen) for providing the Egyptian glass samples; *The Roman Glassmakers* (Andover, Hampshire) for providing the colourless glasses comparable in composition to New Kingdom Egyptian and Roman colourless glasses; *Instituto Valencia de Don Juan* and the *Ashmolean Museum* for providing the lustre ceramics analysed, and, *Vetraria Muñoz de Pablos S.L.* for providing the stain glass pieces studied.

Special thanks area also given to the human sources from Centre for Micro Analyses of Materials (CMAM), Centre for Research in NanoEngineering (CRNE) and Scientific and Technological Centers of the University of Barcelona (CCiTUB) for their help and advice with the use of technical equipment. Special thanks are also given to Chaoren Liu for his help with DSC measurements.

At a personal level I would like to express my special acknowledgement to Salvador Mañosa, sculptor and ceramist and to Isabel Serres and Joan Martínez, ceramists, for all I learned from them and for their kindness. To all my colleagues at Departament de Física i Enginyeria Nuclear and Departament de Física Aplicada who made me feel at home. To my family and friends for their support and the many hours that my dedication to the research work took from them. Finally I would like to thank Trinitat Pradell i Cara and Judit Molera i Marimon for their generosity and infinite patience.

Contents

Chapter 1

Introduction

This thesis is centred in the study of bulk colour and surface decoration of historic glass and glazed wares and the role of micro and nanoparticles in their optical properties. It arises from a multidisciplinary approach that has two goals: scientific and historical. From the scientific point of view the purpose is to identify the materials, learn about their stability and methods of production and to relate them to their optical properties. From the historical point of view we expect to obtain information on the transfer of knowledge between cultures and regions.

For this, the main hypothesis is the existence of a correlation between the advances in technology and the aesthetic innovations. Advances in the scientific knowledge or technological processes naturally result in the development of new materials which may initiate a new aesthetic paradigm which, if successful, is adopted and adapted by other cultures and regions.

The materials studied have in common to be produced by the presence of micro or nanoparticles embedded into the glass/glaze for obtaining yellow or red glasses, and gold or coppery lustre glazes. The samples studied comprise an extended chronology including New Kingdom Egyptian (approximately 1500 BC) and Roman antimony yellow glass, various productions of lustre decorated glazed Abbasid (9^{th} century AD) and Syrian (12^{th} to 14^{th}

centuries AD) ceramics and silver stain glass from early Renaissance cathedrals (15^{th}-16^{th} AD) in Spain. In each case different specific queries are addressed:

- The relationship between New Kingdom Egyptian and Roman antimony yellow glass.
- The method of production of polychrome red copper in combination with yellow-golden, white-silvery or black silver lustre decorations from Iraq, 9^{th} century.
- The study of the relationship between Syrian and the Egyptian Fatimid lustre production.
- The production parameters and materials used to obtain yellow and red silver stains in 15^{th} century stain glass and the reasons for the dichroic effect.

The experimental methodology comprises the analyses of the materials complemented by replication of the materials based on written historical treatises and the data obtained from the analyses of the bulk colour glass and decorations. The analytical techniques used vary in each case depending on the characteristics of each material; thin nanometric layers, minor chemical elements, nano- and micro- precipitates, presence of alterations due to either aging or weathering of the materials, size of the samples available, among many more. For this reason, chemical and microstructural analyses are performed using a selection of complementary Microscopic and Spectroscopic techniques that are the most adequate for the analyses of each material. Physical optical properties (colour, reflectivity, transmittance, opacity) are measured by means of UV-Vis spectroscopy and also modelled.

This memory is structured is 6 chapters. Chapter 1 is the introduction of this memory and includes a summary of the history and technological advances of colour and decorated glass and glaze ceramics. A specific section is dedicated to stain glass and lustre ware decorations due to the relevance of those types of decorations in the thesis and also to the technological complexity and important changes in the materials and processes along the history.

Chapter 2 is about the technology of productions of yellow glasses with lead antimoniate and the relationships between yellow glasses from New Kingdom Egypt and the Roman Empire ones.

Chapter 3 is the study of technology of production of polychrome lustre from Iraq, 9^{th} century.

Chapter 4 is the study of Syrian lustre pottery and its relations with contemporany Fatimid lustres from Egypt (12-14th centuries AD)

Chapter 5 is the study of colour and dichroism of silver stained glasses from 15-16th century AD.

And, finally, Chapter 6 are the conclusions.

Decorated glass and glazed ceramics history

Obsidian was the first glass used by mankind, is a natural glass found in sites dating the Upper Palaeolithic (10000 BC); it was used for the production of ritual objects, fabrication of arrow heads among other daily tools. Although has been neither chronologically nor geographically verified, it is generally accepted that the first artificial glass was first obtained in the Mesopotamian area at the beginning of the Bronze Age (3300-2100 BC) as a by-product of metallurgical activities (Fernandez, 2003); the treatment of copper minerals is known to produce vitreous coloured and opaque slags. Quartz melts at 1670ºC, consequently glass could only be produced provided that elements able to decrease it (*fluxes)* were added, which in Mesopotamia consisted in alkaline salts obtained from plant ashes. Metals such as copper, cobalt or iron dissolved in the glass or lead antimony and calcium antimony oxides forming small crystalline precipitates were also incorporated giving colour to the glass. The earliest glass objects, turquoise blue beads were found in the excavations of the cemetery of Ur (2500 BC). By the end of the second millennium BC, Syria became also an important glass production centre and later between approximately 1500 and 1300 BC (18th dynasty), glass was also produced in Egypt reaching its maximum splendour at the glass workshop of Tell-el-Amarna. It is worth to mention that during this period Syria had already been conquered by Thutmose III who took the best artisans from the conquered area. The Egyptian glass was of the type high soda-high lime type made of *natron* (a highly hydrated variety of sodium carbonate found in the valley of Wadi al Natrum in Egypt). Glass was mainly used to produce ornamental objects and for the production of precious small colourful flask and bottles. The methods of production used in Egypt were described by Sir Flinders Petrie from data obtained in the Tell-el-Amarna (Harden, 1956) excavations. The technique followed was that of the sand nuclei covered by successive layers of soft colour glass. By 1200 BC mould shaped and cut glass objects started being produced and the application of threads and drops of colour glass over the soft glass was the main decorative technique utilised. The Egyptian ground glass used in this period is dark (violet-blue and brown) decorated with yellow, orange, white, light-green and turquoise-blue glasses (Figure 1.1). Those

glass objects were exported to Greece, all the Mediterranean area and later to China, Japan and south-east Asia through India. The Egyptian supremacy in glass production lasted until the resurgence of the Assyrian glass industry in the last millennium BC.

The glass conserved from the Assyrian resurgence is of the type high-potash, high-magnesia soda-lime glazes obtained from plant ashes, usually colourless with a light greenish tinge and the decorations are inscriptions in cuneiform script.

Figure 1.1. Two-handled jar ca. 1539-1295 BC New Kingdom – 18th Dynasty - Reign of Amenhotep III. Gift from Charles Lang Freer. The Smithsonian's Museums of Asian Art.

The oldest treatise on the fabrication of glass was found in the Palace of Assurbanipal (668-626 BC), a set of tablets in cuneiform script containing recipes for the production of both colourless and colour glass (Forbes, 1956). Phoenician glass production became particularly important since the 8th century BC and during the pre-Roman time.

During the Roman Empire many technological innovations were introduced and glass reached the highest quality standards. In particular the Romans improve the technique known as mosaic glass or "millefiori" of Egyptian origin, probably introduced by artisans from Sidon and Alexandria. This technique consists in small cans of colour glass fused together, cut and then stuck together to produce objects.

In the middle of the 2nd century BC, the glass centre of Sidon invented the blowing pipe which happens to be one of the most important technical advances in the glass fabrication processes. Artisans from Sidon moved to Rome and the blown glass technique soon expanded all over the Roman Empire, allowing for the first time "serial" fabrication of glass. Then glass became a more daily use and less sumptuary material. In parallel, colour glass became less important and thanks to the addition of manganese as a decolorizing element, colourless glass blown became of general use.

During the 3rd and 4th century AD, enamel decorations were applied although very scarcely probably due to the difficulties controlling the process; the enamel is a paint made of a suspension of a vitrifiable colour in an organic medium which after firing is fused on to the glass

surface. This technique was perfected and widely used in Islamic times. Cool gold applications started also being used although is during the Byzantine Empire that was extensively used to produce mosaics.

During the 4th century AD exquisite objects of the highest quality were obtained: cameo glass was produced by etching and carving through fused layers of diverse colour glass to produce designs, usually with white opaque glass figures and motifs on a dark-colour background (Figure 1.3.); dichroic glass, such as the Lycurgus cup (Figure 1.2.), red in transmission and green in reflection, was obtained adding gold and silver colloidal metallic particles. Lead oxide is also a *flux*, and during Roman times was directly applied on ceramic wares to produce a high lead glaze. Those glazes were mainly used to waterproof and protect the ceramic objects. The colours obtained were yellow-green due to the presence of Fe^{3+} and Fe^{2+} dissolved in the glaze. However, alkaline based glazes were not applied on ceramics during Roman times.

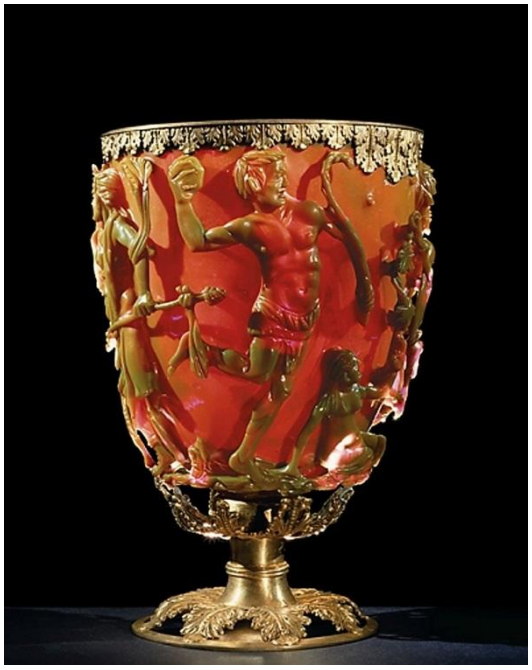

Figure 1.2. Lycurgus cup, in transmission. British Museum.

Figure 1.3. Side A of the Portland Vase. Cameo-glass, probably made in Italy ca. 5-25 AD. British Museum.

The Islamic culture expanded through North of Africa, Persia and the Middle East including some of the most important glass production centres of Egypt and Syria. Transparent glass decorated with *enamel paints* was mainly produced during this period. The most important novelty was the production of *silver stain* also called *lustre* decorations. *Silver stain* is a thin surface micro-layer made of small metallic silver and/or copper nano-particles embodied in the

glassy matrix. The range of colours obtained varies between green, yellow, orange and brown depending on the amount of copper and silver in the layers.

At the beginning of the 8th century, and due to the contact with the Chinese ceramics through the Silk's route, green, yellow and brown lead glazed ceramics imitating the Tang *sancai* productions and later decorated alkaline and mixed lead-alkaline glazed ceramics started being produced. One of the most important innovations was the introduction of tin oxide as a white opaque pigment in the glazes to highlight the colour decorations during the 9th century AD. Tin glaze ceramics became of general use in the Islamic lands and expanded to all the Mediterranean and Europe between 10th and 16th centuries. Several underglaze and overglaze colour decorations were used with varying colours and designs. *Lustre* decorations started being used on tin glaze ceramics during the 9th century AD most probably produced in Bashra (Iraq).

Although during the Middle Age the glass production is kept to a very low level and in very small workshops across Europe, they will later be the germ of the stain glass production which had its maximum exponent during the gothic period. The first reference of the use of stain glass is dated between 969 and 988 AD in the cathedral of Reims. The colours of the glasses were obtained either by the incorporation of metal ions into the bulk glass, grisailles (made of iron oxides mixed with powdered lead glass and an organic medium such as Arabic gum and fixed onto the flat glass surface by firing) and also *silver stains* since the beginning of the 14th century (Fernandez, 2003). Later colour was given also by the application of layers of colour glass onto the transparent glass (*plaque* glass) and *enamels*.

Silver stain and lustre decorations

Silver stains and *lustre*, as mentioned before, share the same technology of production. *Silver stains* normally referring to the decorations applied on glass while *lustre* is normally related to the decorations applied on glazed ware; both names referring to the visual appearance attained in each case. Silver stains were first produced on glass from which it was transferred to decorate glazed wares. Consequently they share a common history and also a common technology which will be summarised herewith.

History

According to the latest reported archaeological finds the earliest existing examples of silver stain glass were of Syrian origin during the Umayyad period (660–750) (Ashmolian, 2004). Abundant Umayyad glass silver stain fragments are found at Qasr al-Hayr al-Sharqī that

was built in (728–9) by the Umayyad Caliph Hishām ibn ‘Abd al-Malik, who governed between 723 and 742. The glass found at the ancient site of Pella in Jordan included also Umayyad silver stain and gilded fragments (O’Hea, 2003).

Apart from these early fragments of Umayyad silver stain glass, two surviving complete glass cups one from Fustāt and the other from Damascus dated 779 and 786 respectively (Scanlon, 2001) are found. After the rise of the Abbasid Caliphate in 750, Syrian glass-workers may have been encouraged to migrate to Iraq (Halett, 2000) and silver stain glass started been produced in Basra, Kufa and Samarra in the eighth and ninth centuries. According to Ya‘qūbī, Basran glassworkers were among the artisans brought to work on Sāmarrā by the Caliph al-Mu‘tasim (833–842).

Figure 1.4. Bowl with a red ruby glaze. Irak, 9th century. Musée du Louvre. OA6700.

It is generally accepted that silver stain glass is the origin of lustre wares (Caiger, 1985). And that the first painters of lustre inherited some of their techniques from glass-workers, and may actually have been glass-painters as well. The lustre wares started being produced in, Iraq (Abbasid) 9th century AD, (Figure 1.4.) and coincided with the introduction of lead oxide and tin oxide to the glazes. The first was probably added to improve the thermal properties of the glazed wares and reduce cooling glaze cracking, the second to obtain a white opaque glaze thanks to the precipitation of small cassiterite (SnO_2) micro-crystallites in the glaze. However, as we will see in the technology description both produced a dramatic change in the visual appearance of lustre decorations.

The first notice about the stain-glass technology appears in “The book of the Hidden Pearl (Kitāb al-Durra)” written by Jābir ibn Hayyān (c. 721–c. 815) who was philosopher and chemist. The paper by Ahmad Y Al-Hassan compares the recipes of Kitāb al-Durra with the results of modern analyses of existing Islamic stained glass objects.

The manuscript of this practical treatise was discovered recently. Jābir ibn Hayyān wrote a unique treatise of technical recipes dealing with the manufacture of coloured glass, making silver stain glass, colouring gemstones, purifying of pearls and making artificial ones and other useful objects.

The essay contains 118 recipes for talāwīh (silver stain glass), in addition to nine recipes inserted by al-Marrākushī, the editor. We extract two of the original recipes: one for making a golden-lustre and the other for silver-lustre:

"*Recipe 63, fol. 14a, gold lustre (mulawwah dhahab): One part of magnesia, two of marcasite (marqashīthā), one of copper, three of litharge (martak), two of arsenic (zarnīkh). They are worked with good vinegar and exposed to fire (talwīh) and it comes out golden."*

Recipe 91, fol. 16a, silver lustre. Take one uqiyya from each of Yemeni alum, Egyptian alum and sal-ammoniac. Take one mithqāl from ceruse (isfīdhāj), borax of goldsmiths, tinkār and natron. Combine and pulverize with white vinegar for two hours; adorn with it and expose to fire."

"The Book Of The Hidden Pearl (Kitāb al-Durra)" written by Jābir ibn Hayyān and edited by Ahmad Y Al-Hassan (2009)

The oldest known description about the materials and process of manufacture of lustre glazed pottery is the Abu'l Qasim's work, dated at 1301 AD. This treatise of ceramics from Kashan (Iran) said:

"*Those (vessels) that come out of the firing white they paint with the enamel of two firings, or with lâjvard, or with pure turquoise. The enamel (lustre pigment) is composed as follows: Take one and a half mans (or: parts) of red and yellow arsenic, one man (or: part) og gold and silver marcasite (types of iron pyrites), one Batman (or: half a part) of Tisi (or: Tabasi or Cypriot) yellow vidriol (probably iron sulphate) and a quarter (of a part) of roasted copper, and mix to a paste and bring it. A quarter of this is mixed with six dirhams of pure silver which has been burned and ground (with sulphur) and is ground on a Stone for twenty-four hours until it is extremely fine. Dissolve this in some grape juice or vinegar and paint it on to the vessels as desired, and place them in a second kiln specially made for this purpose, and give them light smoke for seventy-two hours until they acquire the colour of two firings (which is like gold). When they are cold take them out and rub them with damp earth so that the colour of gold comes out. Other people add certain preparations like sirinj (lead oxide) and sanjâr (verdigris or copper acetate) to this enamel. In fact shâdanej Stone (no identified) with roasted silver serves the same purpose. That which has been evenly fired reflects like red gold and shines like the light of the sun."*

(From Abu'l Qasim's Treatise on Ceramics translated and annotated by J.W. Allan, Iran, IX, 1973, p.114)

The first lustre decorations applied on glazed pottery were found in the Caliphs' palace in Samarra (836-883 AD), although they were most possibly produced earlier, in the time of Harun-al-Rashid (766-809 AD). Abbasid lustres were found as well in the Mosque of Kerouian in Tunisia (Bobin, 2003), the court of the Hammanid princess in Qal'a (Algeria), and also in the court of Ahman ibn Tulun (Fustat, Egypt) who was the administrator of the Samarra court posted to Egypt in 868 AD, and who rebuilt the city of Fustat in pretend of the luxury exhibited in Samarra. Although the earlier separation of Egypt from the Abbasid caliphate (Caiger, 1991) and its rule by the Tulunids (868–905 AD) has sometimes been associated with the transfer of lustre technology from Iraq to Egypt, analyses of the so called Tulunid lustres has demonstrated their Iraqi origin (Mason, 2004).

The 9th century AD Abbasid lustres are polychrome showing two, three and sometimes four lustre colours, the designs are intricate and the effect striking. Typical colours are olive green; brown and amber; orange, yellow and crimson and also extremely dark, almost black, red. Most of the time, they do not show metallic shine but instead appear as iridescent stains. Sometimes, metallic and non-metallic lustre colours of different composition appear mixed in the same piece.

During the 10th century AD the earlier polychrome lustre of the 9th century was substituted by a more standardised green-golden monochrome production (Pradell et al, 2008) associated with new shapes as well as new designs (Caiger, 1991). The occupation of Egypt by the Fatimids in 969 AD started the production of Egyptian Fatimid lustre with the resulting decline of the Abbasid lustre produced in Bashra.

The earliest Egyptian Fatimid lustre decorations display strong stylistic links with the Iraqi monochrome lustre but soon later (11th century AD) exhibit new motifs and also incised lustre decorations (Philon, 1980; Mason, 2004). The colours of Egyptian lustre are quite varied; the most common being yellow, green and brown-golden lustres (Figures 1.5, 1.6). The destruction of Fustat in AD 1168 by Shirkuh was followed by the rule of his nephew Salah-el-Din. During the late Fatimid period, Syria was in a state of nearly permanent war, but periods of relative peace did permit the development of the ceramic industry (Porter, 1981). Syrian lustre is particularly interesting as it shows technological innovations with respect to the earlier Abbasid and Fatimid lustre productions with the use of transparent tin-free glazes (often alkaline) and stonepastes. *Tell Minis* and *Raqqa* lustres date to this period. *Tell Minis* wares show similar ceramic forms, lustre designs and colours to the Fatimid lustres, and have been attributed to

Egyptian potters arriving at Syria after 1075 AD (Mason, 2004). Some local low quality lustre productions seem to happen until the first quarter of the 13th century AD when a chocolate brown and yellowish green lustre was produced in *Raqqa* (Porter and Watson, 1987; Mason, 2004). In AD 1250 the Mongol occupation of Syria destroyed large areas in the north of the country, terminating the *Raqqa* production. Jars and albarellos of golden lustre over cobalt-blue and white grounds continued to be exported from Syria in large quantities during the 14th century AD. This production is typified by a jar with a green-golden lustre on a cobalt-blue glaze and signed by Yusuf from Damascus (Porter, 1981).

Figure 1.5. Bowl fragment with lustre decoration. Egypt, 11th century. Musée du Louvre. K3484.

Figure 1.6. Vessel shards of blown glass with lustre decoration. Egypt, 10th – 11th century. Musée du Louvre. MAO 490/69.

Watson (1985) disregards the link between late 12th century Iranian lustre and earlier local Persian ceramics production and instead establishes a direct link between the beginning of the lustre production in Persia and the fall of the Fatimid dynasty. The earliest dated lustre piece from Persia is from AD 1179 and shows similar designs and decorations to Fatimid lustre (Watson, 1985). During the first quarter of the 13th century AD standardised high quality lustre was produced in Kashan. The Persian lustre ware is made on a stonepaste body with a tin-opacified glaze and is of a homogenous dark-brown-golden colour. The Mongol invasion of AD 1220 disrupted lustre production, until after 1260 AD (Watson, 1985) a large tile manufacture was produced in Kashan (Watson, 1985; Porter, 1995).

Lustre technology expanded also to the Islamic kingdoms in Spain. The first examples of lustre that was made in Spain were found in Murcia and date back to the twelfth century AD, although main productions are also described in Almeria (12th century) and Malaga (13th and 14th century). Subsequent developments following the Islamic tradition in the Hispano Moresque pottery, 13th–15th centuries (Figure 1.7.), and Italian majolica, 15th–16th centuries, created highly prized items that were extensively exported. Different recipes allowed potters to obtain several colours, such as yellow, green, olive green, brown, amber, chocolate, ruby red, and also several metallic sheens (copper, gold, and silver).

Figure 1.7. Deep dish from Spain, after 1475, tin-glazed earthenware with lustred decoration, Victoria and Albert Museum, London. 1680-1855.

Technology

The lustre decorations are extremely thin surface micro-layers made of exceptionally small metal silver and/or copper nano-particles inside the glaze matrix, as can be seen in Figure 1.8. The peculiar optical properties of lustre, including the golden and coppery shine, are directly related to the size and volume fraction of the metal particles.

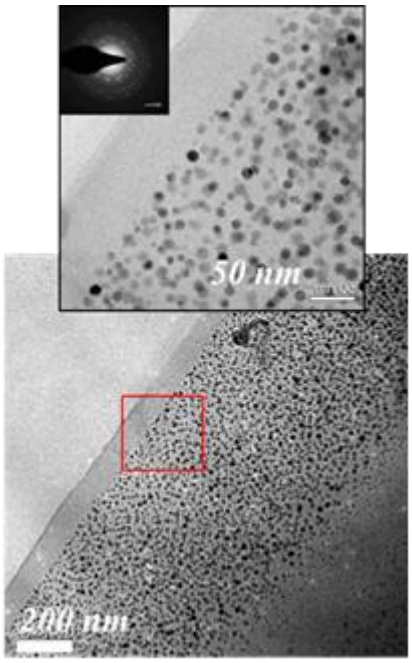

Figure 1.8. TEM image from a replica of a copper lustre thin layer made on an alkaline glass.

The analyses of both laboratory replicas and historical lustres, demonstrated that the colour of the lustre layers is mainly related to the size of the nanoparticles and the amount and oxidation state of copper or silver in the layer, while the metallic shine is related to the presence of a high volume of metal nanoparticles in the layer. Although both size and density of particles in the lustre depend on the composition of the glaze and on the firing temperature and atmosphere, the composition of the glaze has proved to be the essential parameter that regulates the density of particles in the layer and consequently the metallic shine. In particular the addition of lead oxide in the glaze is directly responsible for the formation of

more dense and thinner lustre layers. Moreover, the analyses of historical lustre layers has shown an increase in the lead oxide content of the glazes from early Abbasid to later Fatimid lustre productions suggesting deliberate addition to improve the possibility of obtaining a successful golden lustre.

Lustre was produced following a highly ingenious procedure in which the lustre design was painted (copper, silver and sulphur containing compounds), onto the glaze which is then subjected to a firing at a relatively low temperature (500-600ºC). Ag^{+} and Cu^{+} ions diffuse into the glaze substituting the alkalis (either Na^{+} or K^{+}) from the glaze. The introduction of an external reducing atmosphere into the kiln favoured the precipitation on the metal particles, which formed in a thin layer close to the glaze surface. The paint was washed off after firing to leave the colourful lustre decoration which if successful exhibited a metal like shine, golden shine. Previous studies have shown that silver always appears as metal nanoparticles whilst copper, being more difficult to reduce to metal than silver, often appears either as Cu^{+} or Cu^{2+} ions dissolved in the glaze. Only when very reducing conditions are applied, or metals capable of reducing copper such as iron or tin are added, can the copper ions form nanoparticles of cuprite (Cu_2O) and metal copper. The several colours shown by lustre are not only related to the type and size of metal particles present but also to the presence of Cu^{+} and/or Cu^{2+} dissolved in the glaze. Summarising, metal silver particles give a yellow-greenish colour while metal copper particles a red colour. The addition of copper then helps the reduction of silver to the metallic state and the growth of silver nanoparticles while copper is kept either as Cu+ or Cu^{2+}, resulting in yellow-orange to brown colours. If the reducing atmosphere is strong enough to reduce also copper to the metallic state, then a combination of red coppery and white silvery spots is obtained.

References

Y. Al-Hassan Ahmad (2009). An Eighth Century Arabic Treatise on the Colouring of Glass: Kitāb Al-Durra Al-Maknūna (the Book of the Hidden Pearl) of Jābir Ibn Ayyān (C. 721–C. 815).

Ashmolian. Abbasid Ceramics, Revolution or Evolution? The Development of a True Islamic Style in Ceramics. A Web-Based Teaching Course in Islamic Ceramics. http://archaeology.about.com/gi/o.htm?zi=1/XJ&zTi=1&sdn=archaeology&cdn=education&tm=134&f=00&su=p284.13.342.ip_&tt=33&bt=5&bts=45&zu=http%3A//islamicceramics.ashmolean.org/MainMenu/index.htm

Bobin O. et al. (2003) Where did the lustre tiles of the Sidi Oqba Mosque (AD 836–63) in Kairouan come from? Archaeometry 45, 4, 569-577. UK

Caiger-Smith A. (1985). Lustre Pottery (New Amsterdam, 1985), p. 10 and 17.

Caiger Smith A. (1991), Luster Pottery. New Amsterdam Books, New York.

Fernández Navarro, J. Mº (2003). El Vidrio. CSIC. Sociedad Española de Cerámica y Vidrio.

Forbes, R.J. (1956). Studies in ancient Technology. Edit. Brill. Leiden.

Halett J. (2000). Trade and Innovation: The Rise of the Pottery Industry in Abbasid Basra, Ph.D. Thesis, Oxford University, vol. I, p. 231.

Harden, D.B. (1956) A history of Technology, II. Glass and glazes. Edit. Oxford

Mason, R.B., (2004). Shine like the sun. Luster-painted and associated pottery from the Medieval Middle East. Bibliotheca Iranica. Islamic Art and Architecture Series, 12. Mazda Publishers, Inc., Costa Mesa (Canada).

O'Hea M. (2003) ''Umayyad to Fatimid glass: finds at Pella'', Historians of Islamic Art Newsletter, XIII, p. 5.

Philon H. (1980). Early Islamic Ceramics. Ninth to Late Twelfth Centuries, Catalogue of Islamic Art. Benaki Museum Athens. London, Islamic Art Publications,

Porter, V., (1981). Medieval Syrian Pottery (RaqqaWare). Ashmolean Museum publications, Oxford.

Porter, V. (1995). Islamic Tiles. London: British Museum Press

Porter, V., Watson, O., 1987. Part II: Tell Minis' wares. Syrian and Iran, three studies in medieval ceramics. Oxford Studies in Islamic Art, IV. Oxford University Press, Oxford (UK), pp. 175–248.

Pradell T., Molera J., Smith A.D., Tite M.S. (2008) The invention of lustre: Iraq 9th and 10th centuries AD. J. Arch. Sci. 35 2649–2662

T. Scanlon G. and Pinder-Wilson R. (2001). Fustat Glass of the Early Islamic Period. London, p. 210.

Watson, O. (1985). Persian Lustre Ware. London; Faber & Faber, Incorporated, 1985

Chapter 2

Production technology and replication of lead antimonate yellow glass from New Kingdom Egypt and the Roman Empire

Introduction

Antimony-based opacifiers (i.e., lead antimonate yellow and calcium antimonate white) were used from the beginnings of glass production in the Near East and Egypt around 1500 BC through into the Roman period (Turner and Rooksby, 1959). Towards the end of the Roman period (i.e., from about 4th century AD onwards), lead stannate replaced lead antimonate in the production of opaque yellow glasses (Tite et al., 2008), and it was not until the late 15th century AD that lead antimonate started to be used again both in glass production in Venice (Biringuccio, 1966), and as a yellow pigment in Italian Renaissance paintings (Dik et al., 2005) and in Italian maiolica production (Tite, 2009).

As observed by Mass et al. (2002) and Shortland (2002a) for NewKingdom Egyptian yellow glasses and by Mass et al. (1998) and Freestone and Stapleton (2013) for Roman yellow glasses, a significant proportion of the lead antimonate particles exhibit an irregular, ragged morphology and a clumped distribution, whereas other particles exhibit euhedral morphologies suggesting that they were formed during cooling from the melt. It is therefore argued that preformed lead antimonate, rather than separate lead and antimony compounds, was added to the glass melt. The lead antimonate then suffered partial dissolution in the molten glass, resulting in both surviving clastic particles and euhedral particles that had crystallised from the melt.

In a study of early Roman coloured glasses (1st century BC to 1st century AD), Freestone and Stapleton (2013, Figures 2.9 and 2.10) observed that the reduced compositions of yellow glasses (i.e., renormalized composition after the subtraction of lead, antimony and iron oxides) exhibited elevated silica contents together with lower lime, potash and magnesia contents relative to the reduced values for other colours. They therefore suggested that the yellow colorant was added to the colourless glass in the form of a lead-antimony-silica mixture comparable to the anime used in the production of yellow glasses in Venice in the 18^{th} and 19^{th} centuries AD (Moretti and Hreglich, 1984). Calculation of reduced compositions from analytical data for 1st to 4^{th} century AD Roman glass published by Mass et al. (1998) again show that, as compared to white and turquoise glasses, opaque yellow and green glasses, the latter coloured by a combination of lead antimonate and copper oxide, exhibit elevated silica contents (Figure 2.1a). There is also a tendency for the opaque yellow and green glasses to have lower lime contents, but there is no differentiation in the potash and magnesia contents, the majority of which are less than 1 wt%, between the four colours. However, on the basis of the elevated silica and reduced lime contents, it can still be argued that *anime* continued to be used in the production of lead antimonate glasses through to the later Roman period. In contrast, on the basis of the analytical data for New Kingdom glass from Egypt published by Shortland and Eremin (2006), there are no significant differences in the reduced silica, lime, potash and magnesia contents of opaque yellow glasses relative to the other glasses (Figure 2.1b). Therefore, the Egyptian yellow glass was most probably produced by adding a pigment, made by firing a mixture of lead and antimony oxides, to raw colourless glass.

In both the New Kingdom Egyptian and Roman yellow glasses, the PbO/Sb_2O_5 ratios of the bulk glass are typically in the range 5-15, and significantly higher than the ratio (1.38) for the stoichiometric $Pb_2Sb_2O_7$ particles found in the yellow glasses. Therefore, both the lead antimonate pigments and *animes* used respectively in these two types of yellow glass would have contained an excess of lead. It is generally argued that excess lead facilitates the initial formation

of lead antimonate, the mixing of the pigment or *anime* into the colourless glass, and the subsequent stability of the lead antimonate within the glass (Shortland, 2002a; Freestone and Stapleton, 2013).

In the context of Roman glasses, both Mass et al. (1998) and Freestone and Stapleton (2013) noted that the yellow glasses normally exhibited higher iron contents that those in most other colours, and Mass et al. (1998) further noted that the lead antimonate crystals were themselves contaminated with iron.

More recently, Lahlil et al. (2011) have shown that the lead antimonate crystals in New Kingdom Egyptian yellow glasses contain up to about 7 wt% of iron oxide and up to about 5 wt% zinc oxide, and that those in Roman yellow glasses again contain up to about 7 wt% iron oxide, but instead of zinc oxide, they contain up to about 20 wt% tin oxide. In the present chapter, in order to supplement and extend the data previously obtained by Lahlil et al. (2011), lead antimonate particles present in a small group of New Kingdom Egyptian yellow and green glasses and in a single Roman yellow glass were first investigated. The compositions of the particles were determined using analytical scanning electron microscopy (SEM) and their crystallographic structure using X-ray diffraction (XRD). In an attempt to obtain information on the production procedures employed for these glasses, a number of lead antimonate pigments and *animes* were synthesised taking into account the procedures described in the historical treatises, and were similarly analysed using a combination of SEM and XRD. The stability of the lead antimonate particles in glass, and their conversion to calcium antimonate, was then investigated by firing pigments and *animes* together with colourless glasses. Because lead antimonate based pigments, *animes* and glasses exhibit a wide variety of colours, special emphasis was given to the investigation of the colour parameters, measured using UV-vis reflectance spectrometry, as a function of the synthesis parameters. Finally, on the basis of the compositions of the ancient glasses together with the results of the various pigment and anime syntheses, yellow lead

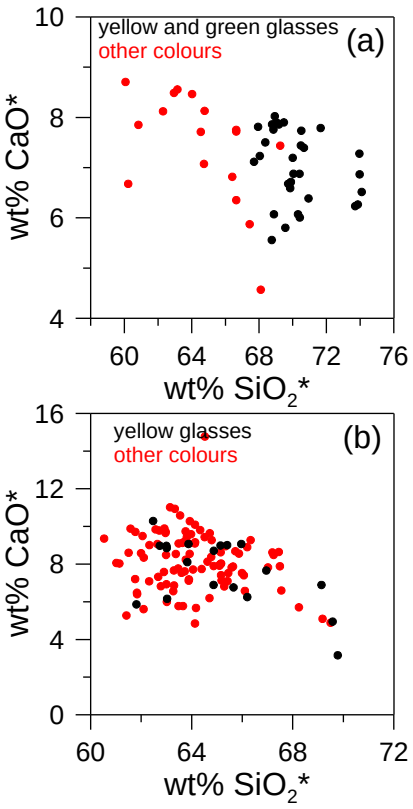

Figure 2.1. Plots of reduced lime content versus reduced silica content comparing (a) opaque yellow and green Roman glasses with other colours (Mass et al.,1998) and (b) opaque yellow New Kingdom Egyptian glasses with other colours (Shortland and Eremin, 2006).

antimonate glasses, comparable in composition, crystallographic particle structure, and colour to those produced in New Kingdom Egypt and in the Roman period, were successfully replicated.

Experimental procedures

Ancient glass samples

Samples from five New Kingdom yellow glasses from Malkata (prefix 'UPP') and Amarna (prefix 'COP'), and one Roman yellow mosaic tessera (116a) from the early medieval workshop at San Vincenzo (Italy), all containing lead antimonate particles, were studied. In addition, one New Kingdom green glass from Malkata (UPP14), coloured by a combination of lead antimonate and copper oxide, was also studied.

Laboratory replications

- ***Lead antimonate pigment***

For the laboratory replication of the lead antimonate pigment, $Pb_2Sb_2O_7$, a stoichiometric mixture of 58 wt% lead oxide (PbO) and 42 wt% antimony oxide (Sb_2O_5) (PG1) (Table 2.1) was first used. This mixture was fired to temperatures of 800ºC or 1000ºC for 2h. Subsequently, the replication was repeated using the stoichiometric PbO-Sb_2O_5 mixtures to which varying amounts of iron oxide (1-8 wt% FeO) and zinc oxide (1-2 wt% ZnO) were added (PG2-6). In this case, the mixtures were all fired to 1000ºC for 2h. Stoichiometric mixtures, rather than those containing excess lead, were used principally in order to provide a reference material to compare with the lead antimonates identified in the ancient glasses, to see how the lattice parameters changed with the addition of iron and zinc, and to investigate the effect of composition and firing temperature on the observed colour.

Further, both the Renaissance treatise on the potters art (Piccolpasso, 2007), and Renaissance painting treatises (Dik et al., 2005) indicate that an alkali flux (eg, common salt or wine lees)was used in the production of yellow lead antimonate pigments. Therefore, replicate pigments were also produced using either a pure stoichiometric mixture (PG7) or mixtures containing 1 wt% FeO (PG8) and 2 wt% ZnO (PG9) to which some 10 wt% sodium chloride flux (NaCl) had been added. The pure mixture was fired to 800ºC, 900ºC or 1000ºC for 2h, and the iron and zinc containing mixtures to 1000ºC for 2 h.

Table 2.1
Chemical compositions of replicate lead antimonate pigments and animes.

		PbO	Sb_2O_5	FeO	ZnO	SnO_2	SiO_2	NaCl	PbO/Sb_2O_5
Pigments	PG1	58,0	42,0						1,38
	PG2	57,4	41,6	1,0					1,38
	PG3	55,8	40,4	3,8					1,38
	PG4	53,7	38,8	7,5					1,38
	PG5	56,9	41,1		2,0				1,38
	PG6	56,0	40,6	2,4	1,0				1,38
	PG7	52,7	38,2					9,1	1,38
	PG8	52,2	37,8	1,0				9,0	1,38
	PG9	51,8	37,5		1,8			8,9	1,38
	PG-EG	85,0	13,3	0,8	0,9				6,4
Animes	AN1	80,9	10,1				9,0		8
	AN2	83,7	7,0				9,3		12
	AN3	64,4	8,0				27,6		8
	AN4	65,4	6,5				28,0		12
	AN-RG	75,0	10,4	3,5		1,5	9,7		7,2

For these and subsequent replications, a Hobersal laboratory furnace (HD-230) with PXR-9/4 programmer was used, and all firings were in air. The heating rate up to the maximum temperature was 5ºC/min, except in the range 90-110ºC when a slower heating rate of 1ºC/min was used in order to eliminate humidity. The cooling rate was 2.5ºC/min down to 700ºC after which the furnace cooled naturally. All experimental mixtures were heated in ceramic crucibles, and the outer layer in contact with the crucible was subsequently removed in order to minimize contamination.

- ***Lead-antimony-silica anime***

For the laboratory replication of the lead-antimony-silica *anime*, four mixtures of lead oxide, antimony oxide and silica were prepared (AN1-4) (Table 2.1). $PbO:Sb_2O_5$ ratios in the range 8:1 to 12:1 were chosen in order to span the ratios typically observed in New Kingdom Egyptian and Roman yellow glasses. The amounts of added silica were such that, after the formation of lead antimonate, there was sufficient lead oxide remaining to produce lead-silica glasses with $PbO:SiO_2$ ratios equal to either 90:10 or 70:30. These mixtures were fired to 900ºC for 2 h.

- ***Stability of lead antimonate particles in glass***

In order to investigate the temperature stability of the lead antimonate particles in glass and their conversion to calcium antimonate, powdered lead antimonate pigments and *animes* were fired together with powdered colourless glasses. In the case of lead antimonate pigments, glasses were produced by adding 12 wt% of the stoichiometric pigment to a colourless glass (RGM-CEG) of composition comparable to that of New Kingdom Egyptian glass (Table 2.2). The pigment mixtures were produced both without and with the addition of 10 wt% NaCl flux (PG1 and PG7 respectively) and were fired to 1000ºC for 2 h. The powdered pigment and glass mixtures were fired to temperatures of 800ºC, 900ºC, 1000ºC or 1050ºC for 2 h. Similarly, in the

case of lead antimonate *animes*, glasses were produced by adding 12 wt% of the low silica, lower PbO/Sb_2O_5 ratio anime (AN1), fired to 900ºC for 2 h, to a colourless glass (RGM-CRG) of composition comparable to that of Roman glass (Table 2.2). The powdered *anime* and glass mixtures were fired to temperatures of 900ºC or 1000ºC for 2 h.

- ***Lead antimonate yellow glasses***

In the replication of "Egyptian type" yellow glass, a lead antimonate mixture was prepared such as to provide a pigment with the approximate formula $Pb_2Sb_{1.8}Fe_{0.25}Zn_{0.25}O_7$, and sufficient excess lead oxide so that PbO/Sb_2O_5 ratio of the mixture matched the average ratio of 6.4 observed for New Kingdom Egyptian yellow glasses. The required pigment mixture whose composition is given in Table 2.1 (Pigment PG-EG) was fired to 1000ºC for 2 h, and then mixed with a colourless glass (Table 2.2 - RGM-CEG) of composition comparable to that of New Kingdom Egyptian glass.

Table 2.2 Chemical compositions of New Kingdom Egyptian and Roman glasses.

		SiO_2	Na_2O	K_2O	CaO	MgO	Al_2O_3	FeO	PbO	Sb_2O_5	ZnO	SnO_2
Lead antimonate yellow glasses												
New Kingdom Egyptian[1]	Average - 19	62,0	17,0	2,1	7,2	4,1	0,7	0,6	5,2	0,8	0,3	
Replicate "Egyptian type" (PG-EG + RGM-CEG-1000°C)	SEM-EDS (x50)	58,5	14,5	2,1	7,2	7,2	1,2	0,5	6,9	1,4	0,4	
Roman[2]	Average - 6	48,4	11,6	0,5	4,7	0,4	1,8	1,4	28,5	2,6		b.d
Roman[3]	Average - 20	59,4	14,7	0,6	5,8	0,5	2,1	0,8	14,8	1,4		b.d
Roman	sample 116a	67,3	18,0	0,7	6,8	0,7	2,1	0,8	2,7	1,0		b.d
Replicate "Roman type" (AN-RG + RGM-CRG-900°C)	SEM-EDS (x50)	64,6	13,0	0,7	5,8	1,6	2,1	0,7	12,6	1,2		0,3
Colourless glasses												
Reduced NK Egyptian [1]	Average - 19	66,1	18,1	2,3	7,7	4,3	0,8	0,7				
RGM-CEG[4]	Theoretical	65,0	18,0	2,0	9,0	4,5	1,0	0,5				
Reduced Roman[2]	Average - 6	70,3	16,8	0,7	6,9	0,6	2,7	2,0				
Reduced Roman[3]	Average - 20	70,8	17,5	0,7	6,9	0,6	2,5	0,9				
Reduced Roman	sample 116a	69,9	18,7	0,7	7,1	0,7	2,1	0,8				
RGM-CRG[4]	Theoretical	71,0	16,5	1,0	8,0	0,5	2,5	0,5				

In the replication of "Roman type" yellow glass, the starting point for the composition of the *anime* mixture was the average composition of the lead antimonate particles present in the Roman glass sample, 116a; that is, 56.7 wt% PbO + 35.7 wt% Sb_2O_5 + 5.1 wt % FeO + 2.4 wt% SnO_2. With the addition of silica and excess lead oxide together with slight increases in the iron and tin oxide contents, based on the *anime* compositions given by Moretti and Hreglich (1984,

278), the composition chosen for the *anime* mixture is given in Table 2.1 (*Anime* AN-RG). This *anime* mixture was fired to 900ºC for 2 h, and then mixed with a colourless glass (Table 2.2 – RGM-CRG) of composition comparable to that of Roman glass.

Analytical methods

Chemical compositions

The chemical compositions of the individual lead antimonate particles and the surrounding glass phase were determined for the ancient glasses and replicate "Egyptian type" and "Roman type" glass using a Stereoscan S-360 SEM equipped with an energy dispersive X-ray spectrometer (EDS), PCXA LINK EDX. The accelerating voltage was 20 kV and the probe current 1.5 nA. The bulk compositions of the Egyptian glasses, as determined by wavelength dispersive spectrometry (WDS), were reported previously by Shortland and Eremin (2006), and only the average composition is given in Table 2.2. For the Roman yellow glasses, average compositions, determined from the EDS and WDS analyses reported by Mass et al. (1998) and Freestone and Stapleton (2013), are given in Table 2.2, together with the bulk composition of Roman glass 116a as determined for areas including lead antimonate particles by EDS using the Stereoscan S-360 SEM.

In the current study of lead antimonate, it is the detection limits for tin and antimony that were of particular importance. For tin, the detection limits were about 0.2 wt% SnO_2 and 0.02 at% Sn. For antimony, when tin was also present, they were about 0.4 wt% Sb_2O_5 and 0.1 at% Sb, and when tin was absent, about 0.2 wt% and 0.05 at% respectively. The equipment was calibrated using mineral standards.

Structural analyses

For the New Kingdom Egyptian glasses, the mineralogy of individual lead antimonate particles was determined using Synchrotron Radiation µ-XRD, performed on beamline BM16 at the ESRF (Grenoble, France) in transmission geometry with a collimated beam with 50 µm x 50 µm spot size and monochromatic 16 keV energy (λ= 0.78 Å) X-rays on thin (about 100 µm) slices cut out of the glasses. The XRD patterns were recorded using a CCD detector. For the Roman tessera, and the replicate lead antimonate pigments, *anime* and yellow glasses, bulk XRD measurements were undertaken using a conventional diffractometer, Siemens D-500 with Cu-Kα radiation. The two theta range was 4-80º. Identification of the compounds has been performed

based on the Powder Diffraction File (PDF) database from the International Centre for Diffraction Data (ICDD).

Colour

For Roman tessera, and the replicate lead antimonate pigments, *anime* and yellow glasses, colour analyses was performed by recording the UV-vis spectra in reflection mode, using a double beam UV-vis-NIR spectrophotometer (Shimadzu 3600) equipped with an ISR 3100 Ulbricht integrating sphere. The spot size was a slit of 5 mm x 1 mm, and measurements were made between 200 nm and 800 nm at 1 nm resolution. A D_{65} standard illumination source was used and barium sulphate provided a white standard. The colour coordinates were determined following the International Commission for Illumination (CIE) recommendation. The colour coordinates are evaluated by CIE 1976, the method being based on the evaluation of the tri-stimulus coordinates (XYZ) equivalent to the eye response to the light and corrected by the emission of a standard illuminant (D_{65}) corresponding to the emission of the blackbody at 6500 K. The XYZ coordinates are not uniformly spaced, and for this reason the Commission established the CIE Lab* standard measure to produce a homogeneously spaced colour system. From the original XYZ colour coordinates, a new set called **a***, **b*** and **L*** are determined, where positive **a*** corresponds to red, negative **a*** to green, positive **b*** to yellowand negative **b*** to blue, and **L*** stands for the lightness. From this international standard system the hue ($\mathbf{h}^* = \arctan(\mathbf{b}^*/\mathbf{a}^*)$) and saturation or chroma ($\mathbf{c}^* = (\mathbf{a}^{*2} + \mathbf{b}^{*2})^{1/2}$) may also be evaluated.

Results

New Kingdom Egyptian and Roman glasses

As previously noted by, for example, Mass et al. (2002) and Shortland (2002a) for New Kingdom yellow glasses, and by Mass et al. (1998) for Roman yellow glasses, significant variation in composition with stripes of glass richer in lead, in which the concentration of lead antimonate particles tends to be higher, was observed in all these glasses in polished section in the SEM (Figure 2.2). The size of these lead antimonate particles is highly variable, ranging from a few µm up to about 60 µm, and the volume fraction of particles never exceeds 7% of the total volume of the sample.

Up to about five lead antimonate particles were analysed by EDS in each of the seven glasses with larger particles being selected in order to minimise the contribution from the surrounding

glass, only those analyses containing less than 5 wt% SiO_2 being considered. Even so, the analyses contained a few wt% of silicon and sodium, and these elements were removed in order to obtain the composition of the lead antimonate particles. The average molar compositions of the particles, normalised to two atoms of lead, are given in Table 2.3.

- ***New Kingdom Egyptian glasses***

The plots of at% of antimony, iron and zinc versus at% of lead for particles in all the glasses, and for the glass surrounding the particles of sample UPP9 are shown in Figure 2.3. From Figure 2.3a, it is seen that, in all the glasses, the lead antimonate particles contain less antimony than lead and show a correlation of about 0.93 Sb atom for every Pb atom. In addition, as previously observed by Lahlil et al. (2011) in New Kingdom Egyptian glasses, the particles contain small variable amounts of iron and zinc which do not show a clear correlation with the lead content (Figure 2.3b and c). Overall, the average composition of the lead antimonate particles is 55.8 wt% PbO + 37.8 wt% Sb_2O_5 + 2.5 wt% FeO + 1.7 wt% ZnO, with the amounts of FeO and ZnO varying quite a lot between particles. From the corresponding plots for the glass phase surrounding the lead antimonate particles in sample UPP9 (Figure 2.3d, e and f), it is seen that the antimony, iron and zinc contents show some correlation with the lead contents. However, the amount of antimony present in the glass is significantly lower than what would be expected from dissolution of the lead antimonate particles, the at% Sb/at% Pb ratio being about 1:6 in the glass as compared to about 1:1.1 in the particles. In contrast, although the amounts of iron and zinc in the glass are again lower than those in the lead antimonate particles, the at% Fe/at% Pb and at% Zn/at% Pb ratios are comparable in the glass and lead antimonate particles.

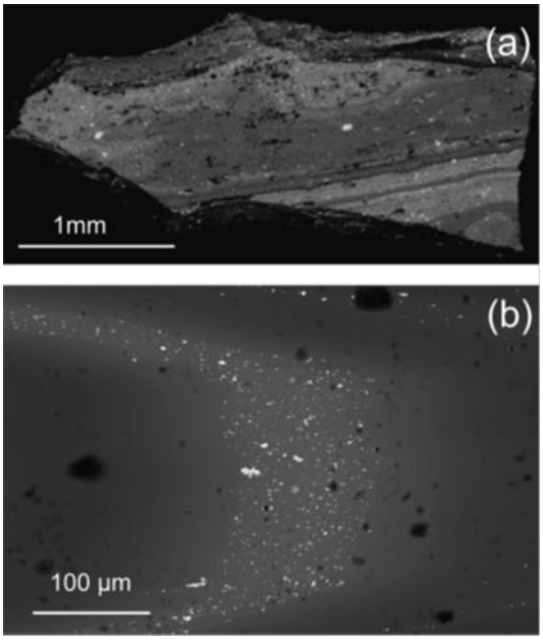

Figure 2.2. SEM photomicrographs in backscatter mode of polished sections through (a) New Kingdom yellow glass from Malkata (UPP9) showing stripes of glass both richer in lead (lighter grey) and poorer in lead (darker grey) and (b) Roman yellow glass (116a) showing, in the central region, a concentration of lead antimonate particles (white) within a lead rich area of glass (lighter grey). Surrounding this are regions of glass poorer in lead (darker grey) which contain far fewer lead antimonate particles.

Micro XRD on individual lead antimonate particles showed that, with one exception, they were all of the type $Pb_2Sb_2O_7$ with a cubic crystallographic structure, space group Fd-3m (lattice parameters a = b = c, and $\alpha = \beta = 90^o$)

known as pyrochlore structure. The majority show the presence of cubic lead antimonates with lattice parameters equal to 10.44, 10.46 and 10.48Å which, as discussed below, are associated with lead antimonates containing iron and zinc (Table 2.4). Pure lead antimonate with lattice parameter equal to 10.40Å was only observed in one glass (UPP11). In addition to the cubic lead antimonates, the green glass (UPP14) contains $PbSb_2O_6$ which has a hexagonal crystallographic structure, space group P312 (a = b = 5.29Å, c = 5.36Å, $\alpha = \beta = 90^o$, $\gamma = 120^o$). Other crystalline phases, such as calcium silicates and calcium magnesium silicates, were also found in all the glasses except UPP10 (Table 2.4). The precipitation of calcium and calcium magnesium silicates is ex expected as Egyptian glasses contain large amounts of calcium and magnesium oxides (typical averages of 7.2 wt% and 4.1 wt% respectively) as compared to Roman glasses (typical averages of 4.7-5.8 wt% and 0.4-0.5 wt% respectively) (Table 2.2). The plot of the reduced lime and silica wt% contents for the glass phase in sample UPP9 shows that there is no significant difference in the composition near to and away from lead antimonate particles (Figure 2.4a). This result is consistent with the observation that, for New Kingdom Egyptian glasses, there are no significant differences in the reduced silica and lime contents of yellowglasses relative to the other colours (Figure 2.1b), and suggests that minimal silica was included in the lead antimonate pigment used in the production of these glasses.

- ***Roman glass***

The plots of at% of antimony iron and tin versus at% of lead for the particles and in the glass surrounding the particles are shown in Figure 2.5. From Figure 2.5a, it is seen that the lead antimonate particles again all contain less antimony than lead and show a correlation of about 0.86 Sb atoms for every Pb atom. In addition, as previously observed by Lahlil et al. (2011) in Roman glasses, the particles contain small variable amounts of iron and tin. In contrast to the

Table 2.3
Molar composition of the lead antimonate particles after normalisation to 2 atoms of Pb (average number of atoms and standard deviation (in brackets) among N particles).

Samples	N particles	At Sb	At Fe	At Zn	At Sn	At O
Egyptian - UPP7	2	1.84 (0.00)	0.60 (0.24)	0.53 (0.36)		7.2 (0.4)
Egyptian - UPP9	5	1.79 (0.08)	0.29 (0.15)	0.16 (0.10)		7.6 (0.6)
Egyptian - UPP10	1	1,75	0,14	0,28		8,1
Egyptian - UPP11	3	1.86 (0.13)	0.33 (0.20)	0.17 (0.07)		7.1 (1.4)
Egyptian - COP20	4	1.83 (0.05)	0.26 (0.12)	0.10 (0.02)		7.3 (1.6)
Egyptian - UPP14	4	1.94 (0.02)	0.07 (0.01)	0.14 (0.04)		5.8 (0.4)
Replicate "Egyptian type" glass (PG-EG + RGM-CEG-1000°C)	9	1.89 (0.29)	0.20 (0.12)	0.06 (0.09)		6.1 (0.47)
Roman - 116a	6	1.77 (0.15)	0.56 (0.06)		0.13(0.05)	7.3 (0.5)
Replicate "Roman type"glass (AN-RG + RGM-CRG-900°C)	7	1.45 (0.11)	0.41 (0.03)		0.23 (0.08)	8.2 (0.9)

situation for the Egyptian glasses, the iron and tin contents correlate well with the lead content (Figure 2.5b and c).

Overall, the average composition of the lead antimonate particles is 56.7 wt% PbO + 35.7 wt% Sb_2O_5 + 5.1 wt% FeO + 2.4 wt% SnO_2. It should be noted, however, that the bulk tin oxide content of the glass itself is below the detection limit (about 0.2 wt% SnO_2) for analyses by EDS.

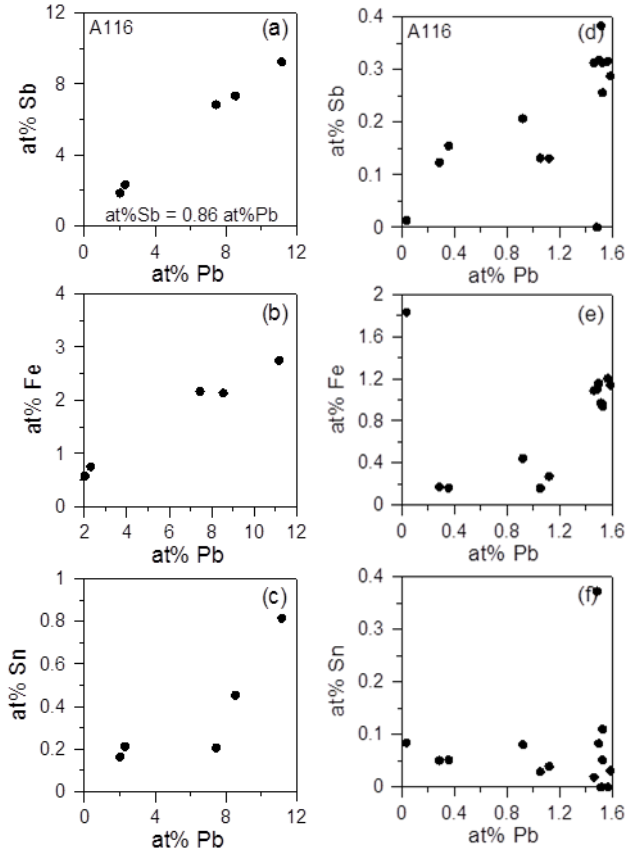

Figure 2.3. Correlation between Pb at% and (a) Sb, (b) Fe and (c) Zn at% for the lead antimonate particles in New Kingdom Egyptian yellow glasses, and between Pb at% and (d) Sb, (e) Fe and (f) Zn at% for the glass phase surrounding the lead antimonate particles in New Kingdom Egyptian yellow glass (UPP9).

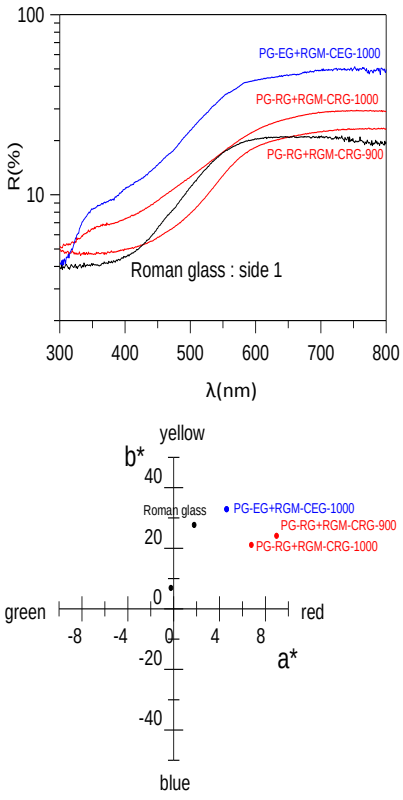

Figure 2.6. (a) UV-vis reflectance spectra and (b) CIE-Lab* colour coordinates (a* and b*) for Roman glass (116a), and for replicate "Egyptian type" glass (PG-EG þ RGM-CEG-1000ºC) and "Roman type" glass (AN-RG + RGM-CRG-900ºC and 1000ºC).

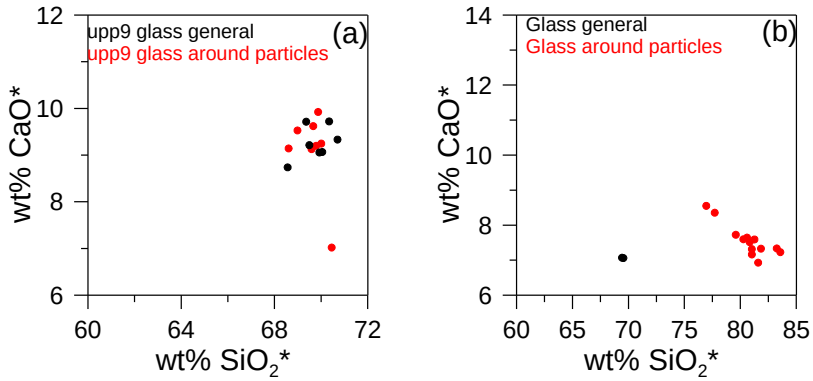

Figure 2.4. Plots of reduced lime content versus reduced silica content around and away from lead antimonate articles for (a) New Kingdom Egyptian glass UPP9) and (b) Roman glass (116a).

From the corresponding plots for the glass phase surrounding the lead antimonate particles, it is seen that the antimony and iron contents show some correlation with the lead contents (Figure 2.5d and e). However, the amount of antimony present in the glass is again significantly lower than what would be expected from dissolution of the lead antimonate particles, the at% Sb/at% Pb ratio being about 1:4 in the glass as compared to about 1:1.1 in the particles.

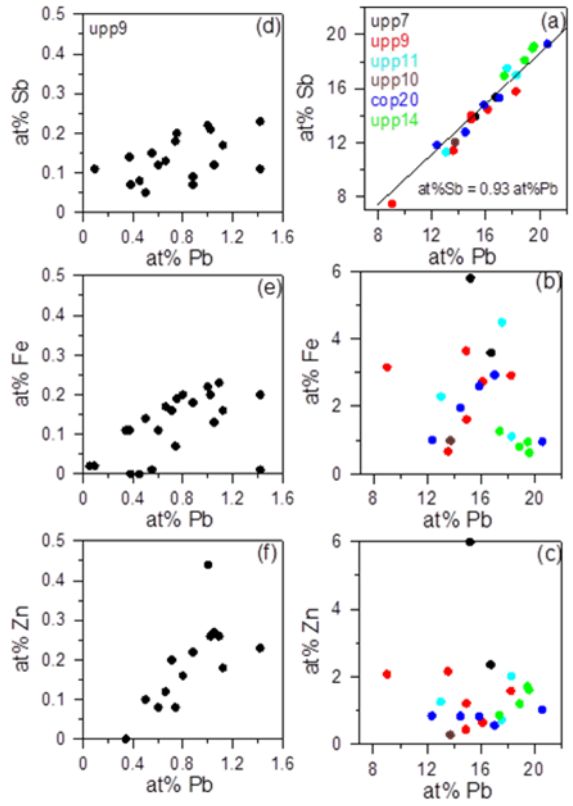

Figure 2.5. Correlation between Pb at% and (a) Sb, (b) Fe and (c) Sn at% for the lead antimonate particles, and between Pb at% and (d) Sb, (e) Fe and (f) Sn at% for the glass phase surrounding lead antimonate particles in a Roman yellow glass (116a).

In contrast, the tin contents are not correlated with the lead contents (Figure 2.5f) and both the low and high lead glass areas contain about 0.05 at% Sn, which is consistent with the low solubility of tin in the glass. Bulk XRD measurements showed that all the lead antimonate particles were of the type $Pb_2Sb_2O_7$ (with Sb partly substituted by either Fe and/or Sn) again with a pyrochlore crystallographic structure, cubic space group Fd-3m (lattice parameters a = b = c, and $\alpha = \beta = 90^o$). As a result of iron and tin present in the lead antimonate particles, the majority have lattice parameters equal to 10.48Å, but on one side of the sample, there appears a second cubic lead antimonate with a smaller lattice parameter (10.46Å) (Table 2.4), thus indicating heterogeneity in the composition of the yellow particles added to the glass. The CIE-Lab* colour coordinates, calculated from the measured UV-vis spectra (Figure 2.6a), are presented in Table 2.5 and plotted in Figure 2.6b. These results show that the colours of the two sides of the sample are slightly different. One side has a large yellow component (**b*** = 26.6) and a small red component (positive **a***) whereas the other side has only a small yellow component (**b*** = 8.2) and an even smaller green component (negative **a***).

The plot of the reduced lime and silica wt% contents for the glass phase shows that the silica contents are significantly higher near to lead antimonate particles as compared to those away from the particles (Figure 2.4b). This result is consistent with the observation that, for Roman glass, the more reduced compositions of yellow glasses exhibit elevated silica contents together with lower lime contents relative to the other colours (Figure 2.1a and Freestone and Stapleton, 2013; Figs. 2.9 and 2.10), and again suggests that silica was included in the lead-antimony mixture used in the production of Roman yellow glasses.

Table 2.4. Lattice parameters for lead antimonate particles and other mineral phases detected in the New Kingdom Egyptian and Roman glasses.

Samples	$Pb_2Sb_2O_7$ lattice parameter (Å)	other crystalline compounds
Egyptian - UPP7	10,44	diopside, ca-mg silicate, wollastonite
Egyptian - UPP9	10.44, 10.48	diopside, ca-mg silicate, wollastonite
Egyptian - UPP10	10.44, 10.48	
Egyptian - UPP11	10.40, 10.44, 10,.48	diopside, ca-mg silicate, wollastonite
Egyptian - COP20	10,46	ca-mg silicate
Egyptian - UPP14	10.44, 10.48	$PbSb_2O_6$
Replicate "Egyptian type" glass (PG-EG + RGM-CEG-1000°C)	10.46, 10.48	diopside, quartz
Roman - 116a	10.46, 10.48	quartz
Replicate "Roman type"glass (AN-RG + RGM-CRG-900°C)	10,48	
Replicate "Roman type"glass (AN-RG + RGM-CRG-1000°C)	10,44	$Ca_2Sb_2O_{6.5}$ (a = 10.37 Å)

- ***Replication of "Egyptian type" lead antimonate glass***

In the replication of "Egyptian type" lead antimonate glass, the first step was the synthesis of various lead antimonate pigments based on a stoichiometric mixture of 58 wt% lead oxide and 42 wt% antimony oxide (Table 2.1). The temperature stability when the stoichiometric pigment was fired with colourless glass was then investigated, and finally, based on the compositions of the New Kingdom glasses, an "Egyptian type" lead antimonate glass was replicated.

- ***Synthesis of lead antimonate pigments***

For the lead antimonate pigments produced from the stoichiometric mixture (PG1), the bulk XRD results, presented in Table 2.6, shows that several lead antimonate compounds were formed. Pure cubic $Pb_2Sb_2O_7$, with lattice spacing 10.40Å, is present for both firing temperatures, but it is only one of several lead antimonates present. After firing to 800ºC for 2h, $Pb_2Sb_2O_7$ is present in trace amounts and the dominant lead antimonate is $Pb_{3+x}Sb_2O_{8+x}$. After firing to 1000ºC for 2 h, both these lead antimonates are present in medium amounts. The CIE-

Lab* colour coordinates for these pigments, which were calculated from the measured UV-vis spectra, and which are presented in Table 2.5 and plotted in Figure 2.7, are consistent with the observed yellow colour; that is, positive **b*** (23-25) with small positive **a*** (5-6) indicative of a red component. For the lead antimonate pigments produced by firing the stoichiometric mixture with the addition of varying amounts of iron oxide and zinc oxide (PG2-6) at 1000ºC for 2h, the bulk XRD results show that several lead antimonate compounds were again formed but that cubic $Pb_2Sb_2O_7$ is now dominant in all cases (Table 2.6). However, due to the incorporation of both Fe and Zn into the cubic lattice, the lattice spacing is greater than that for pure lead antimonate formed previously (a = 10.40Å), and ranges from 10.46Å for 1 wt% FeO to 10.51Å for 2 wt% ZnO. In contrast, the XRD results for the pigment used to produce "Egyptian type" yellow glass (PG-EG), which contained small amounts of iron and zinc together with excess lead, show that two cubic lead antimonates ($Pb_2Sb_2O_7$) were formed, with lattice parameters of 10.425Å and 10.479Å, characteristic of the incorporation of Fe and Zn into the cubic lattice. In addition, some orthorhombic $Pb_2Sb_2O_7$, a mixed Fe-Zn oxide and Sb_2O_4 were formed.

The CIE-Lab* coordinates for the stoichiometric pigments (Table 2.5, Figure 2.7) are again consistent with the observed yellow colour with positive **b*** (10-34) and small positive **a*** (2-7.5) indicative of a red component. However, there is no clear correlation between colour and composition of the pigment, and only the pigment mixtures containing either 4 wt% FeO (PG3) or 2 wt% ZnO (PG5) exhibit a significantly stronger yellow colour (i.e., **b*** approximately 34 and 29 respectively) than that of the stoichiometric mixture without the addition of iron or zinc oxides. For the lead antimonate pigments produced from the stoichiometric mixture to which some 10 wt% sodium chloride flux (NaCl) was added (PG7), the bulk XRD results, presented in Table 2.6, show that cubic $Pb_2Sb_2O_7$, with lattice spacing approximately 10.40Å, is already the major component after firing to 900ºC, and after firing to 1000ºC, it is the only lead antimonate present.

In contrast, when small amounts of iron or zinc were included in the NaCl containing pigments (PG8-9), two cubic lead antimonates ($Pb_2Sb_2O_7$) with lattice parameters of 10.386 and 10.453Å for PG8, and 10.400 and 10.462Å for PG9 were formed, as in the case of pigment PG-EG containing excess lead. The observed colours of these pigments are a more intense and homogeneous yellow than those observed for pigments produced from the stoichiometric mixtures without the addition of NaCl flux. This difference is reflected in the CIE-Lab* coordinates (Table 2.5, Figure 2.7) for which **b*** is in the range 33-46 as compared to 23-34 without the addition of NaCl flux.

Table 2.5 CIE-Lab* colour coordinates.

Sample	L*	a*	b*	c*	h*
Roman yellow glass (116a)					
Side 1	33,4	-0,3	8,2	8,2	92,1
Side 2	48,3	1,7	27,6	27,7	86,5
Replication of "Egyptian type" glass					
Replicate pigment - PG1 (no NaCl)(fired for 2h)					
800ºC	55,5	5,2	23,4	24,0	77,5
900ºC	58,1	4,0	18,7	19,1	77,9
1000ºC	58,1	5,8	24,8	25,5	76,8
Replicate pigments with FeO and ZnO (no NaCl)(fired 1000°C for 2h)					
PG2 - Fe 1 wt%	46,4	5,2	20,5	21,1	75,8
PG3 - Fe 4 wt%	61,1	7,5	34,2	35,0	77,6
PG4 - Fe 8 wt%	55,2	6,5	27,5	28,3	76,7
PG5 - Zn 2 wt%	56,9	6,9	29,3	30,1	76,7
PG6 - Zn 1 wt%+Fe 2.5 wt%	37,1	2,3	10,5	10,7	77,6
Replicate pigment - PG7 (10 wt% NaCl)(fired for 2h)					
800ºC	62,6	5,6	34,0	34,5	80,6
900ºC	58,3	5,5	33,0	33,5	80,5
1000ºC	65,5	9,5	43,3	44,3	77,6
Replicate pigments with FeO and ZnO (10 wt% NaCl)(fired 1000°C for 2h)					
PG8 - Fe 1 wt%	73,1	5,4	46,1	46,4	83,3
PG9 - Zn 2 wt%	71,8	1,3	46,2	46,2	88,4
Stability of lead antimonate particles					
PG1 + RGM-CEG (fired for 2h)					
800°C	84,5	2,7	31,8	31,9	85,1
900°C	72,9	-4,1	29,4	29,7	97,9
1000°C	73,0	-5,2	21,2	21,8	103,8
1050°C	53,2	-3,0	8,9	9,4	108,6
PG7 + RGM-CEG (fired for 2h)					
800°C	67,2	-3,6	25,0	25,3	98,2
900°C	66,4	-7,9	27,1	28,2	106,3
1000°C	63,0	-6,8	23,6	24,6	106,1
1050°C	57,3	-6,1	14,8	16,0	112,4
"Egyptian type" glass					
(PG-EG + RGM-CEG -1000°C)	65,7	4,6	32,9	33,2	82,0
Replication of "Roman type" glass					
Replicate anime (fired 900°C for 2h)					
AN1	62,4	6,1	34,1	34,6	79,9
AN2	38,0	1,6	9,4	9,5	80,3
AN3	81,6	-0,1	7,5	7,5	90,8
AN4	43,0	0,2	1,7	1,7	83,3
Stability of lead antimonate particles					
AN1 + RGM-CRG (fired for 2h)					
900°C	59,0	-5,5	13,9	14,9	111,6
1000°C	58,7	-2,2	3,1	3,8	125,4
"Roman type" glass					
(AN-RG + RGM-CRG -900°C)	43,6	9,1	24,2	25,9	69,4
(AN-RG + RGM-CRG -1000°C)	49,6	6,8	21,1	22,2	72,1

Table 2.6.
XRD data for replicate lead antimonate pigments, fired for 2 h (*: major; m: median; t: traces).

Replicate pigment	JPDF file	Compound	Lattice parameter	Crystalline structure
PG1 (no NaCl)				
800ºC	00-034-1196	$Pb_{3+x}Sb_2O_{8+x}$*		
	01-084-1423	$PbSb_2O_6$ t		
	00-042-1355	$Pb_2Sb_2O_7$ t		cubic (Fd-3m)
	00-039-0834	$Pb_2Sb_2O_7$ t		orthorhombic
1000ºC	01-084-1423	$PbSb_2O_6$*		
	00-034-1196	$Pb_{3+x}Sb_2O_{8+x}$ m		
	00-042-1355	$Pb_2Sb_2O_7$ m	a=10.398(1)	cubic (Fd-3m)
	00-039-0834	$Pb_2Sb_2O_7$ t		orthorhombic
PG2-PG6 (no NaCl), fired 1000 °C				
PG2-Fe 1 wt%		$Pb_2Sb_2O_7$-type *	a=10.457(6)	cubic (Fd-3m)
	01-084-1423	$PbSb_2O_6$ m		
	00-034-1196	$Pb_{3+x}Sb_2O_{8+x}$ m		
	00-039-0834	$Pb_2Sb_2O_7$ m		orthorhombic
PG3-Fe 4 wt%		$Pb_2Sb_2O_7$-type *	a=10.490(4)	cubic (Fd-3m)
	01-084-1423	$PbSb_2O_6$ m		
PG4-Fe 8 wt%		$Pb_2Sb_2O_7$-type *	a=10.488(5)	cubic (Fd-3m)
	01-084-1423	$PbSb_2O_6$ m		
	00-034-0372	$PbSbO_4$ t		
	01-079-1741	Fe_2O_3		
PG5-Zn 2 wt%		$Pb_2Sb_2O_7$-type *	a=10.508(7)	cubic (Fd-3m)
	01-084-1423	$PbSb_2O_6$ m		
	00-034-1196	$Pb_{3+x}Sb_2O_{8+x}$ m		
	00-039-0834	$Pb_2Sb_2O_7$ m		orthorhombic
PG6-Zn 1 wt%+		$Pb_2Sb_2O_7$-type *	a=10.494(1)	cubic (Fd-3m)
FeO 2.5 wt%	01-084-1423	$PbSb_2O_6$ m		
	00-034-1196	$Pb_{3+x}Sb_2O_{8+x}$ t		
PG7 (10 wt% NaCl)				
800ºC	00-034-1196	$Pb_{3+x}Sb_2O_{8+x}$		
	00-042-1355	$Pb_2Sb_2O_7$	a=10.396(4)	cubic (Fd-3m)
	00-039-0834	$Pb_2Sb_2O_7$ t		orthorhombic
900ºC	00-042-1355	$Pb_2Sb_2O_7$	a=10.391(1)	cubic (Fd-3m)
	00-034-1196	$Pb_{3+x}Sb_2O_{8+x}$ t		
	01-084-1423	$PbSb_2O_6$ t		
1000ºC	00-042-1355	$Pb_2Sb_2O_7$	a=10.398(1)	cubic (Fd-3m)
PG8-PG9 (10 wt% NaCl), fired 1000 °C				
PG8-Fe 1 wt%	00-042-1355	$Pb_2Sb_2O_7$	a=10.386(7)	cubic (Fd-3m)
		$Pb_2Sb_2O_7$-type	a=10.453(3)	cubic (Fd-3m)
PG9-Zn 2 wt%	00-042-1355	$Pb_2Sb_2O_7$	a=10.400(5)	cubic (Fd-3m)
		$Pb_2Sb_2O_7$-type	a=10.462(1)	cubic (Fd-3m)
PG-EG, fired 1000 °C				
	00-042-1355	$Pb_2Sb_2O_7$-type	a=10.425(2)	cubic (Fd-3m)
		$Pb_2Sb_2O_7$-type	a=10.479(2)	cubic (Fd-3m)

- ***Stability of lead antimonate particles***

The bulk XRD measurements on glasses produced from mixtures of stoichiometric pigment without the addition of NaCl flux (PG1) and colourless glass (RGM-CEG) (Table 2.2) indicate that trace amounts of cubic $Pb_2Sb_2O_7$ (a = 10.40Å) are present for firings up to 1000ºC. However, for a firing at 1000ºC, hexagonal $CaSb_2O_6$ is also present, and when the glass is fired to 1050ºC, the cubic $Pb_2Sb_2O_7$ is converted to orthorhombic calcium antimonate, $Ca_2Sb_2O_7$.

The CIE-Lab* colour coordinates (Table 2.5) reflect the changes in the antimonate phases present in the glasses fired to different temperatures, as determined by XRD measurements. Thus, as a result of the partial conversion from $Pb_2Sb_2O_7$ to $CaSb_2O_6$, the **b*** colour coordinates are reduced from 31.8 and 29.4 for the glasses fired at 800ºC and 900ºC respectively, to 21.2 for the glass fired at 1000ºC.

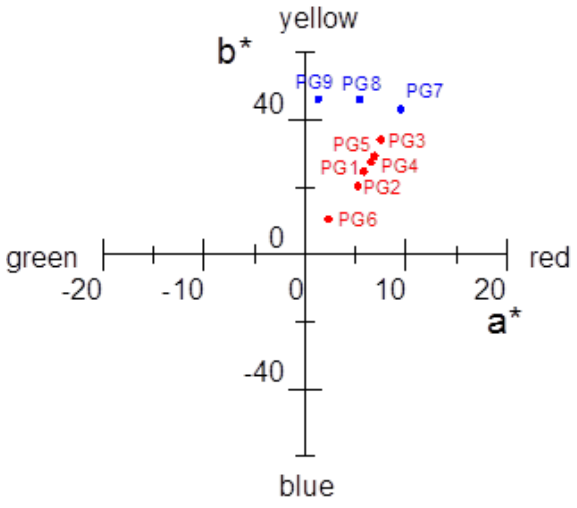

Figure 2.7. CIE-Lab* colour coordinates (a* and b*) for replicate pigments PG1 (no NaCl), PG2-6 (no NaCl but added Fe and/or Zn), PG7 (10 wt% NaCl), and PG8-9 (10 wt% NaCl plus added Fe or Zn), all fired at 1000ºC.

Although these **b*** values are comparable to that for the original pigment (**b*** = 24.8), the glasses differ from the pigment in having small, negative **a*** coordinates (-5 to -3) and being yellow-green in colour, whereas the original pigment had a small positive **a*** coordinate (+5.8) and was yellow-red in colour. Finally, at 1050ºC, the decomposition of the lead antimonate and the formation of calcium antimonate results in the decolouration of the glass (i.e., **b*** = 9).

In contrast, when stoichiometric pigment with the addition of NaCl flux (PG7)was used, bulk XRD measurements showed that the pure cubic $Pb_2Sb_2O_7$ (a = 10.40Å) suffers some transformation to a cubic antimonate with a smaller lattice parameter (10.38Å at a firing temperature of 800ºC and 10.34Å at 900ºC and 1000ºC). These changes are most probably the result of Ca substituting for Pb to form an intermediate cubic lead-calcium antimonate $(Pb,Ca)_2Sb_2O_7$. Then, at a firing at 1050ºC, this intermediate cubic antimonate decomposes to form orthorhombic calcium antimonate, $Ca_2Sb_2O_7$. The CIE-Lab* colour coordinates reflect this early transformation to an intermediate cubic antimonate in that the **b*** for firing temperature of 800ºC and 900ºC (25.0 and 27.1) are lower than the corresponding values (31.8 and 29.4) for the pigment without the addition of NaCl flux.

- ***Replication of "Egyptian type" yellow glass***

Since Egyptian yellow glasses did not exhibit elevated silica contents relative to the other colours, replicate "Egyptian type" glass was produced using a lead antimonate pigment containing no silica. The composition of the pigment, which contained small amounts of iron and zinc together with excess lead oxide is given in Table 2.1 (PG-EG). 12 wt% of this powdered pigment was added to 88 wt% powdered colourless glass (RGM-CEG) with composition comparable to that of New Kingdom Egyptian glass (Table 2.2), and the combined mixture was fired at 1000ºC for 2 h.

The resulting the replicate glass (PG-EG + RGM-CEG-1000ºC) showed a mottled pattern of bright yellow and white areas (Figure 2.8a). In polished section in the SEM, it can be seen that, because the glass was not stirred when molten, there are areas of glass with higher and lower lead oxide contents, and the lead antimonate particles are not well distributed, are frequently clustered together and are very variable in size (Figure 2.8c).

From the plots of at% of antimony, iron and zinc versus at% of lead for the particles and glass phase, as determined by EDS analyses (Figure 2.9a-c), it can be seen that the glass phase contains no antimony but small amounts of iron and zinc. In the lead antimonate particles, the antimony content correlates with the lead content, and their compositions are close to the theoretical stoichiometric composition, with the iron and zinc contents being very variable between particles. The average molar concentrations of the particles, normalised to two atoms of lead, are compared with those for the New Kingdom Egyptian glasses in Table 2.3, and the bulk composition of the replicate glass is given in Table 2.2.

The bulk XRD pattern shown in Figure 2.10a for the replicate glass indicates that, as for the New Kingdom Egyptian glass, the lead antimonate particles are of the cubic $Pb_2Sb_2O_7$ type with two high lattice parameters (a = 10.46Å and 10.48Å) associated with various iron and zinc contents (Table 2.4).

The CIE-Lab* colour coordinates, calculated from the measured UV-vis spectra (Figure2. 6a), are included in Table 2.5 and plotted in Figure 2.6b, and indicate a strong yellow colour (**b*** = 32.9) with a small red component (**a*** = 4.6). Thus, the colour coordinates for a glass produced using a pigment with excess lead correspond well with those for the replicate lead antimonate pigments containing FeO and ZnO, some of which show similar yellow components (eg., **b*** equal to 29.3 and 34.2) together with small red components (**a*** equal to 6.9 and 7.5) (Table 2.5).

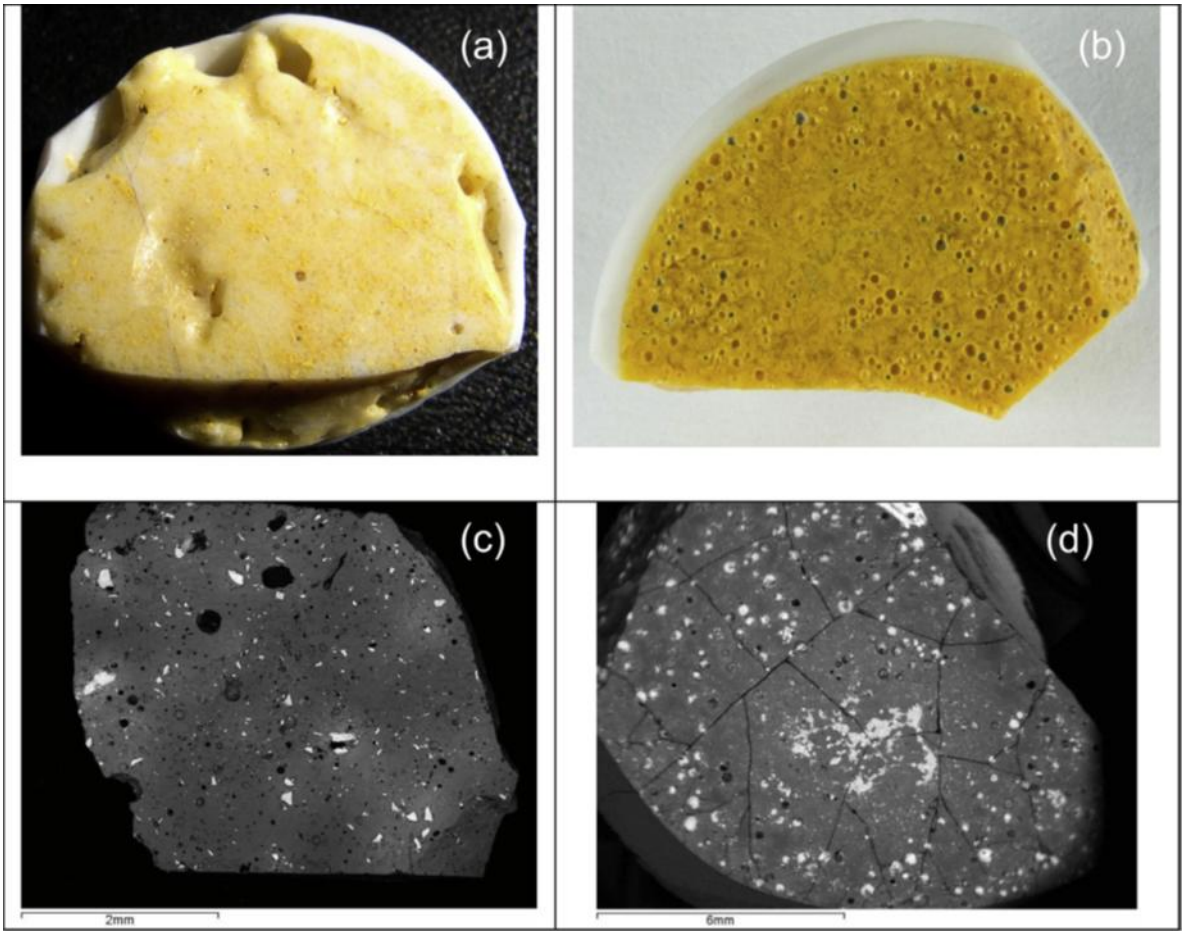

Figure 2.8. Replicate (a) "Egyptian type" (PG-EG + RGM-CEG-1000 _C) and (b) "Roman type" (AN-RG + RGM-CRG-900ºC) lead antimonate glasses, and SEM photomicrographs in backscatter mode of polished sections throughthese replicate (c) "Egyptian type" and(d) "Romantype" glasses showing a scatter of lead antimonate particles(white) together with areas of glass both richer in lead (lighter grey) and poorer in lead (darker grey).

- ***Replication of "Roman type" lead antimonate glass***

In the replication of "Roman type" lead antimonate glass, the first step was the synthesis of various lead-antimony-silica *animes* containing excess lead (Table 2.1). The temperature stability when *anime* was fired with colourless glass was then investigated, and finally, based principally on the compositions of the Roman glasses, a "Roman type" lead antimonate glass was replicated.

- ***Synthesis of lead-antimony-silica anime***

In terms of colour, only the two replicate *anime* mixtures with low silica contents (AN1 and AN2 in Table 2.1) exhibit a yellow colour, although AN2 is very pale. In contrast the high silica *animes* (AN3 and AN4) are essentially white.

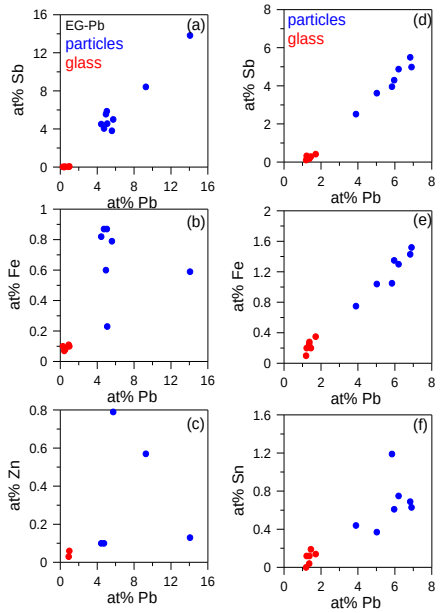

Figure 2.9. Correlation between Pb at% and (a) Sb, (b) Fe, and (c) Zn at% for the lead antimonate particles and surrounding glass phase in replicate "Egyptian type" (PG-EG + RGM-CEG-1000ºC) and between Pb at% and (d) Sb, (e) Fe, and (f) Sn at% in replicate "Roman type" (AN-RG + RGM-CRG-900ºC) lead antimonate yellow glasses

.

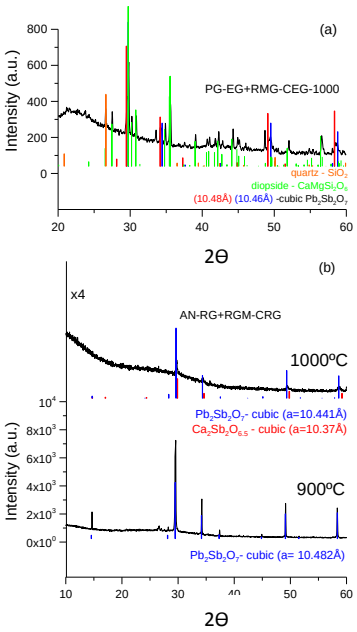

Figure 2.10. XRD patterns for replicate (a) "Egyptian type" (PG-EG + RGM-CEG-1000ºC) and (b) "Roman type" (AN-RG + RGM-CRG) lead antimonate glasses, the latter fired to 900ºC and 1000ºC.

The bulk XRD measurements (Figure 2.11) showed that none of the animes contained the lead antimonate pyrochlore, $Pb_2Sb_2O_7$. Instead the dominant phases in the two mixtures with low silica contents (AN1 and AN2) are $Pb_{3+x}Sb_2O_{8+x}$ and the lead silicate, $Pb_2(SiO_3)O$ whereas those in the two mixtures with high silica contents (AN3 and AN4) are quartz and $PbSb_2O_6$. The observed colour and the lead antimonate phases present are reflected in the CIE-Lab* coordinates (Table 2.5). Thus, of the low silica *animes*, AN1 with the lower PbO/Sb_2O_5 ratio (8 as compared to 12) exhibits a much more intense yellow than AN2 (**b*** = 34.1 and 9.4 respectively), and the two white, high silica *animes* exhibit even lower **b*** values (7.5 and 1.7 respectively).

- ***Stability of lead antimonate particles***

The glass resulting from firing a mixture of the low silica, lower PbO/Sb_2O_5 ratio *anime* (AN1) and colourless glass (RGM-CRG) to 900ºC is mottled yellow in appearance. Under the optical microscope, a mixture of yellow and white particles together with some particles with a yellow core and a white edge are visible. The bulk XRD pattern indicates the presence of a pyrochlore with a lattice parameter close to 10.30Å which is again most probably the result of Ca substituting for Pb to form an intermediate cubic lead-calcium antimonate

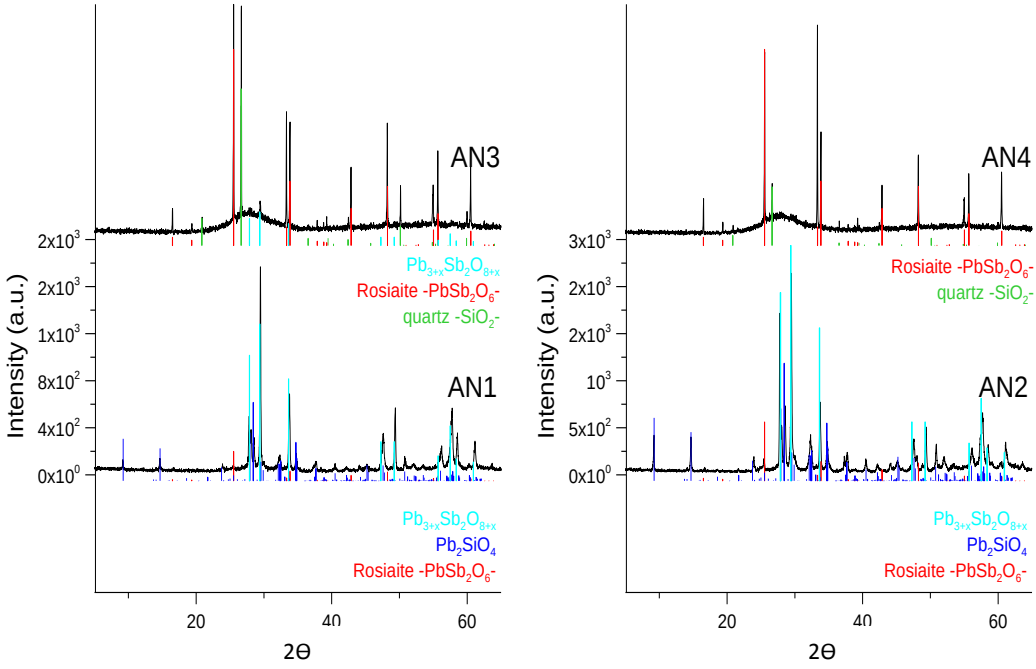

Figure 2.11. XRD patterns for replicate animes AN1-4.

$(Pb,Ca)_2Sb_2O_7$. The CIE-Lab* colour coordinates (Table 2.5) indicate a fairly weak yellow colour (**b*** = 13.9) with a small green component (**a*** = -5.5). In contrast, the glass resulting from firing this same mixture to 1000ºC is opaque white with **b*** coordinate equal to only 3.1.

- ***Replication of "Roman type" yellow glass***

Since Roman yellow glasses exhibited elevated silica contents relative to the other colours, replicate "Roman type" glasses were produced using a lead-antimony-silica *anime*, rather than a lead antimonate pigment containing no silica. The composition of the *anime* (AN-RG), which contained small amounts of iron and tin together with excess lead oxide is given in Table 2.1. Mixtures of this powdered *anime* and powdered colourless glass (RGM-CRG) with composition comparable to that of Roman glass were used (Table 2.2) (20 wt% *anime* + 80 wt% glass) and (12wt% anime + 88 wt% glass) mixtures being fired at 900ºC and1000ºC, respectively, for 2 h.

The resulting replicate "Roman type" glass fired to 900ºC (AN-RG + RGM-CRG-900ºC) is a definite yellow-orange colour (Figure 2.8b). In polished section in the SEM, it can be seen that, because the glass was not stirred when molten, the lead antimonate particles are again not well distributed, are frequently clustered together and are very variable in size (Figure 2.8d).

From the plots of at% of antimony, iron and tin versus at% of lead for the particles and glass phase, as determined by EDS analyses (Figure 2.9d-f), it can be seen that the glass phase contains no antimony but small amounts of iron and tin. In the lead antimonate particles, the antimony and iron contents correlate with the lead content, but the tin contents are more variable between particles. The average molar concentrations of the particles, normalised to two atoms of lead, are compared with those for the Roman glass sample, 116a, in Table 2.3, and the bulk composition of the replicate glass is given in Table 2.2.

The bulk XRD pattern (Figure 2.10b) for the replicate glass indicates that, as for the Roman glass sample, the lead antimonate particles are of the cubic $Pb_2Sb_2O_7$ type with a high lattice parameter (a = 10.482 (1) Å) associated with the incorporation of iron and tin into the lattice (Table 2.4). The CIE-Lab* colour coordinates, calculated from the measured UV-vis spectra (Figure 2.6a), are included in Table 2.5 and plotted in Figure 2.6b, and indicate a strong yellow colour (**b*** = 24.2) together with a significant red component (**a*** = 9.1) which is most probably due to the high iron content of the *anime*.

The plot of the reduced lime and silica wt% contents for the glass phase shows that the silica contents are significantly higher near to lead antimonate particles as compared to those away from the particles (Figure 2.12). This result is as expected with the use of lead antimonate *anime* rather than lead antimonate pigment, and consistent both with the results obtained for the Roman glass sample, 116a (Figure 2.4b), as well as those reported for early Roman glass by Freestone and Stapleton (2013) and those calculated from data published by Mass et al. (1998) for later Roman glass (Figure 2.1a).

The replicate "Roman type" glass fired to 1000ºC (AN-RG + RGM-CRG-1000ºC) also results in a yellow-orange colour, but one that is less saturated than for the glass produced by firing to 900ºC. The CIE-Lab* colour coordinates, calculated from the measured UV-vis spectra (Figure 2.6a) and included in Table 2.5 and plotted in Figure 2.6b, are similarly slightly reduced, although both these observations could be the result of less *anime* being included in the mixture (12 wt% as compared to 20 wt% for the 900ºC mixture). However, the bulk XRD pattern (Figure 2.10b) for this replicate glass indicates that, in addition to cubic lead antimonate particles (lattice parameter a = 10.44Å), some cubic calcium antimonate particles ($Ca_2Sb_2O_{6.5}$ with a = 10.3Å) are also present. Therefore, in spite of the glass still appearing yellow in colour, there has been partial conversion from lead antimonate to calcium antimonate for a firing temperature of 1000ºC, and the glass produced does not fully replicate the ancient Roman glass.

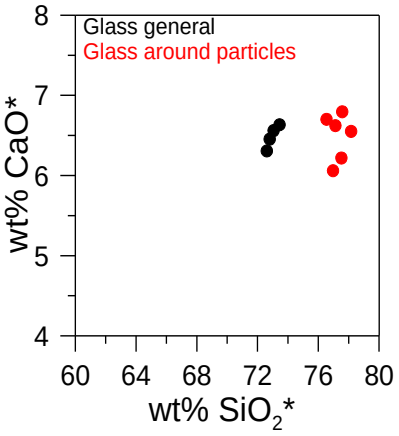

Figure 2.12. Plot of reduced lime content versus reduced silica content around and away from lead antimonate particles for replicate "Roman type" lead antimonate yellow glass (AN-RG + RGM-CRG-900ºC).

Discussion

New Kingdom Egyptian and Roman glasses

The results presented above confirm that New Kingdom Egyptian and Roman yellow glasses are similar in terms of the composition (Table 2.3) and crystallographic structure (Table 2.4) of their lead antimonate particles. The principal difference is that, in addition to the iron present in both types of glass, tin has replaced zinc as the second impurity substituting for antimony in the lead antimonate particles in the Roman glass.

Lead antimonate is a cubic pyrochlore oxide with general formula $A_2B_2O_7$ which has two interpenetrating lattices, an A_4O tetrahedra and a BO_6 vertex sharing octahedra. The A cations occupy part of large sites and help charge balance (either A^{2+} and B^{5+} or A^{3+} and B^{4+}, whereas the Sn^{4+}, Zn^{2+} and Fe^{2+} cations substitute the octahedral sites (Sb^{5+}), modifying the charge valence and distorting the structure. In general and taking into account the detection limits and error in the lattice parameter determination and the statistics, the lead antimonate particles in all the glasses contain seven oxygen atoms and their At Sb/At Pb ratios vary between 1.75:2.0 and 1.9:2.0. These results, together with the observed lattice parameters, are consistent with those previously reported by Rosi et al. (2009).

The fact that at% of iron, zinc and tin show some correlation with at% lead, either in the lead antimonate particles or in the glass surrounding these particles, suggests that the iron, zinc and tin were added with the pigment or *anime*. However, the higher at% Sb/at% Pb ratios, but similar at% Fe/at% Pb, at% Zn/at% Pb and at% Sn/at%Pb ratios, in the particles as compared to the surrounding glass suggests that much of the iron, zinc and tin present in the pigment and *anime* was not originally incorporated into the lead antimonate particles, and therefore, on addition to the glass, was readily dissolved in the glass phase. In contrast, there was only limited dissolution of the lead antimonate particles which contained the bulk of the antimony in the pigment and *anime*.

Mass et al. (1998) proposed, in the context of the production of Roman yellow glasses, that the lead antimonatewas produced from antimonial litharge (i.e., litharge contaminated with antimony) which they argued was a by-product of the cupellation of silver produced from

argentiferous lead ores. Subsequently, Mass et al. (2002) suggested that antimonial litharge from the cupellation of silver similarly provided the lead antimonate used in the production of New Kingdom Egyptian yellow glasses. However, as listed in Table 2.2, New Kingdom Egyptian yellow glasses contain some 0.3 wt% zinc oxide (Shortland and Eremin, 2006), and Rehren (2003) has convincingly argued that this concentration of zinc would not have survived the smelting of argentiferous lead ores in the production of silver-containing lead metal, from which silver would have been subsequently extracted by cupellation. Further, Shortland et al. (2000) have established by lead isotope analyses that the Pb-Zn ore from Gebel Zeit on the Red Sea coast of Egypt was the probably source of the lead used in the production of New Kingdom Egyptian yellow glasses, and that silver metal used in Egypt at this period was produced from a non-Egyptian lead ore.

Therefore, as proposed by Shortland (2002a), the lead antimonate pigment used in the production of New Kingdom Egyptian yellow glass was most probably produced by roasting a mixture of galena (PbS) and stibnite (Sb_2S_3) containing excess lead. The result would have been the formation of lead and antimony oxides which then combined to produce lead antimonate. Because of the refractory nature of zinc oxide (m.p. 1975ºC), the loss of zinc in this process would have been limited. It seems reasonable to assume that the Egyptian glass makers would have been able to select and combine these two metal ores since they were also being used for quite different purposes. Thus stibnite was being used in the production of calcium antimonate white glasses (Mass et al., 1998; Shortland, 2002a) and occasionally as a kohl, and galena was being used in the production of both lead metal and silver as well as being used as a kohl (Lucas and Harris, 1962, 80-84). However, although there is strong lead isotope data to show that galena from Gebel Zeit in Egypt was used as a kohl (Shortland et al., 2000), it is uncertain on the basis of limited lead isotope data (Stos-Fertner and Gale, 1979) whether either lead metal or silver was produced from galena from Egypt. Furthermore, the two ores were most probably being obtained from different places, the galena, as discussed above, from Gebel Zeit in Egypt, and the stibnite from the Caucasus where antimony mines that were active in the Late Bronze Age have been discovered (Chernykh, 1992; Shortland, 2002a).

Conversely, because of the absence of zinc from the Roman yellow glasses, antimonial litharge resulting from the cupellation of silver is a possible source of the lead antimonate used in the production of these glasses. However, there are some doubts as to the extent to which cupellation litharge containing sufficient antimony would have been available (Rehren, 2003). The alternative would have again been to roast a mixture of galena and stibnite, but in this case, zinc must have been absent from the galena chosen. A further option would have been to replace

the galena by cupellation litharge from which any zinc originally present would have been lost during smelting.

The origin of the iron present in the New Kingdom Egyptian pigment is probably the result of contamination from iron minerals, such as pyrite, introduced with the galena used in the production of the pigment, and from the clay crucibles in which the pigment was produced. If antimonial litharge was used to produce the Roman pigment then, as discussed by Mass et al. (1998), an additional source of iron could have been contamination from iron tools used during the cupellation process. Also, in the case of Roman yellow glass, Freestone and Stapleton (2013) have suggested that extra iron was deliberately added to the *anime* mixture in order to stabilise the lead antimonate and make a stronger yellow.

The origin of the tin in the Roman yellow glass, which is present in the lead antimonate particles although below the detection limits for EDS analyses in the bulk glass, presents more of a problem. It is not impossible that the tin was introduced as an impurity from the stibnite, in that some 0.5 wt% of tin was detected in a much earlier, 3rd millennium BC, antimony bead from Syria (Shortland, 2002b). Another possibility is that the scrap lead, which was most probably used in the production of the pigment, contained small amounts of tin, as previously observed by Wyttenbach and Schubiger (1973) in the neutron activation analyses of Roman water pipes. In this case, it was suggested that the lead used to make the pipes included scrap lead which had become contaminated by the inclusion of small amounts of solder. Alternatively, if cupellation litharge was used, this could have contained small amounts of tin as a result of contamination from other adjacent metal production or working processes. Finally, in view of its role in increasing the stability of lead antimonate particles in glass, it is not impossible that tin oxide was deliberately added to the *anime* mixture. However, before it will be possible to resolve the origin of the tin, more information is needed on both the frequency with which tin is present in the lead antimonate particles in Roman glass, and the time period over which this occurs.

Replication of "Egyptian and Roman type" lead antimonate glasses

The synthesis of pure stoichiometric lead antimonate pigments has shown that the cubic lead antimonate, $Pb_2Sb_2O_7$, is only one of several lead antimonates formed. However, the addition of NaCl flux to the mixture produces a pigment in which cubic $Pb_2Sb_2O_7$ is the dominant lead antimonate and which exhibits a more intense yellow colour. This greater reactivity is most probably the result of the NaCl melting at 801ºC to form a liquid which wets the surfacesnof the lead and antimony oxide particles, and results in an increase in their

dissolution and the diffusivity between them. Therefore, as indicated in the relevant Renaissance treatises (Dik et al., 2005; Piccolpasso, 2007), the addition of an alkali flux was necessary to produce the intense yellow pigments required for use in paintings and Italian maiolica glazes from the late 15th century AD onwards. In contrast, when the pigment with added NaCl is incorporated into a colourless glass, the cubic $Pb_2Sb_2O_7$ tends to be less stable, and the resulting colour tends to be weaker than that produced using a stoichiometric pigment without added NaCl. Therefore, in the case of the lead antimonate pigment to be used in the production of yellow glasses, the addition of an alkali flux to the pigment mixture would not have been beneficial.

The inclusion of excess lead in a pigment mixture, as in the case of the pigment (PG-EG) used to produce "Egyptian type" yellow glass, results in the formation of two cubic lead antimonates ($Pb_2Sb_2O_7$) with different lattice parameters (10.425Å and 10.479Å), as otherwise observed only for pigments containing both NaCl flux and small amounts of iron or zinc. Thus, the inclusion of excess lead also facilitates the formation of cubic lead antimonates.

Similarly, the *anime* produced from a lead-antimony-silica mixture with excess lead does not contain cubic $Pb_2Sb_2O_7$ and instead, the dominant lead antimonate is $Pb_{3+x}Sb_2O_{8+x}$. However, for a mixture with a PbO/Sb_2O_5 ratio of 8, the yellow colour is more intense than that observed in a pigment produced from the pure stoichiometric mixture without the addition of NaCl flux (i.e., **b*** = 34.1 compared to **b*** = 24.8), but when the PbO/Sb_2O_5 ratio is increased to 12, the yellow colour becomes very pale (**b*** = 9.4).

Comparison of the "Egyptian type" yellow glass produced using a pigment containing small amounts of iron and zinc together with excess lead oxide (i.e., PG-EG + RGM-CEG) with that produced using pure stoichiometric pigment (i.e., PG1 + RGM-CEG) in the context of the stability experiments established that the cubic lead antimonate particles and the intensity of the yellow colour survived to a higher temperature in the former case. In principle, this increased stability could be due to the addition of either iron-plus-zinc or excess lead oxide. However, the addition of iron-plus-zinc seems the more likely explanation since "Roman type" yellow glass produced from *anime* containing small amounts of iron and tin (i.e., AN-RG + PGM-CRG) is more stable than that produced in the stability experiments from a pure lead-antimony-silica *anime* (i.e., AN1 + RGM-CRG), both of which contained excess lead oxide.

The replication experiments suggest that "Roman type" yellow glass (AN-RG + CGM-CRG) is less stable than "Egyptian type" yellow glass (PG-EG + CGM-CEG) in that, after firing to 1000ºC, conversion from cubic $Pb_2Sb_2O_7$ to calcium antimonate, $Ca_2Sb_2O_{6.5}$, has started only for the "Roman type" glass. The lower stability of lead antimonate in Roman glass is probably

due to its lower viscosity compared to Egyptian glass, as observed during the replication experiments. The streaks of lead-rich glass containing lead antimonate, commonly seen in Egyptian glass (Figure 2.2a), reflects this relatively high viscosity and the resultant difficulty in mixing in the pigment. The higher lime and magnesia contents of the Egyptian glasses (Table 2.2) are responsible for their increased viscosity compared to the Roman glasses. The diffusion coefficients of the atoms in the glass are inversely dependent on the viscosity (Einstein-Stokes relationship) and therefore, higher viscosity implies a lower mobility which, in turn, will help the stability of the lead antimonate particles in the glass. Because of the high viscosity of Egyptian glass, the addition of a yellow pigment with excess lead was sufficient to obtain a glass with stable lead antimonate particles. In contrast, the addition of the more stable yellow lead-antimoni-silica *anime* was the method chosen by the Roman glass makers to solve this problem. Nevertheless, Roman yellow glass probably still had to be fired at a lower temperature than Egyptian yellow glass in order to avoid partial conversion to calcium antimonate.

Conclusions

The above analyses of New Kingdom Egyptian and Roman yellow glasses have established that, with one exception, the lead antimonate particles responsible for the yellow colour were of the type $Pb_2Sb_2O_7$ with a cubic crystallographic structure. In the majority of the particles, the antimony was partially replaced by iron and zinc in the case of the Egyptian glasses, and by iron and tin in the case of the Roman glass. It seems probably that these impurities were incorporated into the glass through the raw materials and processes used to produce the lead antimonate pigment or *anime* employed for the Egyptian and Roman glasses respectively. As confirmed by the pigment replications, the impurities partially replacing the antimony in the lead antimonate particles resulted in observed lattice parameters in the range 10.44-10.48Å, as compared to a lattice parameter equal to 10.40Å for pure lead antimonate particles.

Replication experiments have established that both New Kingdom Egyptian and Roman yellow glasses could have been produced by stirring, respectively, lead antimonate pigment or *anime*, containing small amounts of iron, zinc or tin oxides together with excess lead oxide, into a molten colourless glass. The replication experiments further confirmed that, in producing both types of glass, the inclusion of small amounts of impurities, such as Fe, Zn and Sn, into the pigment or *anime* was an important factor in enhancing the stability of the lead antimonate

particles. However, although no conversion of yellow lead antimonate to white calcium antimonate had occurred at a firing temperature of 1000ºC in the case of the replicate "Egyptian type" yellow glass, partial conversion had started at this firing temperature in the case of the replicate "Roman type" glass. As discussed above, the lower stability of lead antimonate particles in Roman glass was probably due to its lower viscosity at equivalent temperatures compared to Egyptian glass, and is the reason why the more stable lead-antimony-silica *anime* was the method chosen by the Roman glass makers, rather than lead antimonate pigment which was used by the New Kingdom Egyptian glass makers.

References

Biringuccio, V., 1966. The Pirotechnia of Vannoccio Biringuccio (C.S. Smith, M.T. Gnudi,Trans.). The MIT Press, Cambridge, MA.

Chernykh, E., 1992. Ancient Metallurgy in the USSR. Cambridge University Press, Cambridge.

Dik, J., Hermens, E., Peschar, R., Schenk, H., 2005. Early production recipes for lead antimonate yellow in Italian art. Archaeometry 47, 593-607.

Freestone, I.C., Stapleton, C.P., 2013. Composition, technology, and production of coloured glasses from mosaic vessels of the Early Roman Empire. In: Bayley, J.,

Freestone, I., Jackson, C. (Eds.), Glass of the Roman Empire. Oxbow Books, Oxford (in press).

Lahlil, S., Cotte, M., Biron, I., Szlachetko, J., Menguy, N., Susini, J., 2011. Synthesizing lead antimonate in ancient and modern opaque glasses. Journal of Analytical Atomic Spectrometry 26, 1040-1050.

Lucas, A., Harris, J.R., 1962. Ancient Egyptian Materials and Industries. Edward Arnold, London.

Mass, J.L., Stone, R.E., Wypyski, M.T., 1998. The mineralogical and metallurgical origins of Roman opaque colored glasses. In: Kingery, W.D., McCray, P. (Eds.), The Prehistory and History of Glassmaking Technology, Ceramics and Civilization. American Ceramics Society, Westerville, Ohio, pp. 121-144.

Mass, J.L., Wypyski, M.T., Stone, R.E., 2002. Malkata and Lisht glassmaking technologies: towards a specific link between second millennium BC metallurgists and glassmakers. Archaeometry 44, 67-82.

Moretti, C., Hreglich, S., 1984. Opacification and colouring of glass by the use of "anime". Glass Technology 25, 277-282.

Piccolpasso, C., 2007. The Three Books of the Potter's Art (R. Lightbown, A. Caiger-Smith, Trans.). Editions la revue de la céramique et du verre, Vendin-le-Vieil.

Rehren, Th, 2003. Comments on Mass, J.L., Wypyski, M.T., Stone, R.E., 2002. Malkata and Lisht glassmaking technologies: towards a specific link between second millennium BC metallurgists and glassmakers. Archaeometry 44, 67-82, and reply. Archaeometry 45, 185-190.

Rosi, F., Manuali, V., Miliani, C., Brunetti, B.G., Sgamellotti, A., Grygar, T., Hradil, D., 2009. Raman scattering features of lead pyroantimonate compounds. Part I: XRD and Raman characterization of $Pb_2Sb_2O_7$ doped with tin and zinc. Journal of Raman Spectroscopy 40, 107-111.

Shortland, A.J., 2002a. The use and origin of antimonate colorants in early Egyptian glass. Archaeometry 44, 517-531.

Shortland, A.J., 2002b. An antimony bead from Jerablus Tahtani. Historical Metallurgy 36, 1-6.

Shortland, A.J., Eremin, K., 2006. The analyses of second millennium glass from Egypt and Mesopotamia, Part 1: new WDS analyses. Archaeometry 48, 581-603.

Shortland, A.J., Nicholson, P.T., Jackson, C.M., 2000. Lead isotope analyses of 18th Dynasty Egyptian eyepaints and lead antimonate colorants. Archaeometry 42, 153-159.

Stos-Fertner, Z., Gale, N.H., 1979. Chemical and lead isotope analyses of ancient Egyptian gold, silver and lead. In: Scollar, I. (Ed.), Proceedings of the 18th International Symposium of Archaeometry and Archaeological Prospection, Archaeo-Physica 10. Rheinisches Landesmuseum, Bonn, pp. 299-314.

Tite, M.S., 2009. The production technology of Italian maiolica: a reassessment. Journal of Archaeological Science 36, 2065-2080.

Tite, M., Pradell, T., Shortland, A., 2008. Discovery, production and use of tin-based opacifiers in glasses, enamels and glazes from the Late Iron Age onwards: a reassessment. Archaeometry 50, 67-84.

Turner, W.E.S., Rooksby, H.P., 1959. A Study of Opalising Agents in Ancient Opal Glasses throughout Three Thousand Four Hundred Years. In: Glastechnische Berichte 32K, VII, pp. 17-28.

Wyttenbach, A., Schubiger, P., 1973. Trace element content of Roman lead by neutron activation analyses. Archaeometry 15, 199-207.

Chapter 3

Technology of production of polychrome lustre from Iraq (9th century)

Introduction

Lustre is a metallic-like decoration applied on ceramic glazes. It consists of a thin surface layer (from few hundreds of nanometres up to several microns) of metal nanoparticles of silver and/or copper incorporated in the glaze and with sizes ranging between 2 and 50 nm (Pérez-Arantegui et al, 2001, 2004; Sciau Ph et al, 2009). The production process comprises first ion exchange between the Ag^+ and/or Cu^+ ions from an initial mixture applied on the glaze surface, which is fully removed after firing, and the Na^+ and K^+ ions from the glaze, followed by reduction of Ag^+ to Ag^0 and Cu^+ to Cu^0 and finally, nucleation and growth of metallic copper/silver nanoparticles (Pradell et al, 2005). The lustre optical properties (colour and metallic-like shine) can be varied by modifying the composition of the initial mixture and/or the glaze. In particular, the addition of PbO in the glaze formulation is known to reduce the diffusivity of Cu^+ and Ag^+ ions and consequently produce more concentrated lustre layers, closer to the glaze surface, and also, to favour the growth of the metallic copper nanoparticles (Molera et al, 2007; Pradell et al, 2007, 2012; Gutiérrez et al, 2010). Moreover, additions of Sn^{2+} and/or

Fe^{2+} to the glaze are also known to help the reduction not only of the silver but also of the copper ions to the metallic state (Barber et al, 2009).

The earliest lustreware was produced in Iraq (Bashra) in the 9th century during the Abbasid caliphate (Caiger, 1991). It is characterized by the use of several colours on the same piece (polychrome lustre) while later productions are mainly monochrome (Sarre et al, 1925; Mason et al, 1991; Bobin et al, 2003; Mason, 2004; Polvorinos et al, 2008). There are several combinations of colours and shines. The shines which are indicated in brackets are golden or silvery for silver-based lustres and coppery for copper-based lustres. The most common combinations are brown, with bluish iridescences resulting from scattering by large single silver nanoparticles, and ochre; brown, again with bluish iridescences, ochre and green (golden); red (coppery) and yellow (golden); red (sometimes coppery) and black and red (coppery) and white (silvery)**.** Polychrome red (coppery) and yellow (golden) was not produced again until the last decades of the 15th century and during the 16th century in Deruta and Gubbio (Italy) (Padovani et al, 2003, 2004; Padeletti et al, 2004, 2010; Bontempi et al, 2006)

Those lustre decorations combining brown, ochre and green have already been studied (Pradell et al, 2008). They were produced under relatively light reducing conditions using an initial mixture applied on the glaze surface containing both copper and silver in various amounts. The green colour was obtained by adding silver while copper is either absent or present in very small amounts; the ochre, by adding both copper and silver in similar amounts; and the brown also by adding both but with silver in higher amounts than copper. The addition of copper helps the reduction of the silver ions to metal together with the precipitation and growth of silver nanoparticles while, conversely, copper is oxidized appearing as Cu^{+} and also Cu^{2+} in larger or smaller amounts depending on the silver/copper ratio. Consequently, green lustres are formed exclusively by silver nanoparticles; ochre lustres contain copper mainly as Cu^{+} and cuprite and metallic silver nanoparticles; and brown lustres contain mainly metallic silver nanoparticles, Cu^{2+} and in lower amounts Cu^{+} and cuprite nanoparticles. The different colours were applied on separate areas of the glaze surface, and in all cases, fired under light reducing conditions. Consequently, all the color decorations could be applied at the same time. They are characterized by the presence of metallic silver nanoparticles and the absence of metallic copper nanoparticles, and so we usually call them silver lustres.

On the contrary red lustres (copper lustres) are characterized by the presence of metallic copper and cuprite nanoparticles and also Cu^{+} in variable amounts, although some small amounts

of silver nanoparticles may also be present (Molera et al, 2007). A stronger reducing environment is required to reduce copper to the metallic state. Consequently, the combination of silver lustres and copper lustres in the same decoration creates some difficulties, and specific methods of production are required. The three types of Abbasid lustreware combining both copper and silver lustre are studied with the object of determining the materials and method followed in their production. Although the three of them are very beautiful, it is quite obvious than these combining red (coppery) and yellow (golden) decorations is most probably the one sought. Therefore, we investigate the specific method of production followed to succeed obtaining this combination. Finally, the reasons for the different colours and shines observed are also studied and related to the specific nanostructures (type, size and distribution of the nanoparticles) of the lustre decorations.

The chemical and microstructural composition of the glazes and of the lustre layers is obtained by combination of Scanning Electron Microscopy with an Energy-Dispersive X-ray Spectroscope attached (SEM-EDS), Focused Ion Beam (FIB), micro X-Ray Diffraction (μ-XRD), Rutherford Backscattering Spectroscopy (RBS) and Ultraviolet and Visible spectroscopy (UV-Vis).

FIB was used to produce polished cross sections of the lustre layers, and subsequently, secondary electrons (SEM) images of the nanostructure were obtained (Sciau et al, 2009); SEM-EDS was used to analyse both the glaze cross sections and the lustre surfaces. RBS was used to determine the cross section composition profiles of the lustre layers. μ-XRD and UV-Vis were performed in order to determine the nature of the metallic nanoparticles in the lustre layers. The colour coordinates of the decorations were also obtained from the reflectance UV-Vis spectra. Finally, the relationship between colour and shine of the lustre decorations and the chemistry and nanostructure observed is then discussed.

Materials and techniques

Figure 2.1 shows the three samples characteristic of the polychrome 9th century Iraqi lustreware production combining copper and silver lustres that were selected for study. P624 and P717 belong to the Ashmolean Museum (Oxford) and IV163 to the Instituto Valencia Don Juan (Madrid). Sample P624 combines red and black decorations, P717 red, red-coppery and white-silvery, and IV163 red, red-coppery and yellow-golden with some green-golden spots.

Figure 3.1. Polychrome lustre samples studied from 9th century AD Iraq. Left: front side and right: rear side.

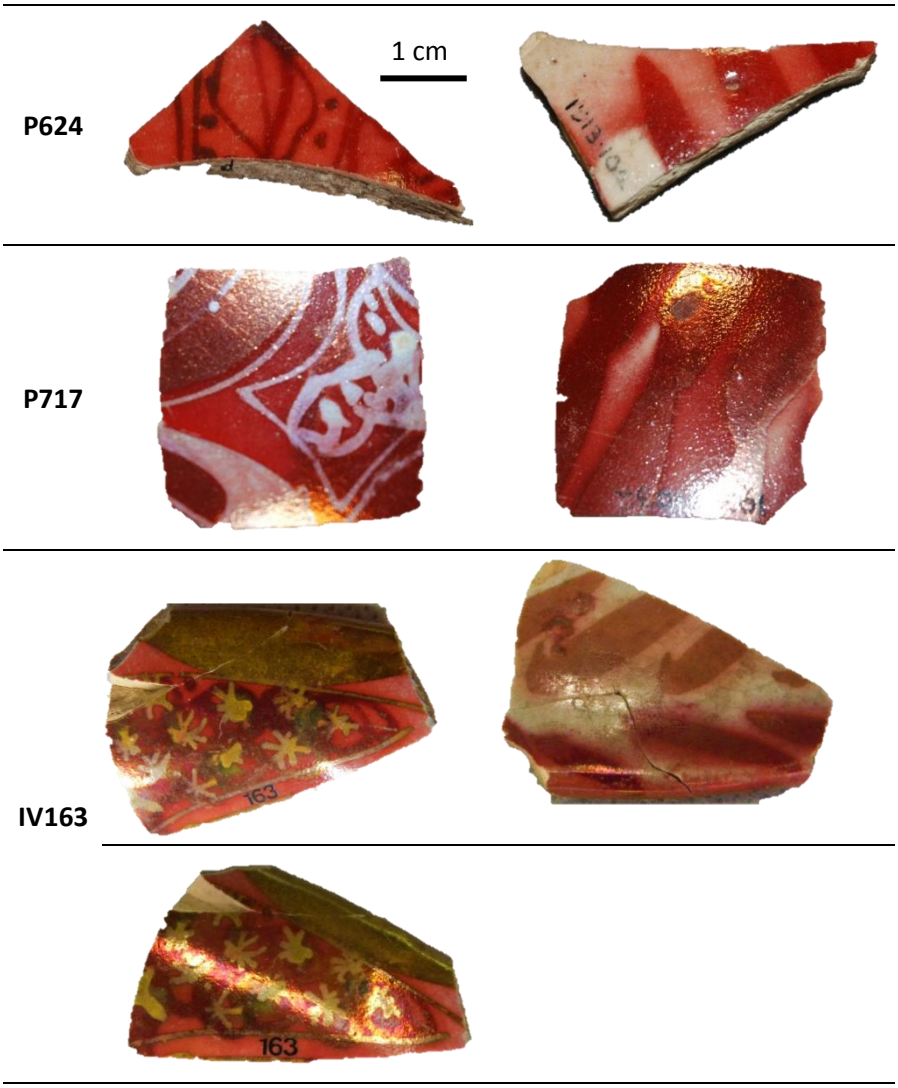

A crossbeam workstation (Zeiss Neon 40) equipped with SEM (Shottky FE) and Ga + FIB columns, was used to prepare cross sections of the lustre layers. First, the sample surface was coated with a thin protective Pt layer (1µm) by ion-beam-assisted deposition; then the cross section was cut and polished and a thin layer of Pt deposited to enhance conductivity. SEM images of the polished cross sections of the lustre layers were obtained at 5 kV and in some cases at 2 kV to minimize the penetration of the electron beam. The compositions of ceramic pastes and glazes were obtained from polished cross sections by SEM-EDS (INCAPentaFETx3 detector, 30mm^2, ATW2 window) operated at 20kV, with 120 s measuring times, and at x50 and x500 on representative areas of paste and glaze respectively; the data are an average of at least 2 measurements. The average lustre composition was obtained by SEM-EDS directly on the surface at 20kV, point and area measurements at x500 being obtained. Finally, Backscattered

Electron (BSE) images were obtained in order to study the microstructures of cross sections of the glazes.

RBS measurements were performed on the 5 MV tandem accelerator (Climent-Font et al, 2004). A 3070keV energy He-beam with square-section (1 mm in diagonal) was used, thus taking advantage of the elastic resonance $^{16}O(\alpha,\alpha)^{16}O$ occurring at this energy and increasing the sensitivity to oxygen concentration by a factor of 23 (Cheng et al, 1993). The samples were kept in vacuum. A careful quantification was performed by employing the simulation code SIMNRA (Mayer, 1997). RBS data was fitted starting from the average chemical compositions obtained from Microprobe analyses of the layers and following a procedure described elsewhere (Pradell et al, 2007; Gutierrez et al, 2010). To determine the lustre cross section chemical profiles, a sequence of layers with varying silver and/or copper content was modelled. The thickness of each layer is given in units of areal densities, which can be converted into absolute thicknesses provided that the mean density of the layer is known. The mean density of the lustre layer was estimated by linear interpolation from the metal nanoparticle and glaze fractions taking 10.49 g/cm^3 for metallic silver, 8.89 g/cm^3 for metallic copper and, for the glaze, the density calculated from the RBS fittings after Fluegel (Fluegel, 2006).

μ-XRD measurements were performed on beamline BM16 of the European Synchrotron Radiation Facility (ESRF) in Grenoble. The measurements were performed in transmission geometry applying a narrow beam (50 x 50 μm) with 15 keV energy (λ=0.83 Å) on thin (about 100 μm) slices cut out of different areas of the lustre layers as described elsewhere (Pradell et al, 2013).

UV-Vis diffuse reflectance (R) measurements were performed directly on the surface of the samples using a double beam UV-Vis spectrophotometer (Shimadzu 2700) equipped with ISR 3100 Ulbricht integrating sphere. The spot size was a slit of 5 mm x 1 mm, and measurements were made between 200 nm and 800 nm at 1 nm resolution. A D65 standard illumination source was used and barium sulphate provided a white standard. The colour coordinates were determined following the International Commission for Illumination (CIE) recommendation.

Results

The chemical compositions of the ceramic pastes are shown in Table 3.1 and correspond in all the cases to the use of a calcareous paste characteristic of this production. It is well known that the composition of the unseen or undecorated glaze surface is often different from the decorated side, and consequently, the glazes from both sides of the samples were analysed with the exception of IV163 from which only the front side was available. The chemical compositions of the ceramic glazes are shown in Table 3.2.

Table 3.1. Analyses of the ceramic pastes in wt%.

sample	luster color	Na_2O	K_2O	Al_2O_3	SiO_2	CaO	MgO	FeO	TiO_2
P624	red/black	2.4 (0.2)	1.4 (0.1)	14.7 (0.1)	43.3 (0.2)	22.6 (0.2)	7.6 (0.2)	7.1 (0.2)	0.25 (0.06)
P717	red/coppery/silvery	2.3 (0.02)	1.2 (0.01)	14.0 (0.2)	42.2 (0.6)	23.8 (0.7)	8.3 (0.2)	7.3 (0.2)	0.35 (0.06)
IV163	red/yellow golden	0.9 (0.04)	1.5 (0.12)	11.2 (1.2)	47.9 (2.3)	20.2 (1.2)	5.8 (0.7)	7.3 (0.01)	0.75 (0.06)

Table 3.2. Analyses of the glazes in wt%.

sample	Glaze side	Na_2O	K_2O	Al_2O_3	SiO_2	CaO	MgO	MnO_2	FeO	SnO_2	PbO
P624	front	7.0 (0.5)	5.0 (0.5)	1.6 (0.3)	75.4 (0.5)	6.3 (1.1)	4.2 (0.7)	0.1 (0.1)	0.5 (0.1)	b.d.	b.d.
	rear	8.0 (0.3)	5.5 (0.1)	2.7 (0.3)	71.3 (1.9)	6.9 (0.8)	4.4 (0.6)	0.1 (0.1)	1.5 (0.7)	b.d.	b.d.
P717	front	8.1 (0.1)	5.0 (0.2)	2.8 (0.2)	61.5 (0.8)	7.5 (0.4)	4.5 (0.2)	0.7 (0.1)	0.8 (0.1)	3.3 (0.7)	5.6 (0.7)
	rear	8.1 (0.2)	5.5 (0.3)	3.2 (0.3)	65.7 (0.9)	9.1 (0.1)	5.5 (0.2)	0.6 (0.1)	1.5 (0.7)	b.d.	b.d.
IV163	front	2.7 (0.1)	4.5 (0.1)	1.8 (0.3)	59.3 (1.2)	5.0 (0.5)	2.1 (0.3)	0.5 (0.2)	1.4 (0.1)	9.4 (0.8)	13.3 (1.1)

The glazes show also the chemistry characteristic of this production; that is, a variable lead and tin content from below detection limits to about 15% PbO and 9%SnO_2 respectively, and between 2 and 5 % MgO together with the presence of small amount of MnO (0.5%) (Bobin et al, 2003; Mason, 2004; Polvorinos et al, 2008; Pradell et al, 2008).

Figure 3.2. SEM backscattering images of cross sections of (A) front glaze and (B) (C) magnifications at the surface from sample P717 where the bright thin layer contains lead and tin.(D) rear glaze from sample P717.

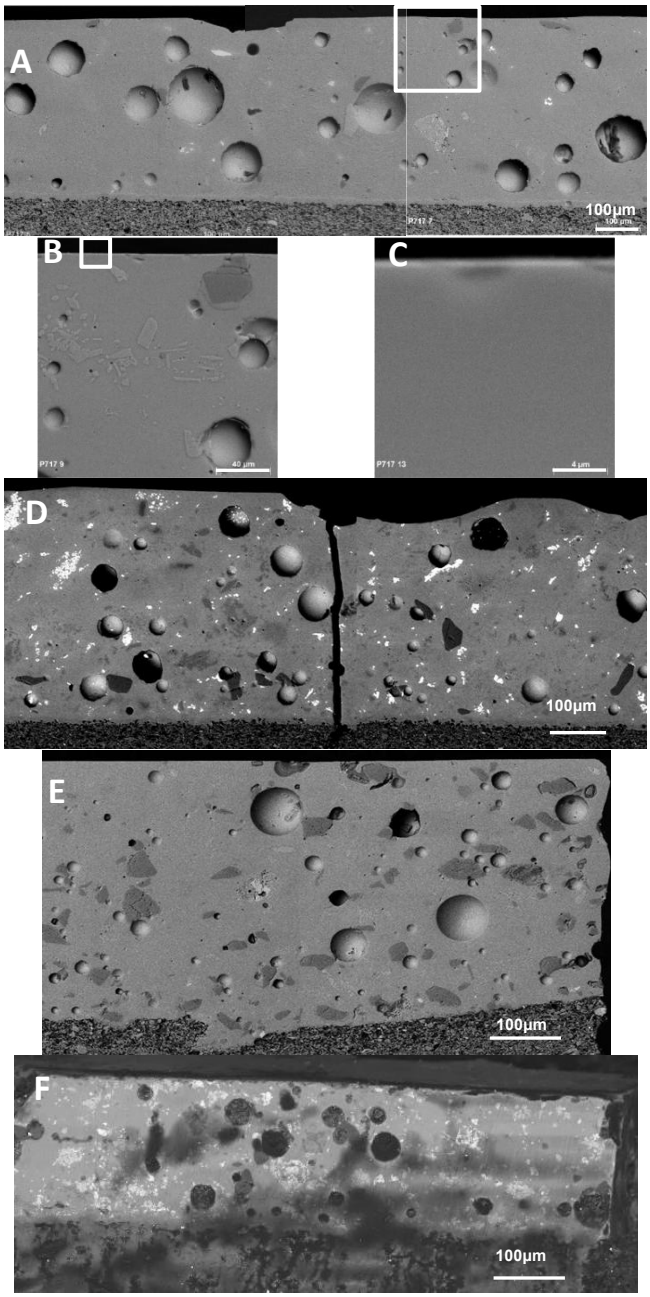

BSE images of cross sections of the glazes are shown in Figure 3.2. The glazes from this production are characterized by a variable thickness and the presence of large numbers of bubbles and small crystallites. Using a combination of EDS analyses and micro-XRD, rounded grains of unreacted quartz, skeletons of the original cassiterite (SnO_2) particles, recrystallized cristobalite crystallites, diopsides ($(Ca,Mg)Si_2O_7$) and nepheline were identified in the glaze section while wollastonite and aluminium rich pyroxenes were found to be concentrated near to the glaze-ceramic interphase as a result of the glaze-ceramic paste reaction during firing (Bobin

et al, 2003; Pradell et al, 2008). Moreover, the glaze surface of the rear lustre decorated glaze from P717 appears enriched in lead and tin, 1.4%PbO and 0.60%SnO_2, Figure 3.2B and Figure 3.2C, and these components could only be incorporated on the glaze surface together with the lustre decorations.

The average compositions of the lustre layers were also measured directly on the glazes surface and are given in Table 3.3 for the different lustre colours and decorations. Although the penetration depth of the SEM beam is larger (2-3 μm) than the typical thickness of the lustre layer (approximately equal to or less than 1μm), the relative ratios between the different specific lustre compounds are essentially correct. The red and red coppery decorations are in all the cases copper rich, above 85 wt% Cu/(Cu+Ag). In contrast, the yellow and green golden decorations are silver rich, below 15 wt% Cu/(Cu+Ag). However, the black and the white-silvery decorations are silver richer than the red decorations but silver poorer than the yellow and green golden decorations, 44 and 63 wt% Cu/(Cu+Ag) respectively. Another interesting result is that although the rear glaze of P717 and both glazes of P624 are lead and tin free, the lustre layers show the presence of small amounts of lead and/or tin. Both lead and tin are present only on the lustre decorated surfaces and are absent from the undecorated glaze surfaces. Consequently, lead and tin must have been incorporated together with the lustre decoration, and therefore, should have been present in the initial lustre mixture.

15μm x15μm cross sections of the different colour decorated areas were also examined by FIB. The corresponding inverse contrast images (5kV or 2kV for the lead free glazes) for the red decoration of P624-r and the black decoration of P624-f are shown in Figure 3, for the white silvery decoration of P717-f in Figure 4, for the red and red-coppery decorations of P717-r in Figure 3.5, and for the red-coppery, green-golden and yellow-golden decorations of IV-163-f in Figure 3.6.

RBS analyses of some of the larger lustre areas (P717-r, P624) was also undertaken, and the corresponding silver and copper cross section profiles were thus obtained, and are also shown in Figure 3.3 and Figure 3.5. Table 3.4 summarizes some average values estimated from these analyses; that is, copper and silver (wt%Cu/(Cu+Ag)), content thickness of the lustre layer and depth at which the lustre layer has the maximum metal content, and the maximum concentration and the maximum volume fraction of silver and copper in the lustre layer. Finally, for the cases where the chemical cross section profiles could not be obtained by RBS, some qualitative SEM-

EDS chemical analyses are also shown, that is, for the white silvery area of P717-f in Figure 3.4 and for the green and yellow decorations of IV163 in Figure 3.6.

Table 3.3. SEM-EDS analyses of the lustre decorations in wt%.

sample	glaze side	luster		SnO_2	PbO	Cu	Ag	Cu/(Cu+Ag)
		color	shine					
P624	rear	red	no	0.5	0.3	3.7 (0.7)	0.9 (0.4)	90 (7)
	front	black	no	b.d.	0.2	2.7 (0.4)	2.3 (0.8)	44 (8)
		red	no	b.d.	0.6	2.9 (0.2)	0.5 (0.1)	83 (5)
P717	front	red	coppery	1.4 (0.4)	3.0 (0.3)	6.4 (0.7)	0.7 (0.2)	91 (2)
		white	silvery	1.5 (0.3)	2.8 (0.2)	5.4 (0.6)	3.1 (0.6)	63 (5)
	rear	red	no	0.7 (0.4)	0.7 (0.1)	2.9 (0.2)	0.2 (0.1)	94 (3)
		red	coppery	0.4 (0.3)	1.0 (0.7)	5.3 (2.0)	0.4 (0.2)	93 (3)
IV163	front	red	no	3.3	10.4	3.7	0.5	89
		red	coppery	2.8 (0.1)	10.5 (0.1)	6.5 (0.2)	1.2 (0.1)	84 (1)
		Yellow decoration	golden	2.5 (0.6)	10.7 (0.2)	0.9 (0.1)	6.3 (1.5)	12 (2)
		Yellow edge	golden	2.4 (1.1)	9.4 (0.1)	0.6 (0.2)	6.7 (1.1)	8 (1)
		green	golden	2.7 (0.7)	10.6 (0.1)	1.2 (0.2)	7.3 (0.6)	15 (2)

From the FIB cross section images shown in Figure 3.3, it is seen that the layers associated with the red lustre from P624-r and of the black and red lustre from P624-f are formed by small copper particles with typical sizes varying between 12 nm and 20 nm. The two layers have a total thickness of 1100 nm and 1350 nm respectively and a top particle-free surface layer of about 110 nm, thicknesses that are in good agreement with the RBS copper and silver cross section profiles also shown in Figure 3.3. Silver appears in small amounts and mixed in the layer with the copper. However, in this case it should be noted that the size of the RBS probe was far larger than the black decoration, and therefore, the profile corresponds to the average of a larger area including red and black.

Table 3.4. RBS analyses of the lustre decorations.

sample	glaze side	luster		composition			thickness	maximum concentration		
		color	shine	wt%Cu	wt%Ag	Cu/(Cu+Ag)	(nm)	position (nm)	at%(Cu+Ag)	Vol.Frac.(%)
P624	rear	red	no	3.5	0.3	91	1911	244	5.6	3.1
	front	red&black	no	3.1	0.3	91	1042	216	7.7	6.2
P717	rear	red	no	6.2	0.2	97	600	299	5.3	4.3

Figure 3.3. SEM images of cross-sections through the red lustre of P624-r and black and red lustre of P624-f (to left) together with corresponding silver and copper composition obtained by RBS analyses (to right).

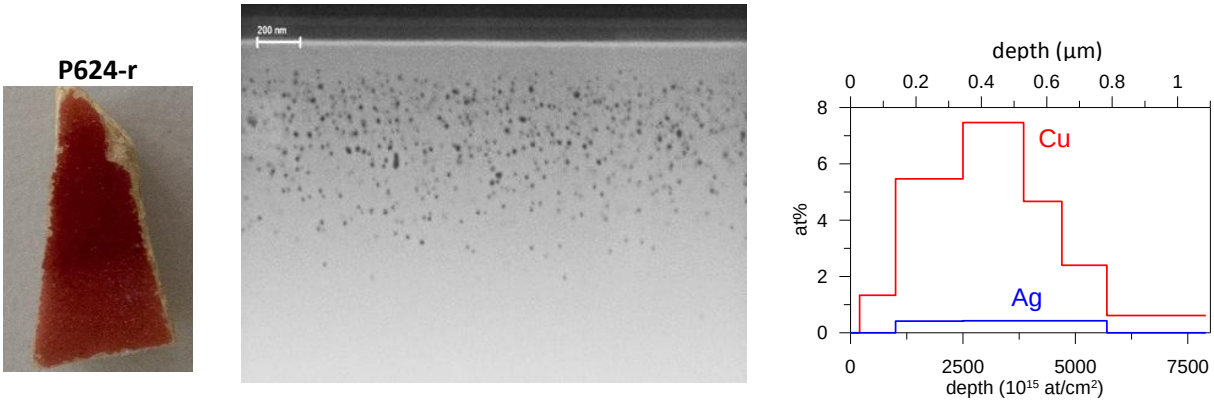

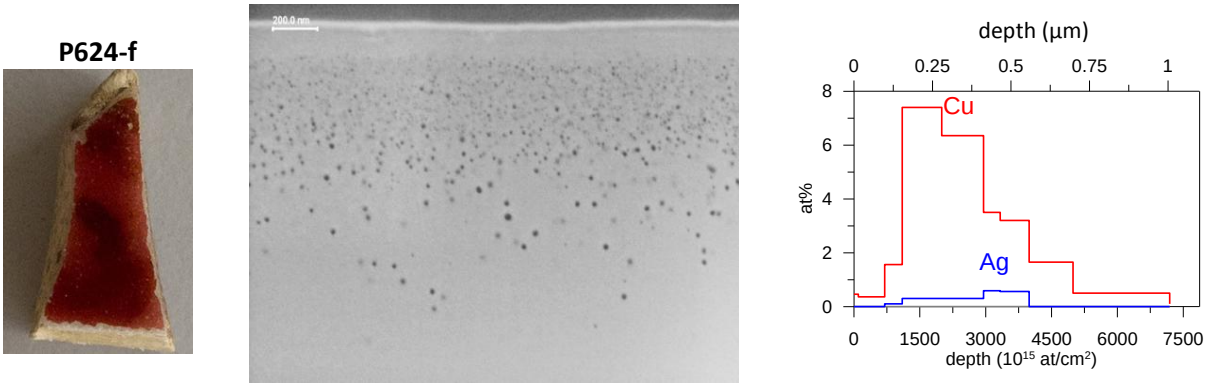

Figure 3.4 SEM Image of uneven glaze surface of P717-f (top). SEM image of cross-section through the white-silvery lustre layer from P717-f (bottom to left) together with EDS analyses for a selection of the particles (bottom to right).

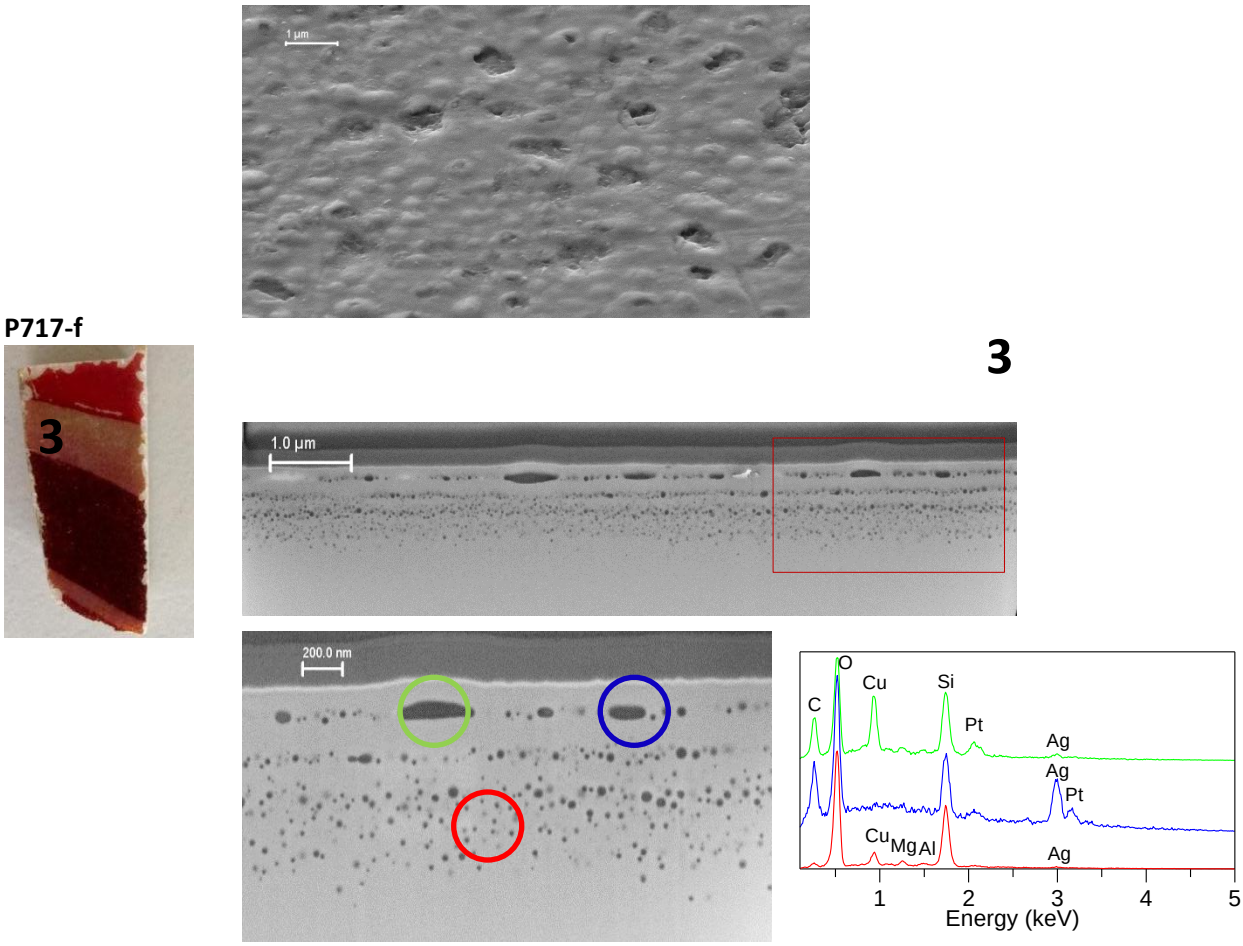

From the FIB cross section images shown in Figure 3.4, it is seen that the white-silvery lustre layer from P717-f appears to be formed by a succession of thin layers of nanoparticles leading to a total thickness of about 1000 nm with a top particle free surface layer of about 110 nm. The inner layer contains small copper particles of typical sizes ranging from 20 nm to 30 nm. The more superficial layer shows the coalescence of the particles into larger non-spherical particles (200-250 nm size) which are responsible for the deformation and unevenness of the glaze surface shown on the top image of Figure 3.4. EDS analyses of those large particles show variable composition from silver-rich to copper-rich particles, and also copper and silver particles grow until they impinge and form aggregates such as those shown on the bottom image of Figure 3.4.

Figure 3.5 SEM images of cross-sections through the red (1) and red-coppery (2) lustre layers from sample P717-r (to left) together with copper and silver composition from (1), as determined by RBS (to right).

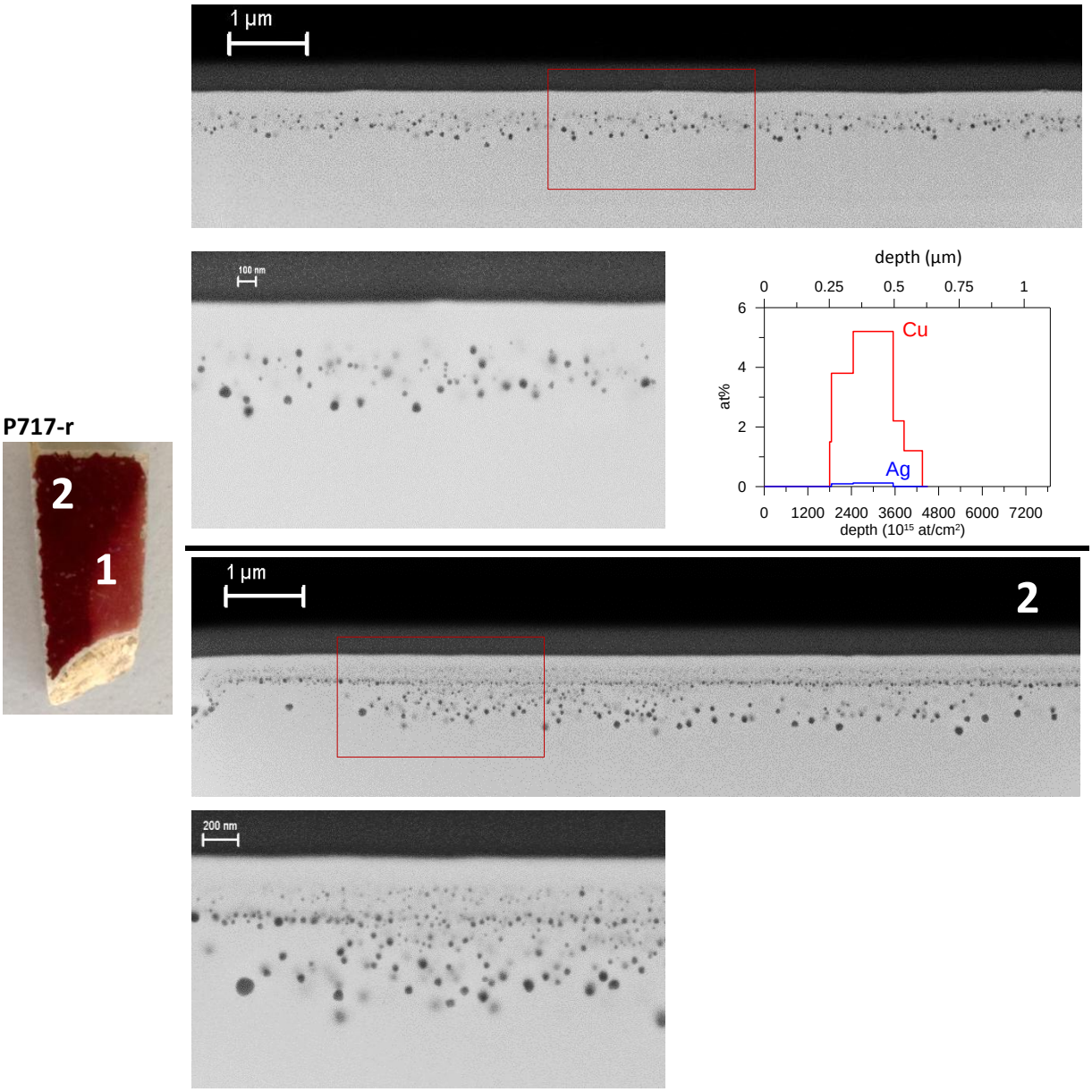

From the FIB cross section images, it is seen that the red lustre layer has a total thickness of about 650 nm and a top particle free surface layer of about 220 nm (Figure 3.5(1)), and that the red-coppery layer has a total thickness of about 1000 nm and a top particle free surface layer of about 150 nm (Figure 3.5(2)). The lustre layers are formed mainly by copper nanoparticles of sizes ranging between 20 nm and 30 nm for the small particles and between 70 nm and 100 nm for the larger particles. The copper and silver cross section profiles from the red area obtained by

RBS agree with the above data, and also show that silver is present in very small amounts and mixed with the copper across all the layers.

Figure 3.6 SEM images of cross-sections through the red-coppery (1), green-golden (2) and yellow-golden (3) lustre layers of IV-163-f (to left) together with EDS analyses of selected areas (to right).

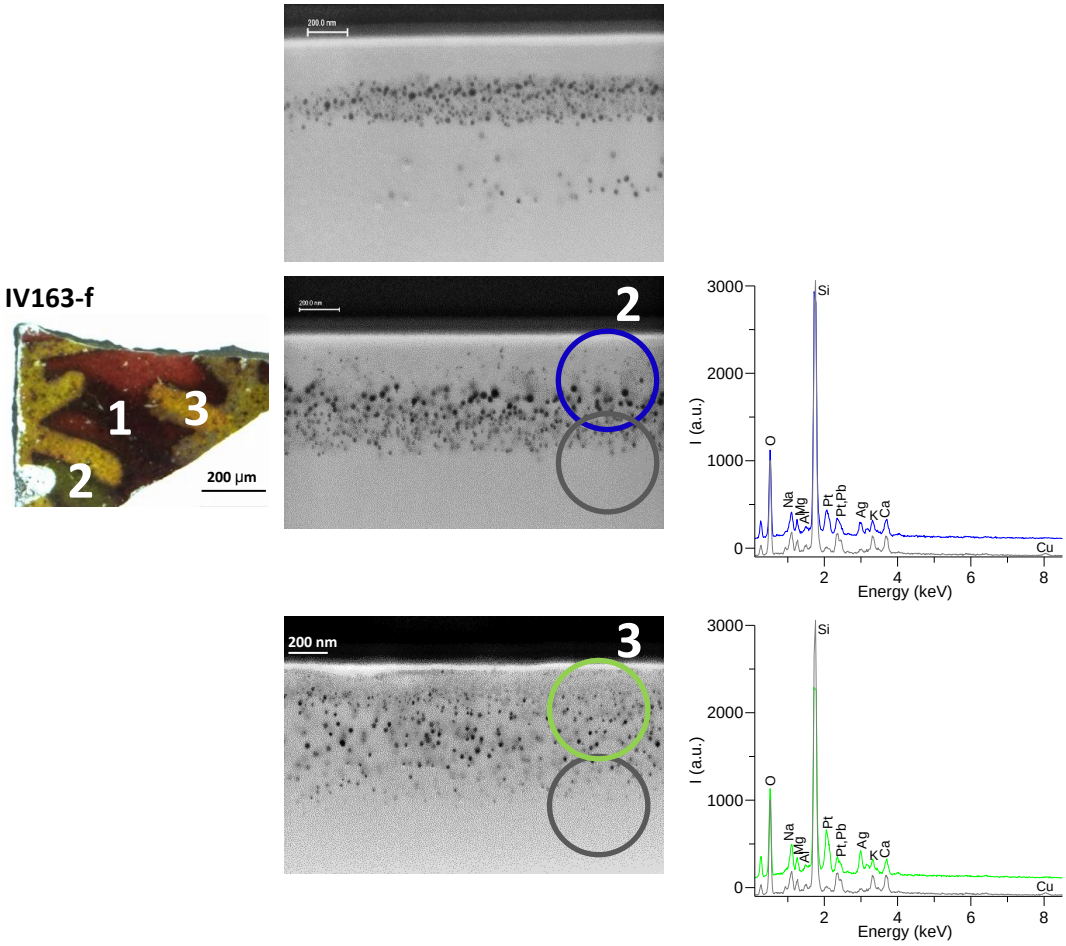

Finally, from the FIB cross section images shown in Figure 3.6, it is seen that the red-coppery, green-golden and yellow-golden lustre layers from IV-163-f all have the same total thickness of about 600 nm. However, the red lustre has a 200 nm particle-free surface layer (Figure 3.6(1)) which is occupied by the silver nanoparticles in the green and in the yellow lustres (Figures 3.6(2) and 3.6(3) respectively). Further, the red lustre layer is formed nearly exclusively from copper nanoparticles while the green and the yellow golden lustres contain both silver and copper nanoparticles. However, in contrast to P624 and P717, silver nanoparticles appear concentrated on the surface layer while copper nanoparticles occupy the inner layer. In particular, the yellow-golden lustre is formed by a first surface layer made of very small (from 2 nm to 10 nm) silver nanoparticles and an inner layer mainly formed by copper nanoparticles (size varying between 10 nm and 20 nm); in the intermediate area a few larger silver

nanoparticles (20 nm) are also formed. For the green-golden lustre, the surface silver rich layer is less concentrated and the intermediate layer contains larger silver nanoparticles (30 nm) than for the yellow-golden lustre.

UV-Vis spectroscopy was also performed to identify the metallic nanoparticles present in the lustre layers. It is well known that the colour of the lustre layers is related to the localized absorption and scattering (Surface Plasmon Resonance, SPR) of the visible light by the metal colloids, and is dependent on their size, shape and concentration (van de Hulst, 1981; Kreibig et al, 1995). Spherical silver nanoparticles absorb and scatter strongly in the blue region of the spectra (around 400-450 nm) but are essentially transparent to the rest of the wavelengths in the visible, and this causes the typical greenish-yellow colour of silver colloidal solutions and the bluish scattering. Larger sizes tend to red shift the Surface Plasmon Resonance, and thus, the colour of the colloids. The SPR absorption band (at 560nm) and electronic inter-band transitions absorbing at shorter wavelengths for copper nanoparticles confer red hues to copper colloidal solutions. The presence of cuprite (Cu_2O) nanoparticles (absorption at about 520 nm) and of Cu^{2+} ions (broad absorption band between 600nm and 1000 nm) dissolved in the glass modifies also the colour shown by the lustre layers. Figure 3.7 shows the Optical Density spectra (OD = log(1/R)) which correspond roughly to the absorbance for small silver and copper nanoparticles for which scattering is negligible compared to absorption. The presence of Cu^o nanoparticles is observed in all the cases (red hue). Ag^o nanoparticles are observed in the white silvery lustre from P717-f and in the Reflectance measured over the whole front surface from IV-163-f. The broader Cu^o SPR peak of P624 compared to P717 indicates the presence of smaller nanoparticles in the former. The broad Ag^o peaks (at 400-450nm) observed for the white-silvery lustre of P717F (Figure 3.7) are related to the large heterogeneity of sizes, non-sphericity and to multi-scattering effects.

The colour coordinates have also been calculated from the diffuse reflectance data using the protocol accepted by the International Commission for Illumination (a*, b*, L* (CIE Lab* 1976)), and are shown also in Figure 3.7 and in Table 3.5. The reds have a hue (h*) varying between 21 and 27 (corresponding to a colour varying between red and deep red) and large saturation (c*) varying between 9 and 20. The white-silvery lustre has h*= 54 (corresponding to orange) but it has a large saturation c*=34 and luminosity L*=47.

Figure 3.7 Optical density OD=log(1/R) (top), together with colour coordinates of the different lustre decorations (bottom).

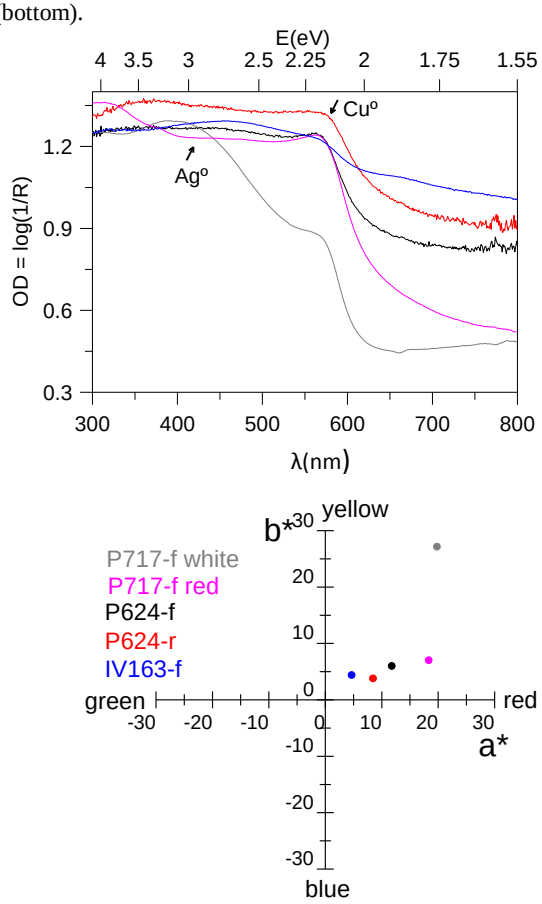

Finally, the whole surface of IV163-f has also been measured and the average colour is yellow-orange (h*=59).

Micro-XRD analyses of the lustre layer were also obtained for some of the cross sections of the lustre decorations. The presence of large metallic copper nanoparticles in P717-r has already been reported elsewhere but cuprite was not found in good agreement with the UV-Vis diffuse reflectance data[27]. Metallic copper nanoparticles of smaller sizes were also identified in P624, but in none of the cases studied was cuprite found.

Discussion

Both the calcareous nature of the ceramic pastes, and the variable lead and tin contents and microstructure of the glazes are characteristic of the 9th century Abbasid lustre production. Taking into account that the addition of PbO to the glaze is known to reduce the diffusivity of copper and silver in the glaze and that the addition of tin also favours their reduction to the metallic state, the absence of lead and tin is believed to make it difficult to produce a shiny lustre in the case of P624. However, we have determined

Table 3.5. Colour coordinates.

sample	glaze side	luster		x	y	Y	L*	a*	b*	c*	h*
		color	shine								
P624	rear	red& black	no	0.3580	0.3327	0.056	28.5	8.1	4.0	9.0	26.0
	front	red	no	0.3756	0.3346	0.069	31.5	11.7	6.0	13.2	27.2
P717	front	red	coppery	0.3980	0.3271	0.077	33.3	18.3	7.0	19.6	21.1
		white	silvery	0.4455	0.3800	0.160	47.0	19.7	27.2	33.6	54.0
IV163	front	red& yellow	coppery& golden	0.3194	0.3330	0.050	27.9	0.7	1.1	1.3	59.1

their presence in the initial lustre mixture used to produce the copper lustre in the lead and tin free glazes, thus helping the reduction of copper to the metallic state, and the growth of metallic copper crystallites, and thus, the development of the copper lustre.

The diffusivity of copper in the glaze is greater than that of silver, resulting in the spread of the red color at the edges of the decorations, and also the formation of deeper copper lustre layers. Copper rich edges are common in silver lustres.

The use of a copper rich initial mixture is demonstrated in the production of the copper lustre. Moreover, the presence of metallic copper nanoparticles and the absence of cuprite nanoparticles indicate also the use of a strong reducing atmosphere for the copper lustre studied here. Nonetheless, the large size and also the coalescence of the metallic particles observed in P717 indicate the use of a stronger reducing atmosphere in this case than in the other samples for which the nanoparticles are smaller.

To obtain the black, white-silvery and yellow-golden decorations, a silver rich initial mixture is used in all the cases, but with different success. In the silver rich "black" decoration of P624, the silver nanoparticles are completely mixed with the copper nanoparticles, and they do not appear concentrated enough to produce a shiny lustre. In contrast, in the silver rich white-silvery decoration of P717, silver appears mainly concentrated near the surface forming very large non-spherical particles that result from the coalescence of smaller silver particles and also with copper particles. The use of a silver rich initial mixture, together with a very strong reducing firing, is responsible for the resulting layered coarse nanostructure.

The large particles and high concentration of silver and copper are responsible for the silvery shine associated with sample P717f. However, the colour of the layer determined from the diffuse reflectance is yellow-orange due to the combination of the red hue due to the presence of copper nanoparticles and also to the broad SPR peak associated to the very large non-spherical silver and silver-copper particles.

IV163 shows clearly the presence of two succeeding layers, the inner one consisting basically of copper nanoparticles and the more superficial one consisting of extremely small silver nanoparticles (between 5 nm and 10 nm in size) which appears yellow. The presence of small silver nanoparticles with typical sizes varying between 10 and 30 nm usually gives a green hue. However, intrinsic size effects happening in very small particles (particles below 20 nm), modify the values of the dielectric functions producing a blue shift and broadening of the SPR

absorption peak (van de Hulst, 1981; Kreibig et al, 1995). Moreover, retardation effects happening in nanoparticles larger than 20 nm are also known to produce a red shift and broadening of the SPR peak. Consequently, the colour is more yellow as a result both of decreasing the size below 20 nm and of increasing the size above 20 nm. Figure 3.8 shows the calculated colour obtained as a function of the size of the silver nanoparticles.

Figure 3.8. Calculated colour coordinates of a suspension of silver nanoparticles in a glass matrix with index of refraction n_g=1.60 as a function of the size of the nanoparticles taking into account the intrinsic size effects and high order terms on the optical response.

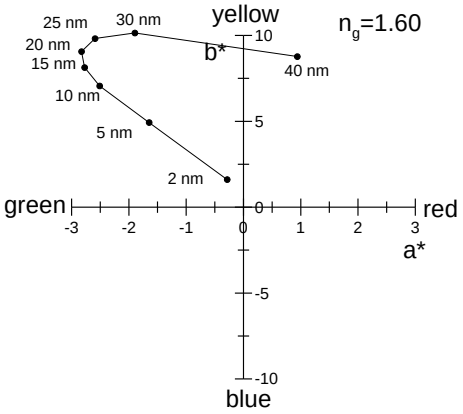

The calculation of the extinction cross section is made using Mie expansion series for silver nanoparticles of variable sizes using the dielectric constants of bulk silver (Johnson, 1975) corrected for the small sizes, in a glass matrix with index of refraction n_g=1.60 (typical of containing lead glazes (Priven et al, 2003) and neglecting multiscattering effects. As a consequence, lustre layers made of silver nanoparticles with sizes between 2 and 5 nm show a yellow colour but with lower saturation (ie smaller b*) similar~~ly~~ to those shown by silver nanoparticles with sizes larger than 25 nm, while silver nanoparticles of sizes ranging between 10 and 25 nm appear greener. Consequently, in the case of IV163, the yellow colour of the golden silver lustre layer is due to the presence of silver nanoparticles smaller than 10 nm, and only in the few areas where silver nanoparticles are larger (ie between 20 nm and 30 nm), is the colour of the lustre green. The silver nanoparticles touching the layer of copper nanoparticles layer from below are larger, because copper helps the reduction and growth of the silver nanoparticles. However, generally they are not larger than 10 nm and only in the green areas, the particles have grown larger.

The presence of extremely small metallic silver nanoparticles in IV163 indicates the use of very light reducing conditions during the production of the silver lustre. In contrast, the presence of metallic copper nanoparticles in the copper lustre indicates the use of a stronger reducing firing. This is only possible if each lustre colour was applied and fired separately, first the copper lustre and afterwards the silver lustre. The presence of lead and tin in the glaze would also have helped the formation of thin, superficial and concentrated lustre layers preventing a mix up of the copper and silver layers and thus, favouring formation of the metallic shine. Copper is known to enhance the reduction of silver and oxidation of copper but also the

formation of silver particles of variable size, heterogeneously distributed in the layer which, as a result, appears brown or white-silvery if the particles coalesce.

Conclusions

The different colours of the silver lustres observed in the Polychrome lustre ware, (black, white, yellow, green) is associated, on the one hand, with the different size of the silver nanoparticles present (ie larger than 100 nm for the white, below 10 nm for the yellow, and about 20 nm for the black and for the green), and on the other hand to their distribution in the lustre layer (ie mixed with the copper nanoparticles in black and white, and in a separate layer in yellow and green).

In particular the polychrome lustre combining red-coppery and yellow-golden decorations in the same object, was successfully developed by:

(1) the application of the lustre decoration over a lead and tin containing glaze, and

(2) the application, first, of a red copper rich lustre mixture which was fired under a strong reducing atmosphere followed by the application of a silver rich lustre mixture fired under a weak reducing atmosphere.

However, objects combining either black and red or white-silvery and red-coppery lustres were also obtained when the procedures or materials used were not optimal. White-silvery silver lustres were obtained on low lead and tin containing glazes under very high reducing conditions and/or high firing temperature and probably submitted to several firings. Red copper and black silver without metallic shine were obtained over lead and tin free glazes.

It has been demonstrated that the Abbasid Iraq potters added lead and tin in the initial lustre mixture. Although adding lead and tin in the initial mixture would certainly help the reduction of silver and copper to the metallic state as well as the growth of the metallic particles, the incorporation of lead into the glaze also reduces the diffusivity of silver and copper in the glaze and facilitates the development of the metallic shine.

References

Barber DJ, Freestone IC, Moulding IC. Ancient copper red glasses: investigation and analyses by microbeam techniques. In: Shortland, Andrew J., Freestone, Ian C., Rehren, Thilo (Eds), From Mine to Microscope. Advances in the Study of Ancient Technology: 115-127. Oxford, UK: Oxbow; 2009

Bobin O., Schvoerer M., Ney C., Rammah M., Daoulatli A., Annequin B., Gayraud RP. Where did the lustre tiles of the Sidi Oqba Mosque (AD 836–63) in Kairouan come from? Archaeometry 2003; 45(4): 569–77

Bontempi E, Colombi P, Depero LE, Cartechini L, Presciutti F, Brunetti B, Sgamellotti A. Glancing incidence x-ray diffraction of Ag nanoparticles in gold lustre decoration of Italian Renaissance pottery. Appl Phys A 2006; 83(4): 543-6

Caiger Smith A. *Lustre Pottery*. New York, EUA: New Amsterdam Books; 1991.

Cheng HS, Shen H, Tang J, Yang F. Cross sections for 170 backscattering of 4He from oxygen in the energy range of 2.0-9.0 MeV. Nucl Instr Meth Phys Res B 1993; 83 (4): 449-53

Climent-Font A, Pászti F, García G, Fernández-Jiménez MT Agulló F. First Measurements with the Madrid 5 MV tandem accelerator. Nucl Instr Meth Phys Res B 2004; 219-220:400-4.

Fluegel, A. Global model for calculating room-temperature glass density from the composition. J Am Ceram Soc 2007; 90 (8): 2622-5.

Gutierrez PC, Pradell T, Molera J, Smith AD, Climent-Font A, Tite MS. Color and Golden Shine of Silver Islamic Lustre. J Am Ceram Soc 2010; 93(8): 2320–8

Johnson PB, Christy RW. Optical constants of noble metals. Phys Rev B 1975; 6 (12): 4370–9

Kreibig U, Vollmer M. Optical Properties of metal clustre. Springer 25. Berlin, Germany: Springer Verlag; 1995

Mason R., Keall EJ. Abbasic glazed ware of Siraf and the Basra connection: Petrographic analyses. Iran 1991; XXIX: 51-68

Mason RB. *Shine like the sun. Lustre-painted and associated pottery from the Medieval Middle East*. Bibliotheca Iranica: Islamic Art and Architecture series 12. Costa Mesa, Canada: Mazda Publisher Inc; 2004

Mayer M. SIMNRA User's Guide, (IPP 9/113 1997): http://www.rzg.mpg.de/; 1997

Molera J, Bayés C, Roura P, Crespo D, Pradell T. Key parameters in the production of medieval lustre colors and shines. J Am Ceram Soc 2007; 90(7): 2245-54

Padovani S, Sada C, Mazzoldi P, Brunetti B, Borgia I, Giulivi A, Sgamellotti A., D'Acapito F,Battaglin G. Copper in glazes of Renaissance lustre pottery: nanoparticles, ions and local environment. J Appl Phys 2003; 93(12): 10058-63

Padovani S, Borgia I, Brunetti B, Sgamellotti A, Giulivi A, D'Acapito F, Mazzoldi P, Sada C, Battaglin G. Silver and copper nanoclustres in the lustre decoration of Italian Renaissance pottery: an EXAFS study. Appl Phys A 2004; 79 (2): 229-33

Padeletti G., Fermo P.. Production of gold and ruby-red lustres in Gubbio (Umbria, Italy) during the Renaissance period. Appl Phys A 2004; 79 (2): 241-5.

Padeletti G, Fermo P, Bouquillon A, Aucouturier M Barbe F. A new light on a first example of lustre majolica in Italy. Appl Phys A 2010; 100 (3): 747-61.

Pérez-Arantegui J, Molera J, Larrea A, Pradell T, Vendrell M, Borgia I, Brunetti BG, Cariati F, Fermo P, Mellini M, Sgamellotti A, Viti C. Lustre pottery from the thirteenth century to the Sixteenth century: a nanostructured metallic thin metallic film. J Am Ceram Soc 2001; 84(2): 442-6

Pérez-Arantegui J, Larrea A, Molera J, Pradell T, Vendrell-Saz M. Some aspects of the characterization of decorations on ceramic glazes. Appl Phys A 2004; 79(2): 235-9

Polvorinos del Rio A, Castaing J, Roehrs S, Vallejo-Triano A, Escudero-Aranda J. Estudio arqueométrico de loza dorada de Madinat al'Zahra, Córdoba. Cuadernos de Madinat al-Zahra 2008; 6: 165-79

Pradell T, Molera J, Roque J, Smith AD, Crespo D, Pantos E, Vendrell M. Ionic-exchange mechanism in the formation of medieval lustre decorations. J Am Ceram Soc 2005; 88(5):1281-9

Pradell T, Climent-Font A, Molera J, Zucchiatti A, Ynsa MD, Roura P, Crespo D. Metallic and non-metallic shine in lustre: an elastic ion backscattering study, J Appl Phys 2007; 101(9): 103518 (8)

Pradell T, Molera J, Smith AD, Tite MS. The invention of lustre: Iraq 9th and 10th centuries AD. J Arch Sci 2008; 35(5): 1201–15

Pradell T, Pavlov RS, Gutiérrez PC, Climent-Font A, Molera J. Composition, nanostructure, and optical properties of silver and silver/copper lustres. J Appl Phys 2012; 112: 054307(11)

Pradell T, Molina G, Molera J, Pla J, Labrador A. The use of micro-XRD for the study of glaze color decorations. Appl Phys A 2013; 111 (4): 121–7

Priven AI, Mazurin OV. Comparison of methods used for the calculation of density, refractive index and thermal expansion of oxide glasses. Glass Technol 2003; 44 (4): 156–66

Sarre F., Herzfeld E., Arnold H. *Keramik von Samarra.* Forschungen zur islamischen Kunst 2. Berlin, Germany; Dietrich Reimer; 1925

Sciau Ph, Mirguet C, Roucau C, Chabanne D, Schvoerer M. Double Nanoparticle Layer in a 12th Century Lustreware Decoration: Accident or Technological Mastery?. J Nano Research 2009; 8:141-6

Sciau P, Salles P, FRoucau C, Mehta A, Benassayag G. Applications of focused ion beam for preparation of specimens of ancient ceramic for electron microscopy and synchrotron X-ray studies. Micron 2009; 40(5-6): 597-604

van de Hulst HC. Light scattering by small particles. New York, EUA: Dover Publications Inc; 1981

Chapter 4

Analyses of Syrian lustre pottery (12th–14th centuries AD)

Introduction

Lustre is an expensive art form developed with a strong scientific background and produced by skilled artisans. Consequently, although it is possible that the movement of artisans within the caliphate spreads lustre technology, the main diffusion occurred after the collapse of dynasties resulting in the migration of artisans to new production centres (Caiger-Smith, 1991). For instance, the occupation of Egypt by the Fatimids in 969 AD started the production of Egyptian Fatimid lustre with the resulting decline of the Abbasid lustre produced in Bashra. Although the earlier separation of Egypt from the Abbasid caliphate and its rule by the Tulunids (868–905 AD) has sometimes been associated with the transfer of lustre Technology from Iraq to Egypt, analyses of the so called Tulunid lustres has demonstrated their Iraqi origin (Mason, 2004). Later the collapse of the Fatimid dynasty circa 1169 AD was followed by the beginning of the so called "Kashan lustreware" in Persia (Watson, 1985). Syrian lustreware began earlier, the so called "Tell Minis" lustreware dating from the late 11th century or beginning of the 12th century. Syria was not a peaceful place during the 11th century as the Byzantines, Fatimids and Crusaders among others fought for the territory until the Seljuk Turks (1084–1086) were able to stabilise the area for about a century. They were defeated by Saladin (1175–1185) who started the Ayyubid dynasty. The so called "Raqqa ware" developed during the Ayyubid dynasty in the

city of Raqqa and continued until Raqqa was destroyed by the Mongols in the 1260 s AD and abandoned in 1288 AD (Jenkins-Madina, 2006). Although in this period (12^{th}–13^{th} century AD) lustreware was also produced in other places (Pérez-Arantegui et al., 1995; Redford and Blackman, 1997), the analytical study made by Dylan Smith demonstrated the existence of a "Raqqa ware" comprising not only the dark brown lustreware (often combined with underglaze cobalt blue) but also the black decoration under turquoise glaze and polychrome ceràmics (Smith, 2006). Other productions include green lustre with splashed purple and turquoise decoration and thick bodies from Gritille (Redford and Blackman, 1997) which appear to be of lower quality (Porter, 1981). Later ceramic productions dating to the Mamluk period (c. 1250 onwards) and concentrated in Damascus are known to include polychrome, blue and white, sgraffito and lustre. Lustrewares from this period are golden on a cobalt blue tinged glaze (Porter, 1981; Smith, 2006; Watson, 2004). One of the characteristics of the Syrian ceràmics is the use of stonepaste, a synthetic ceramic paste made of sand, clay and glass frit, although a small part, and including all the productions, was earthenware.

The existence of the two first groups "Tell Minis" and "Raqqa type" has been confirmed by several analytical studies (Franchi et al., 1995; Mason, 1997, 2004; Smith, 2006); "TellMinis" ware is finer, more compact and contains a higher amount of clay, with a transparent mixed lead–sodium rich alkaline glaze; "Raqqa" ware has a porous structure, is calcium richer, shows relative large variations of the clay content depending on the size and characteristics of the pot, and appears glazed with a sodium rich alkaline glaze. Finally, the stonepaste associated to the Mamluk productions appears to be clay poorer and calcareous richer than "Raqqa" and "Tell Minis", contains large rounded quartz grains, and appears glazed with a sodium rich alkaline glaze (Franchi et al., 1995;Mason, 1997, 2004; Smith, 2006). However, in this case the variability found is large requiring of a more extensive study.

Each lustre production has its own peculiarities not only in the lustre colour, (silver/copper composition and oxidation state) and nanostructure (size and concentration of particles, thickness of the layer) but also in the paste and glaze compositions, processing and firing conditions (Chabanne et al., 2012; Padeletti et al., 2010; Padovani et al., 2003; Pradell et al., 2008a, 2008b). Differences in the lustre colour and shine are in all cases related to a combination of the process of production and materials used. Recent studies have demonstrated that the production of a metallic shining lustre (either golden or coppery) is strongly related to the composition of the glaze, and in particular, that the use of a lead bearing glaze strongly increases the possibility of obtaining a successful metallic shine (golden/coppery) decoration (Molera et al., 2007). The diffusivity of copper and silver is greater in alkaline glazes than in

lead bearing glazes which results in the formation of thicker and less concentrated lustre layers. As the presence of a high concentration of metallic particles is fundamental for obtaining a high reflectance (metallic shine) (Pradell et al., 2007), the use of alkaline glazes reduces the possibilities of obtaining a lustrous layer. However, other strategies may be followed to obtain shiny lustres. For example, the precipitation and growth of the metal nanoparticles may be strongly increased by adding reducing agents such as Sn^{2+} and Fe^{2+} to the glaze composition or those such as Bi and Hg to the lustre paint (Molera et al., 2001; Padeletti et al., 2010). Tin was commonly added to the glazes to increase opacity and iron is also present either added as an impurity with the sand or incorporated into the glaze by diffusion from the ceràmic paste, both being known to be able to reduce copper to the metallic state. Finally, the addition of copper itself is known to reduce silver to the metallic state.

In fact an increase in the lead content of the glazes has been found from the early Abbasid (9th and 10th century AD) through to the later Fatimid period (11–12th century AD) (Gutierrez et al., 2010). Subsequent productions used lead bearing glazes with the exception of some Syrian lustre productions, including Raqqa ware, as well as, 16–18th century Safavid lustre wares in Persia (Mason, 1997, 2004; Padeletti et al., 2010; Pradell et al., 2008b; Roque et al., 2007).

Consequently, the study of Syrian lustreware is particularly interesting not only because of the variety of lustre productions during a relative short period but also because of the novelties introduced as compared to earlier Abbasid and Fatimid Egyptian lustre productions. The use of transparent tin-free and/or lead-free, alkaline, glazes is accompanied by technological variations in order to increase the chances to produce a shiny lustre.

In this chapter we present preliminary analyses of the ceramic pastes, glazes and lustre decorations used on the early Syrian lustre productions belonging to the Ashmolean Museum including Tell Minis (first half 12th century AD), Raqqa and related wares (second half of the 12th century AD and first third of the 13th century AD) and Damascus (second half of the 13th century AD and 14th century AD).

Materials and methods

The materials selected belong to the collections donated by Sir A. Barlow (1956), Mr. G. Reitlinger (1978) and Mr. Bartels (1980) to the Ashmolean Museum (Porter, 1981; Porter and Watson, 1987). The Tell Minis lustreware comprises three sherds from conical bowls, two (EA-

1978-2217 and p8834/36) with scratched arabesque brownish and green lustre decoration respectively (Porter and Watson, 1987) and one (p138) with calligraphic brownish lustre decoration (Mason, 2004). The three Raqqa typewares (p8833, p9404 and p620) are typical conical shaped bowls with a greenish glaze and chocolate Brown coloured lustre. The last two correspond chemically to a group of pots and wasters analysed by Smith (2006) which have been ascribed to 13th century Raqqa lustrewares and are characterised by their Al/Fe ratios/contents while p8833 falls into the so called Raqqa related wares. Finally, the two sherds assigned to Damascus ware were selected, one being from a footring (p8839) and the other being from the base of an albarello (p8830) (Porter and Watson, 1987). p8839 shows a Brown metallic-like lustre on a blue glaze with characteristic interlace designs and p8830 shows a green–yellowish lustre on a blue glaze with disconnected designs. Those two sherds were found together in a context with other Mamluk wares (underglaze painted) (Porter and Watson, 1987) which supports their description as Damascus lustreware.

Chemical analyses of the ceramic pastes, glazes and lustre decorations were obtained by Scanning Electron Microscopy and an Energy dispersive X-ray detector, Stereoscan S-360 SEM, PCXA LINK EDX. The accelerating voltage was 20 kV and the probe current 1.5 nA.

X-ray microstructural analyses of the ceramic pastes and glazes was also obtained on polished thin cross sections (about 50 μm thick) of the samples by micro X-ray diffraction performed at the European Synchrotron Radiation Facility (ESRF). SR-μ-XRD was performed on beamline BM16 at the ESRF (Grenoble, France) in transmission geometry, using 0.78 Å wavelength (16 keV), and, taking advantage of the layered structured, a 100 μm × 30 μm spot size and recorded using a CCD detector.

Results and discussion

The chemical analyses of the ceramic pastes, glazes and lustre layers corresponding to the samples studied are shown in Tables 4.1–4.3 respectively.

The body pastes used are stonepastes all with a creamy colour although showing some differences between them. Tell Minis pastes are very fine (grain sizes below 100 μm) (Figure 4.1) and siliceous rich with very low Na, K, Ca, Mg and Fe contents (Table 4.1). This corresponds to a mixture of very pure quartz sand (about 60%, quartz plus cristobalite as determined by XRD) with clay (about 20%, assuming an illitic clay containing about 25% Al_2O_3) and Na–Ca glass frit (about 20%). The XRD data (Figure 4.2) show the presence of quartz and cristobalite as well as Na-feldspar (albite, $NaAlSi_3O_8$), nepheline ($NaAlSiO_4$) and

diopside ($CaMgSi_2O_6$) formed in the glassy matrix that holds together the quartz and cristobalite grains.

Table 4.1. Analyses of the pastes obtained by SEM-EDS (20 kV, 1.5 mA). Average values and standard deviation (between brackets) of 2 measurements.

		Na_2O	K_2O	Al_2O_3	SiO_2	CaO	MgO	FeO	TiO_2	PbO
TELL MINIS	EA-1978-2217r	2.5 (0.04)	0.9 (0.01)	4.6 (0.1)	88.8 (0.9)	1.6 (0.04)	1.0 (0.1)	0.6 (0.1)		
	p138	2.9 (0.1)	1.3 (0.1)	5.7 (0.3)	87.1 (0.6)	1.5 (0.2)	0.7 (0.1)	0.5 (0.04)	b.d.	
	p8834/36	2.2 (0.2)	0.9 (0.2)	3.1 (0.2)	90.7 (0.6)	1.9 (0.5)	0.8 (0.2)	0.5 (0.63)	b.d.	
RAQQA	p8833	3.5 (0.3)	1.02 (0.01)	4.5 (0.1)	80.3 (0.3)	5.9 (0.2)	2.4 (0.2)	1.9 (0.2)	0.10 (0.05)	
	p9404	2.4 (0.1)	0.88 (0.01)	2.2 (0.3)	85.5 (0.8)	3.2 (0.1)	1.7 (0.2)	2.5 (0.1)	b.d.	
	p620	2.9 (0.4)	0.89 (0.01)	2.5 (0.4)	84.5 (1.3)	4.5 (0.1)	1.9 (0.1)	2.9 (0.4)	0.14 (0.04)	
DAMASCUS	p8830	1.0 (0.2)	0.8 (0.1)	2.2 (0.2)	71.5 (0.8)	18.2 (0.9)	1.3 (0.1)	0.6 (0.1)	0.4 (0.05)	4.4 (0.1)
	p8839	4.7 (0.3)	1.7 (0.1)	12.5 (0.9)	76.1 (1.5)	2.1 (0.1)	1.1 (0.1)	1.0 (0.1)	0.3 (0.04)	

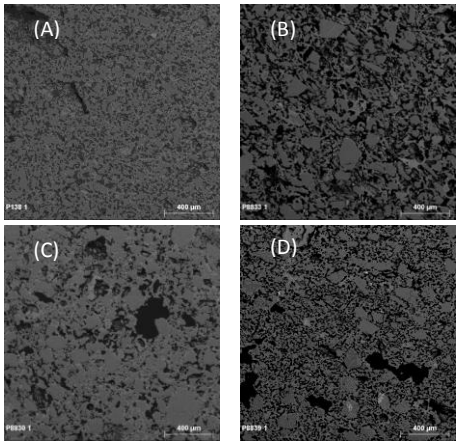

Figure 4.1. SEM backscattering images corresponding to the ceramic stonepastes from (A) Tell Minis (EA1978.2217) (B) Raqqa (p8833), Damascus (C) Ca-rich (p8830) and (D) Damascus Al-rich (p8839).

Cristobalite is stable at temperatures above 1470°C but may metastably crystalise from amorphous silica at lower temperatures. Therefore, it is a usual form found in glassy silica and in all the cases is present in small amounts (between 2 and 10%wt). Raqqa and related wares are also siliceous but contain higher amounts of Ca, Mg and Fe (Smith, 2006) and are coarser (grain sizes up to 200 μm) (Figure 4.1). As before this composition corresponds to a mixture of quartz-rich sand but this time incorporating some calcareous grains with some clay and glass-frit. The lack of correlation between the calcium and the aluminium content between the two Raqqa wares (p9404 and p620) suggests that the calcium was not added with the clay.

The same lack of correlation was observed in the study involving a large selection of Raqqa and other Syrian stonepastes (Smith, 2006). As before XRD data show the formation of the same compounds as in Tell Minis pastes, but with higher amounts of diopsides, which are a consequence of the higher Ca, Mg and Fe contents of Raqqa pastes.

Table 4.2
Analyses of the glazes obtained by SEM–EDS (20 kV, 1.5 mA). Average values and standard deviation (between brackets) of 2 measurements.

		Na_2O	K_2O	Al_2O_3	SiO_2	CaO	MgO	TiO_2	FeO	CoO	CuO	SnO_2	PbO
TELL MINIS	EA-1978-2217r both	13.6 (0.4)	1.9 (0.1)	1.7 (0.1)	57.7 (1.0)	4.9 (0.4)	2.7 (0.2)	b.d.	0.32 (0.3)			b.d.	17.2 (0.6)
	p138 front	13.3 (0.5)	1.6 (0.1)	1.5 (0.3)	55.3 (0.4)	2.7 (0.1)	1.5 (0.1)	b.d.	0.40 (0.1)			b.d.	23.7 (0.7)
	p8834/36 front	10.9 (0.9)	1.6 (0.2)	1.3 (0.3)	64.1 (3.8)	3.7 (0.3)	1.6 (0.1)	b.d.	0.66 (0.1)		0.25 (0.1)	0.32 (0.2)	15.0 (2.7)
RAQQA	p9404 front	15.9 (0.2)	2.1 (0.1)	1.6 (0.1)	70.6 (0.4)	5.0 (0.1)	3.3 (0.2)	0.14 (0.1)	0.89 (0.1)		b.d.		b.d.
	p8833 front	16.9 (0.3)	2.1 (0.03)	2.0 (0.1)	64.3 (0.3)	6.4 (0.1)	2.7 (0.2)	0.10 (0.1)	0.79 (0.1)		b.d.		3.9 (0.3)
	p620 rear	7.6 (0.7)	1.9 (0.4)	1.3 (0.2)	78.6 (2.0)	6.6 (2.0)	2.2 (0.3)	b.d.	1.04 (0.2)		0.10 (0.11)		b.d.
	p620 front	11.6	1.7	1.2	73.0	7.2	2.9	0.11	0.87		b.d.		
DAMASCUS	p8830 both	12.2 (0.5)	3.7 (0.2)	1.9 (0.1)	64.1 (1.6)	10.8 (1.0)	4.1 (0.5)	b.d.	2.3 (0.2)	0.41 (0.2)	0.14 (0.1)		b.d.
	p8839 front	10.0 (0.1)	1.5 (0.01)	2.0 (0.0)	46.5 (0.0)	5.2 (0.1)	2.2 (0.03)	b.d.	1.3 (0.1)	0.54 (0.1)	b.d.	4.9 (0.2)	25.6 (0.2)

Table 4.3
Analyses of the lustres obtained by SEM–EDS (20 kV, 1.5 mA). Average values and standard deviation (between brackets) of at least 4 measurements.

		Na_2O	K2O	Al_2O_3	SiO_2	CaO	MgO	FeO	SnO_2	PbO	Cu	Ag	Cu/(Cu+Ag)
TELL MINIS	EA-1978-2217r	3.0 (0.7)	1.8 (0.1)	1.3 (0.1)	62.5 (2.3)	3.9 (0.4)	2.3 (0.1)	0.6 (0.1)	0.1 (0.1)	13.1 (0.4)	7.9 (0.7)	3.5 (2.3)	69 (11)
	p138	1.8 (0.7)	1.6 (0.1)	1.4 (0.2)	69.1 (2.8)	2.0 (0.2)	1.0 (0.1)	0.6 (0.1)	0.2 (0.2)	11.9 (1.3)	4.7 (0.9)	4.5 (1.5)	52 (7)
	p8834/36	5.4 (0.2)	2.0 (0.0)	1.1 (0.1)	60.3 (0.4)	4.3 (0.2)	1.9 (0.0)	0.7 (0.0)	0.1 (0.0)	14.6 (0.2)	5.2 (0.6)	4.3 (0.2)	55 (4)
RAQQA	p9404	4.3 (1.4)	1.9 (0.2)	1.4 (0.2)	73.4 (1.7)	3.0 (0.1)	2.1 (0.1)	1.1 (0.1)			6.9 (0.8)	2.8 (0.8)	71 (9)
	p8833	5.6 (0.5)	2.2 (0.2)	1.0 (0.7)	67.6 (0.8)	4.8 (0.3)	2.2 (0.2)	0.6 (0.3)	0.4 (0.4)	2.9 (0.2)	9.9 (0.7)	2.9 (0.7)	78 (5)
	p620 rear	4.9 (0.7)	2.2 (0.1)	1.3 (0.3)	74.8 (0.6)	6.5 (0.2)	2.7 (0.1)	1.2 (0.4)	0.3 (0.1)	0.1 (0.1)	5.8 (0.6)	0.1 (0.1)	98 (1)
	p620 front	2.7 (0.1)	1.2 (0.1)	5.9 (1.3)	75.3 (0.1)	5.0 (0.0)	1.8 (0.1)	1.7 (0.2)	b.d.	b.d.	5.5 (0.5)	b.d.	100
DAMASCUS	p8830	3.0 (0.5)	3.3 (0.5)	1.5 (0.1)	72.4 (1.3)	8.8 (1.1)	3.8 (0.8)	1.5 (0.4)	0.3 (0.1)	0.1 (0.1)	4.4 (1.0)	0.4 (0.2)	93 (3)
	p8839	3.6 (0.6)	2.6 (0.5)	1.7 (0.1)	57.0 (1.6)	4.6 (0.2)	1.9 (0.2)	1.5 (0.1)	5.2 (1.5)	18.4 (0.5)	1.6 (0.9)	1.6 (1.2)	54 (6)

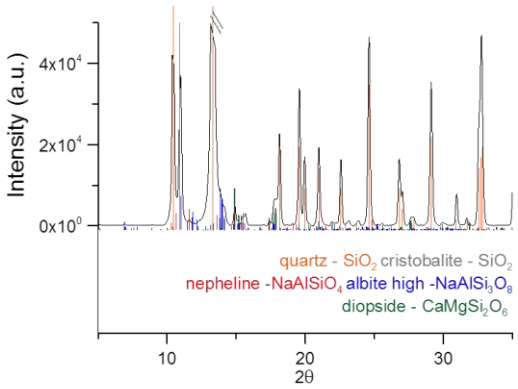

Figure 4.2. XRD pattern from p138 showing the presence of quartz, cristobalite, diopsides, feldspars and nepheline.

The two Damascus wares are also coarse but siliceous poorer (≈75 wt.% SiO_2). However, p8830 is calcium richer while p8839 is aluminium richer. Therefore, the body analyses of p8830 correspond to Ca rich stonepaste and that of p8839 to earthenware. The high calcareous stonepaste, p8830, corresponds well with the data obtained for the Mamluk Syrian productions (Smith, 2006) of probable common Damascus origin. XRD analyses shows that p8830 contains quartz, cristobalite, larger amounts of diopsides than in Tell Minis or Raqqa wares and, about 10 wt% of calcite ($CaCO_3$). XRD analyses of p8839 shows the presence of quartz, cristobalite, and larger amounts of diopsides and feldspars (Ca–Na type) than Tell Minis or Raqqa wares. In both cases XRD data indicate that they contain about 40–50 wt.% of quartz and cristobalite in contrast with the higher content in Tell Minis and Raqqa pastes. Therefore, p8830 was made of a mixture of quartz sand rich in calcite grains with some clay and glass frit. The mineralogical and chemical composition of p8839 indicates the use of ceràmic paste containing about half and a half of quartz sand and clay with a small amount of glass frit. Earthenware was used in Syria contemporary with the use of stonepastes in all the production types (sgraffito, splash painted, moulded, tin glaze) (Jenkins-Madina, 2006; Mason, 2004); in particular tin glazed ceramics were made of a kind of proto-stonepaste containing quartz, clay and also a large amount of glass (Mason, 2004).

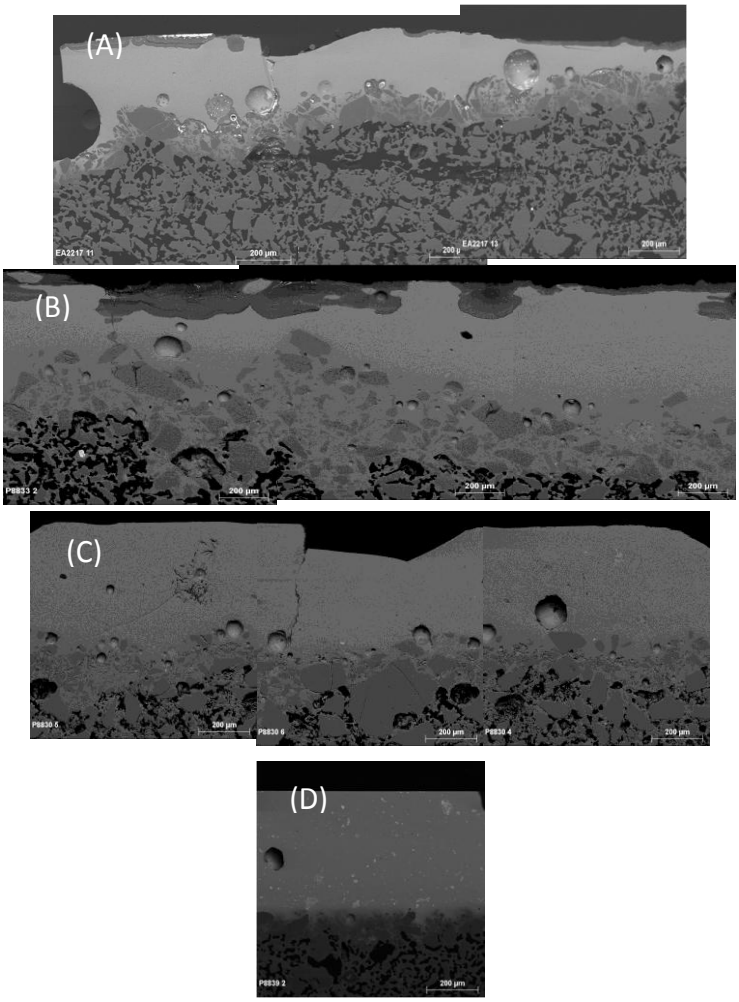

Figure 4.3. SEM backscattering images corresponding to typical alkaline glazes from (A) Tell Minis EA2217, (B) Raqqa, p8833 (C) Damascus, p8830 and (D) tin opacified lead–alkaline glaze from Damascus p8839.

In all the cases the formation of diopsides indicates

temperatures above 950 °C most probably above 1000 °C.

As shown in Table 4.2 Tell Minis glazes are transparent, sodium-rich lead glazes which are not tin-opacified, the use of very light coloured stonepastes making the addition of cassiterite in the glazes unnecessary. The composition of those glazes, although slightly lead poorer, resembles those of Fatimid lustreware. Moreover, some authors have found a reduction of the lead content of the glazes in 12th century Fatimid lustreware (Mason, 2004). Consequently, ignoring the incorporation of cassiterite, Tell Minis lustreware glazes appear very similar to contemporary Fatimid lustreware glazes. Finally, the glazes and bodies were fired in a single firing as the large glaze-paste interactions show in Figure 4.3(A); this is another advantage of the use of stonepastes.

Contrarily, Raqqa glazes (Table 4.2) are mainly alkaline (sodium-rich) and if they contain lead, it is in very small amounts. However, they also contain a higher amount of Fe which, since the glazes are greenish in colour, is probably mainly present as Fe^{2+}. Therefore, its addition is likely to have helped the reduction of copper to the metallic state. The use of iron as reducing agent in the production of copper red glass is a well-known practise in the glass industry since Roman times (Arletti et al., 2006; Barber et al., 2009); the conservation state of these alkaline glazes especially their surfaces is very badwith large areas, appearing to be missing or showing layered structures and scales Figure 4.3(B).

The two Damascus type sherds analysed show two different glaze compositions (Table 4.2). Sherd p8830 is a lime-soda alkaline glaze while p8839 is an alkaline–lead tin opacified glaze. Both are blue and contain Co as well as Fe. SEM backscattering images of the glaze cross sections are shown in Figure 4.3(C) and (D) respectively. Few analyses obtained from the glazes used for polychrome under-glaze painted Damascus wares (Mason, 2004) revealed in all cases alkaline glazes.

The surfaces of the glazes and the lustre decorations were also measured by SEM–EDS, which allows the comparison of the chemistry between non-decorated and decorated areas. It should be noted that the chemical compositions measured directly on the glaze surfaces are not comparable to thosemeasured on the glaze cross sections as the former are heavily affected by the alteration and weathering. For instance even in those cases where the glazes seem in a good state of conservation, as the glaze surfaces appear always depleted in Na and Pb. This is never seen in replicated glazes which have not been affected by the use or burial.

Both Na and Pb leaching are expected in humid and acid environaments affecting the 2 μm depth analysed by means of EDS. Nevertheless, the analyses allow the determination of the Cu and Ag composition of the lustre layers and also detect the presence of other elements

associated to the lustre production process. The results of the analyses obtained for the lustre decorations are shown in Table 4.3.

An overall depletion of sodiumis observed in the glaze, as compared to the results determined on cross sections of the glazes. However, comparison of sodium, copper and silver contents at different points of the lustre decorations shows that those areas containing higher silver or copper also contain lower amounts of sodium. In Figure 4.4 the atomic content of Cu and Ag versus Na corresponding to different areas of the lustre decoration are plotted revealing an inverse correlation which supports the substitution of Na by Cu or Ag. Consequently, all the lustre layers studied herewith were made following the procedure described in the introduction, that is, through ionic exchange between sodium from the glaze and the copper and silver from the applied lustre materials and precipitation of the metal nanoparticles (Padovani et al., 2003; Pradell et al., 2005).

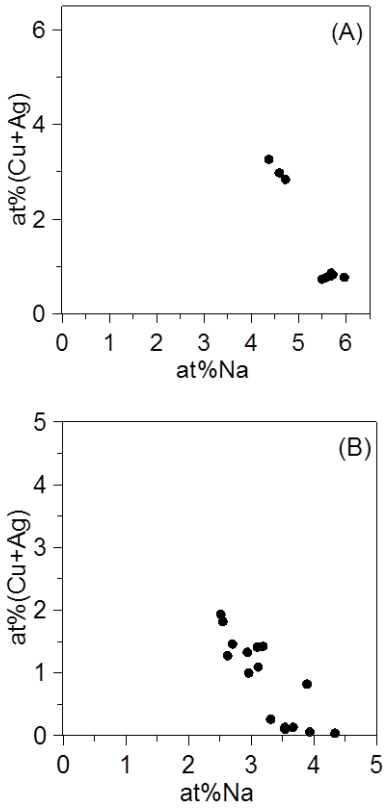

Figure 4.4. at% Na versus at.% (Cu + Ag) in the lustre showing the inverse correlation characteristic of ionic exchange for (A) Tell Minis, p8834-36 and (B) Raqqa, p8833.

The relative copper/silver content of the lustre decoration is also important as it determines the range of colours of the lustre layers. This data is also given in (Table 4.3) as %Cu/(Cu + Ag) for the diferent samples studied. Tell Minis lustres are richer in silver — 50–70% Cu/(Cu + Ag) — than Raqqa lustres — 70–90% Cu/(Cu + Ag) — but richer in copper than Fatimid Egyptian lustres — 10–30% Cu/(Cu + Ag) — and 10th century monochrome Iraqi lustres — 0–10% Cu/(Cu + Ag) — (Gutierrez et al., 2010; Pradell et al., 2008a, 2008b). These results suggest a decrease in the silver content of the lustres produced in the region from 11th century to 13th century AD, which could be related to either difficulty in acquiring silver or a voluntary modification. The increasing copper content results in a shift from green–yellowish to brown colour of the lustre layers. Contemporary Kashan lustreware which is also brown contains 50–70% Cu/(Cu + Ag) and is therefore richer in copper than earlier productions although not as rich as Raqqa ware.

However, the copper/silver contents found show a large variability not only due to the difficulties in controlling the lustre production process but also due to the state of conservation of

the layers. The method of production of lustre that involves ionic exchange (Padovani et al., 2003; Pradell et al., 2005) and the subsequent further growth of nanoparticles is known to develop compressive stresses on the glaze which becomes tougher. This also makes the lustre decorated areas more stable and less affected by burial conditions. However, the lustre layers are formed close to the glaze surface (some tens of nanometers below the surface) and are also very thin (few hundreds of nanometers thick) which is a handicap, as scratches and erosion may degrade them and affect the colour and shine of the layers. In particular, since silver appears in general more concentrated closer to the surface than copper which diffuses deeper inside the glaze surface (Pradell et al., 2012), surface erosion affects silver more than copper. And this ismore important for the lustre layers produced on lead bearing glazes as these are closer to the surface than those produced over alkaline glazes (Gutierrez et al., 2010; Pradell et al., 2007, 2012). This fact has to be taken into consideration when comparing lustres from different productions.

In particular, none of the Tell Minis lustre sherds studied was in a state of good preservation, showing lots of scratches and peelings especially on sherd EA-1978-2217r which shows also the higher copper content. Consequently, the silver content determined is most probably lower than that originally present.

Well preserved TellMinis lustres usually showa yellow–orange colour and golden shine consistent with silver lustres containing some copper and the use of lead glazes. The Raqqa production shows a chocolate brown lustre similar to contemporary Persian lustre from Kashan; this is also consistent with the higher copper content shown by those lustres. However, well preserved Persian lustre normally shows Golden shine consistent with the fact that they were produced over a tin-opacified, lead glaze (Pradell et al., 2008b). Although the increase in the copper content of the lustre layers with respect to earlier lustre productions is observed both in Kashan and Raqqa lustrewares, the silver content in the Raqqa wares is very low. In fact the use of alkaline glazes with copper lustres has the advantage of accepting strong external reducing atmospheres which could not be used with lead glazes. Moreover, strong reducing atmospheres are not desirable for the production of silver lustres (Molera et al., 2007).

Finally, the two Damascus lusters are different. p8830 lustre shows a yellow–green colour and contains only copper which suggests an incomplete reduction while p8839 has a brown colour and metallic shine and contains about 50% Cu/(Cu + Ag). However, since very limited studies concerning Damascus wares are found in the literature (Mason, 2004) and even less concerning lustreware, (Chabanne et al., 2012), some morework should be performed in order to characterise their production.

Conclusions

The results obtained indicate the copper enrichment of the lustres from early 12th century to 13th century productions. Tell Minis and Syrian lustres are more similar in composition and colour to contemporary Fatimid Egyptian lustre (richer in silver), whereas Raqqa lustre is more similar in colour and composition (richer in copper) to contemporary Persian lustre. One of the peculiarities of Syrian lustres is the use of transparent glazes, lead glaze for Tell Minis and alkaline glaze for Raqqa.

The Raqqa and Tell Minis sherds studied correspond well in both paste and glaze compositions, with data from the literature (Franchi et al., 1995; Kaczmarczyk, 1994; Mason, 1997, 2004; Smith, 2006). In contrast, the two sherds of supposedly Damascus ware were completely different from each other (Ca-rich stonepaste with alkali glaze for p8830 and earthenware with tin glaze for p8839), and only p8830 is comparable to the few analyses of Damascus lustreware found in the literature. A more extensive study is therefore necessary in this case.

Tell Minis lustres showing golden shine were obtained on lead bearing glazes. Raqqa lustres were produced over alkaline glazes but neither the sherds studied here nor the pots found in Museums show metallic shine. Finally, from the two Damascus wares studied, the one showing metallic shine was produced over a tin opacified lead glaze. Consequently the results obtained herewith agree with previous studies indicating that the addition of lead to the glaze increases the probability of producing lustre with metallic shine.

Finally, Raqqa lustre and glazes are richer in iron than Tell Minis, Fatimid Egyptian and Persian lustrewares (Pradell et al., 2008b). The addition of iron to the glazes helps the reduction of copper andwas a common practise for the production of Roman copper red glasses (Arletti et al., 2006; Barber et al., 2009), a fact which suggests a direct connection between Raqqa lustreware and the glass industry which should be studied.

References

Arletti, R., Dalconi, M.C., Quartieri, S., Triscari, M., Vezzalini, G., 2006. Roman coloured opaque glass: a chemical and spectroscopic study. Applied Physics A 83, 239–245.

Barber, D.J., Freestone, I.C., Moulding, K.M., 2009. Ancient copper red glasses: investigation and analyses by microbeam techniques. In: Shortland, A., Freestone, I.C., Rehren, Th. (Eds.), From Mine to Microscope. Advances in the Study of Ancient Technology. Oxbow, Oxford (UK), pp.115–127.

Caiger-Smith, A., 1991. Luster Pottery. New Amsterdam Books, New York (UE).

Chabanne, D., Aucouturier, M., Bouquillon, A., Darque-Ceretti, E., Makariou, S., Dectot, X., Faÿ-Hallé, A., Miroudot, D., 2012. Ceramics with metallic lustre decoration. A detailed study of Islamic productions from the 9th century until the Renaissance. Matériaux & Techniques 100, 47–68.

Franchi, R., Tonghini, C., Paloschi, F., Soldi, M., 1995. Mediaeval Syrian fritware: materials and manufacturing technique. In: Vincenzini, P. (Ed.), The Ceramics Cultural Heritage. Editorial Tchna srl, Faenza (Italy), pp. 197–205.

Gutierrez, P.C., Pradell, T., Molera, J., Smith, A.D., Climent-Font, A., Tite, M.S., 2010. Color and golden shine of silver Islamic luster. Journal of the American Ceramic Society 93 (8), 2320–2328.

Jenkins-Madina, M., 2006. Raqqa Revisited. Ceramics of Ayyubid Syria. The Metropolitan Museum of Art, New York.

Kaczmarczyk, A., 1994. www.arch.ox.ac.uk/dl-tite2.html.

Mason, R.B., 1997. Medieval Syrian Lustre-painted and Associated Wares: Typology in a Multidisciplinary Study. Levant, XXIX 169–200.

Mason, R.B., 2004. Shine like the sun. Luster-painted and associated pottery from the Medieval Middle East. Bibliotheca Iranica. Islamic Art and Architecture Series, 12. Mazda Publishers, Inc., Costa Mesa (Cacada).

Molera, J., Mesquida, M., Pérez-Arantegui, J., Pradell, T., Vendrell, M., 2001. Lustre rècipes from a medieval workshop from Paterna. Archaeometry 43 (4), 455–460.

Molera, J., Bayés, C., Roura, P., Crespo, D., Pradell, T., 2007. Key parameters in the production of medieval luster colors and shines. Journal of the Amer. Ceramic Society 90 (7), 2245–2254.

Padeletti, G., Fermo, P., Bouquillon, A., Aucouturier, M., Barbe, F., 2010. A new light on the first example of lustred majolica in Italy. Applied Physics A 100, 747–761.

Padovani, S., Sada, C., Mazzoldi, P., Brunetti, B., Borgia, I., Sgamellotti, A., Giullvi, A., D'Acapito, F., Battaglin, G., 2003. Copper in glazes of renaissance luster pottery: nanoparticles, ions, and local environment. Journal of Applied Physics 93, 10058–11063.

Pérez-Arantegui, J., Querré, G., Kaczmarczyk, A., Bernus-Taylor, M., 1995. Chemical characterization of Islamic glazed ceramics from Northern Syria by particle induced x-ray emission (PIXE). In: Vincenzini, P. (Ed.), The Ceramics Cultural Heritage. Editorial Tchna srl, Faenza (Italy), pp. 475–482.

Porter, V., 1981. Medieval Syrian Pottery (RaqqaWare). Ashmolean Museum publications, Oxford.

Porter, V., Watson, O., 1987. Part II: Tell Minis' wares. Syrian and Iran, three studies inmedieval ceramics. Oxford Studies in Islamic Art, IV. Oxford University Press, Oxford (UK), pp. 175–248.

Pradell, T., Molera, J., Roque, J., Vendrell-Saz, M., Smith, A.D., Pantos, E., Crespo, D., 2005. Ionic-exchange mechanism in the formation of medieval lustre decoration. Journal of the American Ceramic Society 88 (5), 1281–1289.

Pradell, T., Climent-Font, A., Molera, J., Zucchiatti, A., Ynsa, M.D., Roura, P., Crespo, D., 2007. Metallic and non-metallic shine in luster: an elastic ion backscattering study. Journal of Applied Physics 101 (9) (103518-1-8).

Pradell, T., Molera, J., Smith, A.D., Tite, M.S., 2008a. The invention of lustre: Iraq 9^{th} and 10^{th} centuries AD. Journal of Archeological Science 35, 1201–1215.

Pradell, T., Molera, J., Smith, A.D., Tite, M.S., 2008b. Early Islamic luster from Egypt, Syria and Iran (10^{th} to 13^{th} century AD). Journal of Archeological Science 35, 2649–2662.

Pradell, T., Pavlov, R.S., Gutiérrez, P.C., Climent-Font, A., Molera, J., 2012. Composition, nanostructure, and optical properties of silver and silver–copper lusters. Journal of Applied Physics 112 (5) (054307-1-10).

Redford, S., Blackman, M.J., 1997. Luster and fritware production and distribution in Medieval Syria. J Field Archaeology 24 (2), 233–247.

Roque, J., Molera, J., Pérez-Arantegui, J., Calabuig, C., Portillo, J., Vendrell-Saz, M., 2007. Lustre colour and shine from Olleries Xiques workshop in Paterna (Spain) 13^{th} century AD: nanostructure, chemical composition and annealing conditions. Archaeometry 49 (3), 511–528.

Smith, D.T., 2006. Appendix 2: Compositional analyses of early-thirteen-century ceramics from Raqqa and related sites. In: Jenkins-Madina, M. (Ed.), Raqqa Revisited. Ceramics from Ayyubid Syria. The Metropolitan Museum of Art, New York (USA), pp. 221–237.

Watson, O., 1985. Persian Lustre Ware. Faber and Faber, London (UK).

Watson, O., 2004. Ceramics from Islamic Lands. Kuwait National Museum. The Al-Sabah collection. Thames & Hudson, London (UK).

Chapter 5

Color and dichroism of silver stained glasses from Spain (15-16th century)

Introduction

Silver stain is a type of decoration applied to glass that was developed in early medieval times (Heaton 1947). A silver stain consists of a surface layer (between 10 and 300 μm thick) of metallic silver nanoparticles of varying sizes (typically between 1 and 30 nm) dispersed in the glass. The technique was first discovered in Islamic lands (Egypt) in the eighth century AD for the production of stained glass although later was used with some variations in the production of the so-called *luster* ceramics (Pradell et al. 2005; Molera et al. 2007; Colomban 2009). The silver staining technique was transferred to the West through the book ‘‘El Lapidario’’ from the king of Castille Alfonso X where, for the first time, a formula for its production is presented. The translation of this treatise due to Abolais was concluded in 1250 AD (Heaton 1947). Nevertheless, it is not until the end of the thirteenth century or beginning of the fourteenth century that this decorative technique was applied to color window glasses. Its use expanded during the fourteenth century becoming general use in the fifteenth century and particularly in the sixteenth century.

Silver stains were obtained by applying over the glass surface a silver compound dispersed in a clay medium which was then fired (Jembrih-Simbürger et al. 2002; Delgado et al. 2011; Gil et al. 2005; Gil and Villegas 2004). The method resulted in the ionic exchange of the silver ions with the alkali ions (either Na^+ or K^+) from the glass, diffusion in the glass, and subsequent reduction to metal and growth of silver nanoparticles. Reduction of silver ions to the metallic state happens by means of redox reactions with the non-bridging oxygen of the silicate network or with other ions such as Fe^{2+}, Sb^{3+}, As^{3+}, and Sn^{2+} either originally present in the glass or added in the applied silver bearing mixture (Gil et al. 2005; Gil and Villegas 2004). Both diffusion coefficients and redox reactions depend on the composition of the glass. Consequently, the size and volume fraction of the metallic silver nanoparticles and the thickness of the silver stain layer are glass dependent (lime–potash, lime–soda, lead glasses). In fact, the golden-like shine shown by the so-called *luster* in ceramics and glass is consequence of the presence of a high volume fraction of metallic nanoparticles with the consequent change from individual to collective optical behavior (Pradell et al. 2005, 2012; Molera et al. 2007). Moreover, the production parameters, including firing temperature (between 550 and 650ºC) and time (a few minutes at the maximum temperature and slow/free cooling), as well as the composition of the precursor mixture (various silver salts such as Ag_2SO_4, Ag_2O, AgCl, Ag_2S among others, and iron compounds such as clay minerals and oxides) are also important (Jembrih-Simbürger et al. 2002; Barley 1996).

Although in the description of the procedure for silver staining window glasses due to Antoine de Pise (Lautier and Sandron 2008), copper is not mentioned, the interest of producing other colors increased and later in the fifteenth century in Flanders (Caen 2010); the addition of copper is indicated with the purpose of obtaining brighter yellow and orange colors. In fact, the addition of copper has been found to increase the size of the metallic silver nanoparticles in the production of *luster* ceramics under weak reducing conditions unable to reduce copper to the metallic state (Delgado et al. 2011). As a consequence more saturated yellows and also orange colors are produced. Although red silver stain glasses were occasionally obtained, in particular during the sixteenth century, this is less common due to the difficulties in the control of the conditions of production of such glasses which should involve the presence of reducing ions in the glass (Sb^{3+}, As^{3+} and Sn^{2+}) (Gil and Villegas 2004). Even rarer are dichroic glasses, that is, those showing different color in transmission than in reflection. Among them, the most famous is the *Lycurgus cup*, an exceptional cut glass from the fourth century AD opaque greenish-yellow in reflected light and red translucent in transmitted light. The *Lycurgus cup* is among those historical glasses colored by the presence of metal nanoparticles the best known. The dichroic

behavior is attributed to the presence of 50–100 nm silver–gold (7:3 ratio) alloy colloids. However in this case, silver and gold were added to the glass before melting resulting in their partial or total dissolution and further crystallization of the alloy nanoparticles thanks to the redox reactions in which antimoni present in the glass in small amounts must have had an important role (Barber and Freestone 1990).

The color shown by those glasses containing metal colloids is related to the localized absorption and scattering (surface plasmon resonance, SPR) of the visible light which depend on their size, shape, and concentration (Kreibig and Vollmer 1995). Spherical silver nanoparticles absorb and scatter strongly in the blue region of the spectra (around 405 nm for silver nanoparticles of about 30 nm in a glass with a refraction index of 1.52) but are essentially transparent to the rest of the wavelengths in the visible range causing the typical yellow color of silver colloidal solutions and of the bluish scattering. Larger sizes tend to red shift the Surface Plasmon Resonance varying the color of the colloids (Gil et al. 2005; Gil and Villegas 2004; Kreibig and Vollmer 1995). Spherical gold nanoparticles are known to absorb and scatter in the yellow region of the spectra (around 535 nm for gold nanoparticles of about 30 nm in a glass with a refraction index of 1.52) causing the red color of gold colloidal solutions.

The origin of the colors shown by three early Renaissance silver-stained glasses is discussed. Two of these glasses (Avi15 and Pal15) were produced by the same artist, Arnao of Flanders the Elder, belong to the cathedrals of Avila and Palencia, respectively, and date to the last decades of the fifteenth century. The third (Avi16) is from an unknown artist, belongs to the cathedral of Avila and dates to the second half of the sixteenth century. Avi15 and Pal15 are pale and strong yellow, respectively, and Avi16 is dichroic, yellow in reflection and red in transmission. The correlation between the colors observed and the silver stain nanostructure is studied with particular emphasis on the origin of the dichroic behavior. The optical response is computed and compared to the experimental data. Differences in the synthesis parameters responsible for the two non-dichroic and the dichroic silver stains are proposed. This will give insight into the methods used to control of the nanostructures of yellow and red silver stain glasses in the fifteenth and sixteenth century, respectively. It is of particular importance for the restoration/conservation of the glasses, in particular to replicate the glass pieces which have to be replaced.

.

Materials and techniques

The glass pieces studied belong to the set of stain glass windows from the cathedrals of Avila and Palencia restored by Vetraria Muñoz de Pablos S.L. although none of them has been installed back into windows. The pieces sampled and studied belong to the collection of glass panels of the cathedral, and are from historical lost glass windows which were used by the master glaziers for later restorations.

Two of the glasses, Avi15 and Pal15, were produced by Arnao of Flanders ‘‘the Elder’’ master glazier of Flemish origin who worked in Spain between 1480 and 1515 for the cathedrals of Avila, Palencia and Burgos. Avi15 belongs to a window glass from the Cathedral of Avila showing designs similar to others found in the same cathedral which are dated to the last decades of the fifteenth century. Pal15 was found in a bricked up window in front of the organ in the cathedral of Palencia and the authorship is documented in the cathedral archive. Avi16 is from an unknown master but it shows a design which starts being used around 1550. This glass piece could have another origin as the coloration shown is not found in the glass windows existing at present in the cathedral. Nevertheless, the way it was decorated with a thick application, indicates a strategy to produce a red glass which has great technical complexity. It is not until the sixteenth century that the process starts being better controlled involving the addition of copper to the silver stain. However, it is also known that, without the adequate amount of silver and copper and control of the firing process, the stained glass obtained shows a brownish dark color and not the red color wished for (Caen 2010).

The glasses under study were decorated on one side with silver stain and on the other side with *grisaille*. A *grisaille* is a brown-blackish decoration made of iron oxides and also copper, zinc, lead and/or manganese oxides. Some lead glass was also added to the *grisaille*, the lead glass is known to have a lower melting temperature than the window glass which after firing fixes the *grisaille* to the glass surface. Silver stains are usually fired at lower temperatures (between 550 and 650ºC) than the *grisailles* (about 700ºC) (Caen 2010; Verita´ 1996; Perez-Villar et al. 2008). Consequently, the yellow silver stains are often applied on the other side (the external side) of the window glass, as happens in the three cases studied here, and fired once the *grisaille* has been fixed. Pictures of the glasses studied are displayed in Figure 1 showing the decoration including silver stain and *grisaille*. Images of the yellow stains obtained in transmitted and reflected light are also shown. The yellow stains from both Avi15 and Pal15 are essentially yellow both in transmission and reflection while on the contrary the Avi16 yellow stain is dichroic, yellow in reflection and red in transmission.

The thickness and composition of the silver stain layers were determined from polished cross sections of the glass surfaces by using an Electron Microprobe CAMECA SX-50 (Cameca, Gennevilliers, France). The measurement conditions were a 20 kV and 15 nA probe current with a spot size of about 1 µm. A JEOL model JSM-840 microscope (with secondary and backscattered electron detectors), coupled with a LINK AN 10000 microanalyses system was also used. 20 kV acceleration voltage, 1.5 nA probe current and 25 mm working distance were used for observation and analyses.

UV–Vis Transmission measurements were performed using a UV–Vis spectrophotometer (Shimadzu 2700). For the Reflection measurements an ISR 3100 integrating sphere was attached to the spectrophotometer, and the spectra calculated with respect to a reference $BaSO_4$ white. Undecorated areas of the glasses were also measured.

A crossbeam workstation (Zeiss Neon 40) equipped with SEM (Shottky FE) and Ga^+ FIB columns, was used to obtain polished cross sections of the yellow stains. The polishing obtained was good enough to discern the silver nanoparticles. First, the sample surface was coated with a thin protective Pt layer (1 µm) by ion-beam-assisted deposition; then the cross-section was cut and polished. In some cases, a lamella was extracted and transferred to a TEM grid for further TEM investigation. In a final step, the lamella was thinned down to a thickness transparent to the electron beam (<60 nm). High Resolution Transmission Electron Microscopy (HRTEM) characterization was performed on a JEOL JEM-2100 Lab6 electron microscope with an operating voltage of 200 kV.

The glass transition temperature of the glasses was determined by Differential Scanning Calorimetry (DSC) at several heating rates (5, 10, 20, and 40 K/min), in a Netzsch F404 Pegasus. Above the glass transition temperature, the glass behaves as a liquid, and as a consequence atomic diffusion coeficients show a great increase (Greer 1999). Therefore, it is necessary to fire the glass and silver stain precursor compound to temperatures above the glass transition temperature to boost atomic diffusion in the glass. Theoretical scattering and extinction cross-sections for spherical particles are calculated up to third order (Mie scattering) (van de Hulst 1981), using the measured dielectric constants for metallic silver given in Johnson and Christy (1975) and taking into account the particles size dependence of the dielectric constants using the Drude approximation (Kreibig and Vollmer 1995). The refraction index of the matrix is evaluated from the glass composition (Priven and Mazurin 2003). This computation is used to estimate the optical response of the silver stain layers

Figure 5.1 Pictures of the three stained glass pieces studied and the corresponding Optical Microscopy images taken with transmitted light (left), and reflected light (right).

.

Results

The chemical composition of the glasses and of the silver stains is shown in Table 5.1; the three glasses exhibiting a similar composition. It is worth mentioning that in this period the glasses were usually imported from the north of Europe (Flanders or Germany) and consequently, for a relatively long period, they presented a similar composition. The density and refraction index of the glasses are calculated from the composition (Priven and Mazurin 2003; Fluegel 2007) and are also shown in Table 5.1. The glass transition temperatures (T_g) determined from the DSC data taking the middle temperature of the transition at different heating rates are shown in Table 5.2. In the wood fed kilns used at the time of production of the glasses, a typical heating rate (24 h to reach 700ºC) was 0.5 K/min. At these low heating rates, T_g follows an Arrhenius-like dependence which in our case gives T_g = 653ºC. These results are in reasonable good agreement with the values varying between 670 and 725ºC determined for very similar high-lime low alkali sixteenth–seventeenth century glasses (Cable and Smedley 1987).

Table 5.1. Composition of the glasses measured with SEM-EDX.

Glaze	composition											n	ρ	Max.Ag	Max.V_f
(wt%)	Na_2O	MgO	Al_2O_3	SiO_2	P_2O_5	S	Cl	K_2O	CaO	MnO	FeO		(g/cm^3)	wt%	%
Avi15	2.3	2.8	4.9	60.4	3.2	0.1	0.9	4.1	20.3	0.5	0.6	1.56	2.65	1.7	0.4
Avi16	1.8	3.0	4.9	61.0	3.1	0.1	0.6	4.6	19.9	0.7	0.3	1.56	2.64	1.6	0.4
Pal15	2.1	2.7	5.0	60.2	3.3	0.1	0.6	4.3	20.5	0.6	0.4	1.56	2.65	2.4	0.5

Calculated index of refraction after Priven and Mazurin (2003) and density after Fluegel (2007). Maximum wt% and volume fraction of silver nanoparticles in the layer calculated from the chemical analyses obtained by SEM–EDS of the cross section of the glasses

Table 5.2. Glass transition temperature from DSC data as the medium temperature of the transition.

HR (ºC/min)	T_g (K)
5	677
10	686
20	693
40	699

The yellow stain layer has in the three cases a total thickness of about 15 µm, as can be seen in Figure 5.2. However, Avi16 shows the greatest silver concentration (0.44 %) at 10 and 15 µm below the surface while for Avi15 and Pal15 (0.53 and 0.60 % respectively) it appears closer to the surface (between 2 and 5 µm). The yellow stains corresponding to Avi15 and Pal15 contain only silver, but Avi16 contains also copper and lead mainly concentrated near the surface and showing a typical diffusion profile. The maximum wt% of silver in the layer and the corresponding màximum volume fraction of silver nanoparticles in the layer are also given in Table 5.1. Maximum volume fractions which were found to be about 0.5 % are in good agreement with those found in other silver stain glasses (Jembrih-Simbürger et al. 2002).

The transmittance and reflectance corresponding to the three samples studied are shown with solid lines in Figure 5.3. Dashed lines correspond to the undecorated areas of the glasses which were also measured. Reflectance spectra were obtained from both sides of the samples, that is the silver stain layer side (thick line) and the reverse (thin line). We can see that the front side shows a more intense signal than the rear, but both spectra show the same wavelength dependent response. The corresponding color coordinates are evaluated from the transmittance (dots) and reflectance (triangles) spectra using the protocol accepted by the International Commission for Illumination x, y, Y (CIE 1931) and a, b, L (CIE Lab*) 1976) shown also in Figure 5.3. Solid symbols correspond to the silver stains and void symbols to the undecorated glasses. The color of the glasses is slightly yellow–green both in reflection and transmission. Avi15 and Pal15 silver stains each have a similar yellow-greenish hue both in reflection and transmission with transmission being more saturated than the reflection. Avi16 has a stronger color than the other two, both in reflection and transmission, and the color is yellow-greenish in reflection and red with a small blue component in transmission (Table 5.3).

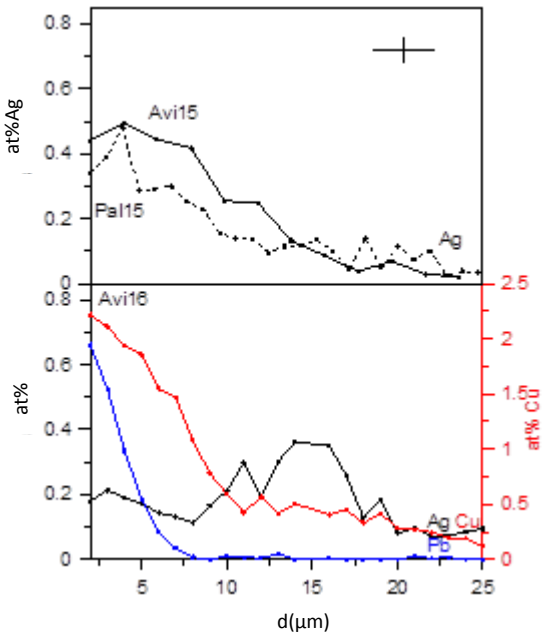

Figure 5.2. Top at% Ag composition profile corresponding to Avi15 and Pal15. Bottom at% Ag, Pb and Cu composition profiles corresponding to Avi16. The horizontal bar of the cross indicates the dimensions of the spot and the vertical bar the typical standard deviation.

The color of the silver yellow stains depends strongly on the size of the metallic silver nanoparticles. For this reason, polished cross-sections of the silver yellow stains were prepared by FIB in a Zeiss Neon 40 workstation. A lamella of sample Avi16 was extracted for further TEM observation, which is shown in Figure 5.4. The silver yellow stains corresponding to samples Avi15 and Pal15 appeared concentrated near the surface, as we have already observed by SEM, Figure 5.2, and the size of the particles was very small with a wide distribution, maximum sizes of about 15 and 30 nm, respectively. The presence of very small particles (2–5 nm) is observed in all the cases. These results agree with those found in other silver-stained glasses (Jembrih-Simbürger et al. 2002).

On the contrary, Avi16 shows particles of sizes below 20 nm in a first layer close to the surface and, separated by some space, a second layer of particles with sizes increasing from 30 to

90 nm with depth as is shown in Figure 5.4. The first layer of silver particles is also characterized by the presence of copper and lead (Figure 5.2) dissolved in the glass.

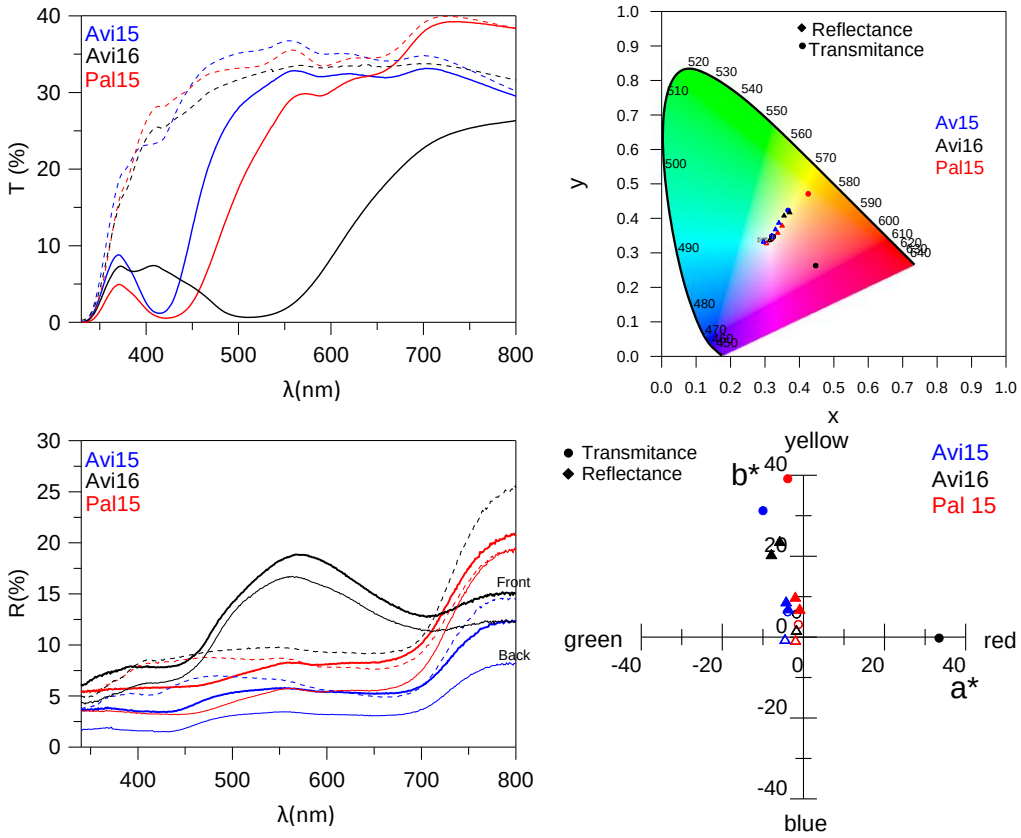

Figure 5.3 Left transmission (top) and reflectance (bottom) UV–Vis spectra of the three silver stains. Dotted lines correspond to the transparent glass. In the Reflectance spectra, the thick lines correspond to the measurements obtained on front side of the glass where the yellow stain is applied and the thin solid lines to the measurements obtained from the back side of the glass. No differences are observed in the reflectance measured on both sides of the glass. Right Locus Cie-1931 color coordinates (top) corresponding to the three yellow stains (solid symbols) and to the glasses (open symbols) both measured in reflection and in transmission. The corresponding Cie Lab* color coordinates (bottom) of the glasses and yellow stains.

Discussion

The three glasses are of the type containing high lime (20 % CaO), high silica (60 % SiO2), and low alkalis (7 % Na_2O + K_2O). They all contain a small amount of MnO which was probably added to decolorize the glass (manganese is known to oxidize Fe^{2+} to Fe^{3+} reducing the greenish color). The density and index of refraction of the glasses estimated from their composition (Priven and Mazurin 2003; Fluegel 2007) are about 2.65 kg/m^3 and 1.56,

respectively. The glass transition temperature, determined by DSC at 2.5 K/min heating rate, is of about 653ºC. Therefore, for the glasses herewith considered the silver stains were produced at temperatures clearly above 653 º C and most probably approaching 700ºC, in reasonable good agreement with those reported for sixteenth–seventeenth century glasses (Cable and Smedley 1987). This is a high temperature, clearly above the temperatures considered in the literature for the production of silver stains.

One of the interesting differences existing between the silver stains from the fifteenth and sixteenth century, respectively, is the presence in the latest glasses of copper and lead.

Table 5.3. Color coordinates calculated form the transmission and reflection UV-Vis spectra. Cie Lab* coordinates are given and the calculated chroma, c* and hue, h* are also given.

Transmittance	**L***	**a***	**b***	**c***	**h***
Avi15 glass	66.2	-3.9	6.2	7.4	122.1
Avi15 silver yellow	62.6	-10.0	31.3	32.8	107.7
Avi16 glass	56.7	-1.7	5.7	6.0	106.8
Avi16 silver yellow	20.2	33.4	-0.2	33.4	359.6
Pal15 glass	42.2	-1.3	3.1	3.4	112.2
Pal15 silver yellow	38.8	-3.9	39.2	39.4	95.7
Reflectance					
Avi15 glass	30.1	-4.6	-0.4	4.6	185.2
Avi15 silver yellow F	28.2	-3.8	7.1	8.1	118.1
Avi15 silver yellow B	21.0	-4.3	8.8	9.8	115.9
Avi16 glass	37.2	-1.8	1.8	2.5	134.1
Avi16 silver yellow F	44.3	-5.9	23.8	24.5	103.8
Avi16 silver yellow B	46.0	-7.9	20.5	22.0	111.1
Pal15 glass	34.8	-2.0	-0.6	2.1	198.1
Pal15 silver yellow F	33.6	-0.9	7.0	7.1	97.6
Pal15 silver yellow B	27.5	-2.0	10.0	10.2	101.5

The diffusion-like chemical profile shown by those elements (Figure 5.2) and their absence in the bulk glass composition indicate that they were incorporated in the glass together with the silver. Therefore, in the case of the dichroic silver stain, Avi16, copper and lead were also present in the precursor material applied over the glass surface. The addition of copper in the precursor material has been reported to enhance the color of the silver stain. Moreover, the presence of copper has already been observed in some silver stain glasses (Caen 2010). Copper has the capability of reducing silver to the metallic form, and therefore enhances the growth of the metallic silver nanoparticles. Moreover, the presence of copper modifies the electronic charge valence favoring the formation of silver aggregates (Quinten and Kreibig 1993). Therefore, larger silver particles, showing usually a heterogeneous size distribution, are obtained if copper is added to the precursor material. In particular, the presence of large silver nanoparticles will certainly increase the absorption and therefore enhance the color of the silver stain. On the contrary, the addition of lead has been reported neither in the historical treatises nor in the analyses of stained glasses. Although the addition of PbO in the glass composition is known to reduce the diffusivity of silver and thus, produce thinner more

concentrated layers (Pradell et al. 2012), its effect when present in the precursor material has not yet been studied.

TEM observation (Figure 5.4) indicates the presence of a very heterogeneous distribution of metallic silver nanoparticles in Avi16 which are arranged in two main layers. The layer

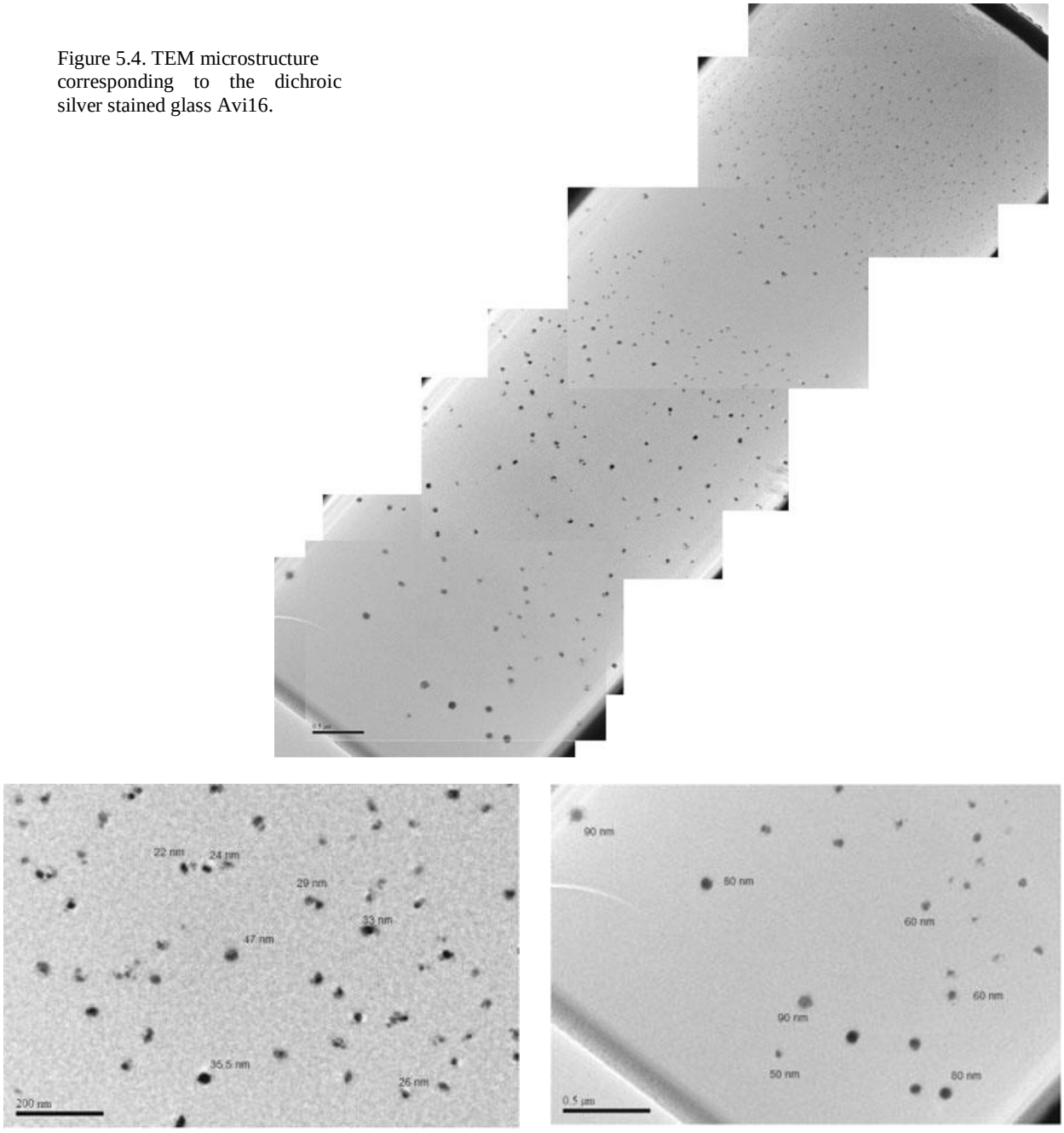

Figure 5.4. TEM microstructure corresponding to the dichroic silver stained glass Avi16.

closer to the surface which is 5 µm in depth and contains copper consists of smaller silver nanoparticles (sizes ranging from 10 to 25 nm), and the second layer which is between 10 and 15 µm in depth contains very large particles (from 50 to 90 nm). Those larger particles are concentrated in the lowest part of the layer. It is worth to note that the thickness of the TEM preparation is of about 70 nm, consequently most of the large particles are cut on the lamella

production process; as the sectioned particles show always an apparent diameter smaller than the actual one, the actual average particle size is larger than that determined from the TEM sample. Although this is a common problem with regard to TEM preparations, it is particularly important when the size of the particles is of the same dimension or larger than that of the lamella. The formation of larger silver nanoparticles may be related to the addition of copper and probably also lead in the precursor material. It is common to find the larger nanoparticles concentrated inside the layer when far long firing times are applied.

The color observed in the glasses both in transmission and in reflection is related to the size and distribution of the metallic silver nanoparticles in the silver stain layer. Silver metallic nanoparticles in a non-absorbing matrix (glass) absorb and scatter the light. Absorption is dominated by the collective resonance of the free electrons resulting from surface polarization, denoted as surface-plasma resonance (SPR). The position and shape of these resonances depend on the optical functions of the metals and of the dielectric matrix. The *extinction* cross-section is defined as the total light loss in the system, either absorbed or scattered. Both *scattering* and *extinction* cross-sections are calculated for spherical particles by a series expansion (Mie scattering) corresponding to spherical multipolar excitations (dipolar, quadrupolar, and octupolar) (van de Hulst 1981). Although the dipolar approximation is sufficient for small particles (up to about 20 nm for silver), larger nanoparticles require the use of higher multipolar orders.

The refraction index of the matrix is evaluated from the glass composition (Priven and Mazurin 2003), which for the glasses herewith studied is of about 1.56 as shown in Table 5.1. The corresponding extinction, absorption, and scattering constants ($\gamma=f\sigma$) evaluated for an equivalent volume fraction of monodispersed particles as a function of the size of the silver nanoparticles are shown in Figure 5.5a. In Figure 5.5b the position (Cmax) of the main SPR peak is plotted against the full width at half maximum (*fwhm*), and from this, we can see how increasing the size of the silver nanoparticles above 30 nm results in a red shift and broadening of the SPR peak from the extinction cross-section. Neglecting multiscattering which is a reasonably good approximation if the fraction of particles is very low, typically from $f \leq 10^{-3}$ to 10^{-5}, and the topology isotropic and statistical, the optical properties may be assumed to be the sum of the optical properties of the individual particles in a quasi-homogeneous effective-medium. Then, the transmittance may be approximately evaluated as the total non-extinct light in the layer, which is $T \approx e^{-2\gamma eL}$ (Nobbs 1985).

Figure 5.5. a) From top to bottom, absorption, scattering and extinction constants for an equivalent volume fraction of particles (γ=fσ); b) Full width at half maximum (fwhm) and position (λ_{max}) of the SPR main peak corresponding to the extinction constant as a function of the size of the silver metallic nanoparticles. c) Color coordinates calculated for the corresponding transmission spectra.

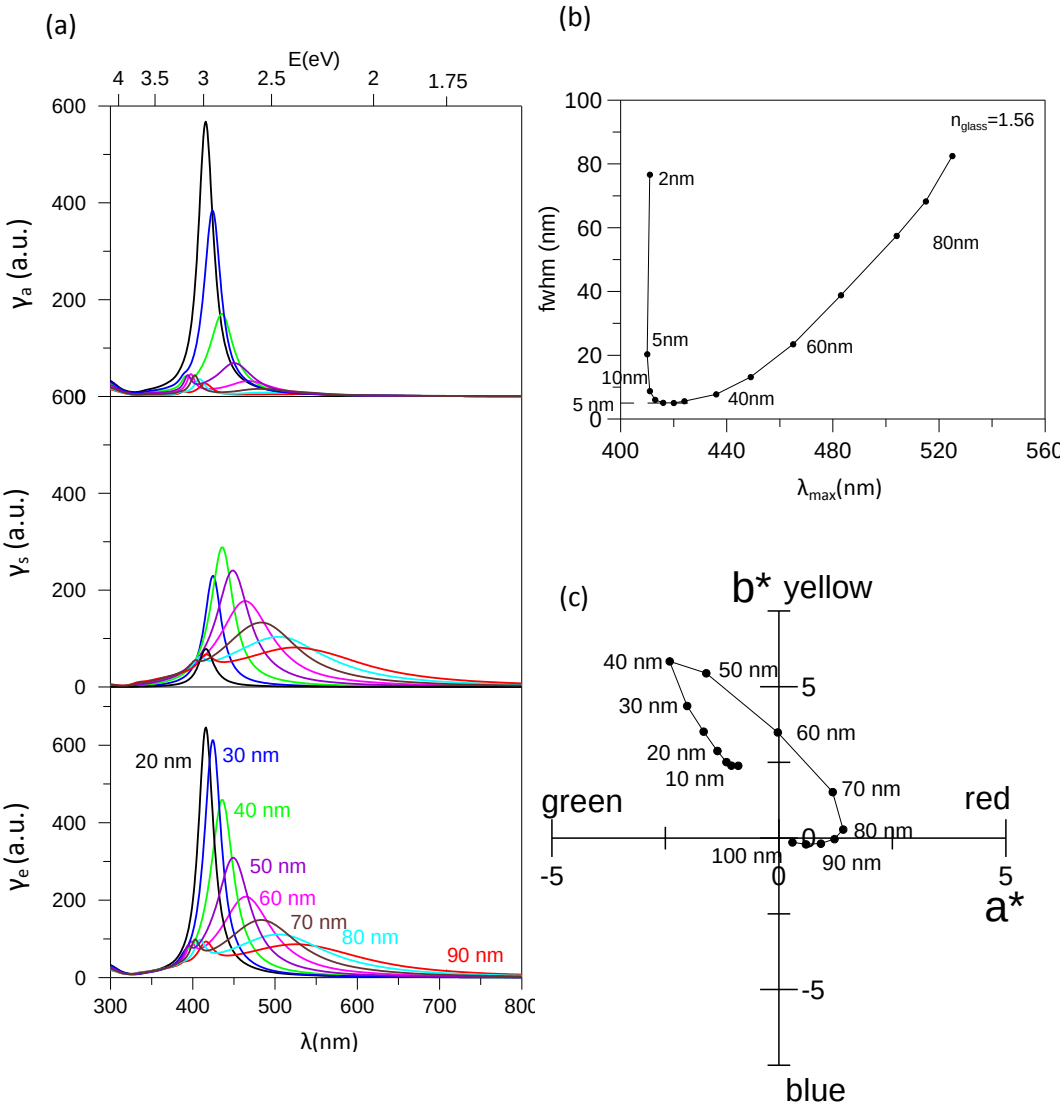

We can see in Figure 5c how to increase the size of the metallic silver nanoparticles, the color changes from green (≤40 nm) to yellow (≈60 nm), orange (≈ 70 nm), and finally red (≥80 nm). Moreover, color saturation intensifies as the particle size increases, reaching a maximum for particles of about 40 nm, and decreases again for larger particles.However, what is more interesting from the above calculations is the relative contribution of scattering and absorption to the total extinction; for small silver nanoparticles (d<30 nm) absorption is the dominant contribution while for larger nanoparticles (d>30 nm) scattering progressively becomes the

dominant contribution. This will affect the color of the glasses measured both in reflection and in transmission.

The maximum volume fraction of particles present in the studied silver stain layers is of about 0.5 % which falls within the order of magnitude required to neglect multiscattering. Therefore we can use the noninteracting particles approximation for the transmittance. The color measured in transmittance gives values of a* = -10.0 and b* = 31.3 for Avi15 and a* = -3.9 and b* = 39.2 for Pal15 (blue and red dots respectively in Figure 5.3). This corresponds to hues of 108º and 96º for Avi15 and Pal15 respectively (i.e., between yellow (90º) and green (180º), with both showing similar saturations (39 and 33). This observation is consistent with the small, but slightly larger for Pal15 than for Avi15, size of the silver nanoparticles observed by electron microscopy in both silver yellow stains. Avi16 shows a large red color a* = 33.4 with a small blue component b* = -0.2, and similar saturation (33.4). This large red component is associated to the large particles (60–90 nm) present in the inner layer. Although smaller silver nanoparticles are also present in the outer layer (20–30 nm), the corresponding volume fraction is small (f = 0.14 %) compared to those from the large nanoparticles (f = 0.36 %), as shown in Figure 5.2. Therefore, the contribution to the color from the small particles is also small. Figure 5.6 shows the Optical density, OD = log(1/T), of the silver stains after subtracting the glass contribution.

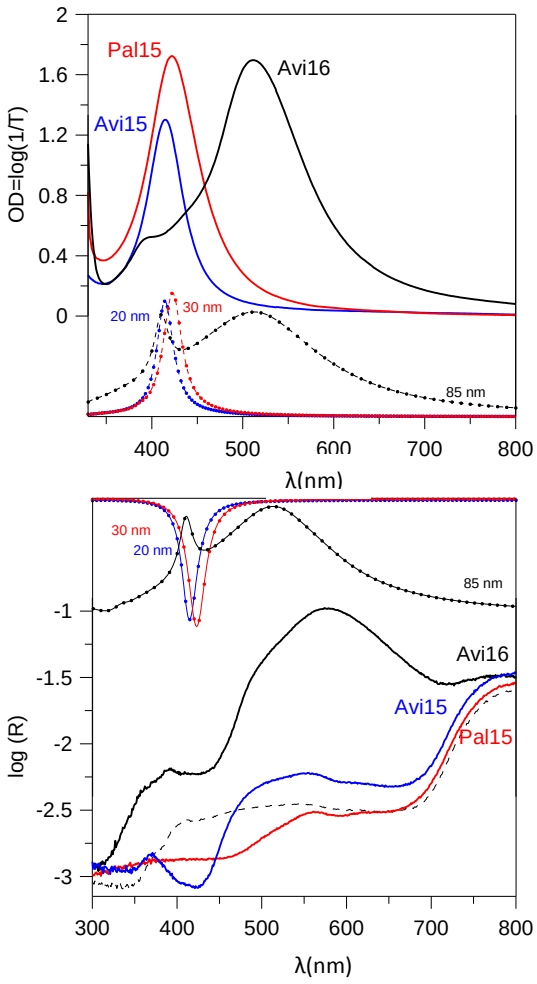

Figure 5.6 (Top) Optical density, OD = log(1/T) from Av15 and Av16 and Pal15 silver stains after subtracting the glass contributions. The dotted lines correspond to the extinction constants for 20, 30 and 85 nm spherical particles in glass which compare to the OD spectra of Avi15, Pal15, and Av16, respectively. (Bottom) log(R) from Av15 and Av16 and Pal15 silver stains. The glass contribution has not been subtracted and is plotted with a dashed line. The dotted lines correspond to the backscatter constant minus the absorption constant calculated for 20, 30 and 85 nm spherical particles in glass. The first two compare directly to the log(R) spectra from Avi15 and Pal15 respectively. A combination of the small and large particles constants compare to the log(R) spectrum from Avi16.

Under the assumptions herewith considered and taking into account reabsorption in the layer thickness, the transmittance can be calculated from the extinction constant by (van de Hulst

1980a, b) $T \approx 2(\gamma_e L)^2 \int_{\gamma_e L}^{\infty} \frac{e^{-t}}{t^3} dt$. The results corresponding to a 10 μm thick layer with a volume fraction, f = 0.3 %, of 20, 30, and 85 nm size nanoparticles are also plotted with dash-dotted lines.

We can see that the computed peak positions match with the experimental data. However, the experimental peaks are broader, due to the presence of a broad distribution of mainly smaller nanoparticles and multiscattering effects.

Although the extinction constant has two contributions, absorption and scattering, the relative importance of both varies greatly with the size of the nanoparticles. Absorption dominates the Optical response for small metallic silver nanoparticles in contrast to what happens for large nanoparticles. This has an important effect on the Reflectance of the silver stains (Nobbs 1985; van de Hulst 1980a, b). The Reflectance measured has two main contributions: on the one hand the light back-scattered by the particles and on the other hand the light reflected on the glassair interface which is transmitted back through the layer. The back-scattering contribution may be determined by integrating the Mie back-scattered light. The difference between the backscattering constant and the absorption constant for 20, 30, and 85 nm particles shown in Figure 6 demonstrates how for large particles backscattering dominates the optical response while for small particles it is dominated by absorption. Consequently, the large nanoparticles present in Avi16 are responsible for the broad reflectance peak at 530 nm. Conversely, the small nanoparticles are responsible for the absorbance at 450 nm of the light transmitted then reflected on the glass-air interface. The combination of both effects results in the observed yellow-greenish reflectance. Scattering is negligible for the small particles present in Avi15 and Pal15 stains and consequently, absorbance of the light transmitted and then reflected at the glass-air interface dominates the optical response resulting in the characteristic yellow-greenish color shown. However, the effect is small, resulting in a very low saturated yellow-greenish reflectance.

Consequently, the simultaneous presence in the silver stain layer of small nanoparticles, for which absorption dominates the optical response and, large nanoparticles, for which scattering dominates the optical response, is responsible for the dichroic behavior shown by Avi16. Moreover, the calculations also show that as long as the conditions herewith considered are accomplished (i.e., a low concentration of metallic nanoparticles which assures negligible multiscattering and the simultaneous presence of particles with very different sizes), the position of the small/large nanoparticles in the layer does not affect the color observed either in transmission and reflection.

The presence of a bimodal size distribution of silver metallic nanoparticles in glass occupying distinct depths has been reported previously to be responsible for a dichroic (yellow/bluish) response (Magruder et al. 2009). However, in this case and contrarily to what happens in our dichroic glass, high order multipolar orders were not present as the silver nanoparticles were not larger than 25 nm and dipole–dipole coupling due to the high density of particles present was responsible for the double shifted peaks present in the reflectance/absorption spectrum.

The origin of the dichroic behavior of Avi16 is the addition of copper and lead in the precursor mixture used to obtain the silver stain. Those elements act as reducing agents enhancing the reduction and growth of the silver nanoparticles. Moreover, copper is known to modify the electronic charge valence favoring the development of a heterogeneous size distribution of silver nanoparticles. Therefore, only the addition of copper and lead together with silver in the precursor compound is responsible for the production of the red silver stain glasses. No other ions such as those (Sb^{3+}, As^{3+}, and Sn^{2+}) (Gil and Villegas 2004; Gil et al. 2005) considered responsible for the production of red stain silver glasses have been found.

In contrast, the yellow silver stains Avi15 and Pal15, where copper or lead were not found, are both characterized by the presence of small silver nanoparticles for which absorption dominates the optical response, resulting in the same yellow-greenish color observed either in reflection and in transmission. The enhancement of the color for Pal15 in comparison with Avi15, observed as an increase in the color saturation, is due to the presence of larger silver nanoparticles in Pal15 than in Avi15. This may be related either to the use of a higher firing temperature or longer firing time.

Finally, the glass transition temperature of the glasses used in this historic period has been determined even for very low heating rates to be higher than 650ºC and establishes a lower limit for the temperature used in the production of the three silver stains.

Conclusions

The fifteenth century yellow silver stains (Avi15 and Pal15) are both characterized by the presence of small silver nanoparticles for which absorption dominates the optical response. On the contrary, the simultaneous presence of small nanoparticles and large nanoparticles for which scattering dominates the optical response is responsible for the dichroic behavior (red transmittance and yellow-greenish reflectance) shown by the sixteenth century silver stain (Avi16). This heterogeneous size distribution of metallic silver nanoparticles is due to the

addition of copper and lead in the precursor mixture used to produce red silver stains in the sixteenth century and not due to the addition of other ions such as Fe^{2+}, Sb^{3+}, As^{3+} or Sn^{2+} in the glass. Finally, the determination of the glass transition temperature of 650ºC establishes a lower limit of circa 700ºC for the temperature of production of the silver stains from this historic period.

References

Barber DJ, Freestone IC (1990) An investigation of the origin of the colour of the Lycurgus cup by analytical transmission electron microscopy. Archaeometry 32(1):33–45

Barley KC (1996) Tests et observations a` propos de l'usage du jaune d'argent in: Grisailles, jaune d'argent, sanguine, e´mail et peinture a` froid. Dossier de la Comission Royale des monuments, sites et fouilles, 3, Forum pour la Conservation et la Restauration des Vitraux, pp 117–121

Cable M, Smedley JW (1987) Liquidus temperatures and melting characteristics of some early container glasses. Glass Technol 28(2):94–98

Caen JMA (2010) The production of stained glass in the county of Flanders and the Duchy of Brabant from the XVth to the XVIIIth centuries: materials and techniques (Corpus Vitrearum, Belgium, Studies). Harvey Miller Publishers- Brepols, Washington

Colomban P (2009) The use of metal nanoparticles to produce yellow, red and iridescent color, from Bronze Age to present times in luster pottery and glass: solid State chemistry, spectroscopy and nanostructure. J Nano Res 8:109–132

Delgado J, Vilarigues M, Ruivo A, Corregidor V, Silva RC, Alves LC (2011) Characterisation of medieval yellow silver stained glass from Convento de Cristo in Tomar, Portugal. Nucl. Instrum Method Phys Res B 269:2383–2388

Fluegel A (2007) Global model for calculating room-temperature glass density from the composition. J Am Ceram Soc 90(8):2622–2625

Gil C, Villegas MA (2004) Ruby coloured lead glasses by generation of silver nanoparticles. Mater Chem Phys 88:185–191

Gil C, Villegas MA, Fernandez-Navarro JM (2005) Preparation and study of superficially coloured lead glass. J Mater Sci 40:6201–6206

Greer AL (1999) Through a glass, lightly. Nature 402(6758): 132–133

Heaton N (1947) The origin and use of silver stain. J Br Soc Master Glass Paint 10:9–16

Jembrih-Simbürger D, Neelmeijer C, Schalm O, Ferderickx P, Screiner M, de Vis K, Mader M, Schryvers D, Caen J (2002) The colour of stained glass- analytical investigations carried out with XRF, SEM-EDS, TEM and IBA. J Anal At Spectrom 17:321–328

Johnson PB, Christy RW (1975) Optical constants of noble metals. Phys Rev B 6(12):4370–4379

Kreibig U, Vollmer M (1995) Optical properties of metal cluster. Springer, Berlin

Lautier C, Sandron D (2008) Antoine de Pise. L'art du vitrail vers 1400. Edition CTHS, Paris

Magruder RH, Robinson SJ, Smith C, Meldrum A, Halabaica A, Haglund RF (2009) Dichroism in Ag nanoparticle composites with bimodal size distribution. J Appl Phys 105:024303-1–024303-5

Molera J, Baye´s C, Roura P, Crespo D, Pradell T (2007) Key parameters in the production of medieval luster colors and shines. J Am Ceram Soc 90(7):2245–2254

Nobbs JH (1985) Kubelka–Munch theory and the prediction of the reflectance. Rev Prog Color 15:66–75

Perez-Villar S, Rubio J, Oteo JL (2008) Study of color and structural changes in silver painted medieval glasses. J Non-Cryst Solids 354:1833–1844

Pradell T, Molera J, Roque J, Vendrell-Saz M, Smith AD, Pantos E, Crespo D (2005) Ionic-exchange mechanism in the formation of medieval luster decoration. J Am Ceram Soc 88(5):1281–1289

Pradell T, Pavlov RS, Gutiérrez PC, Climent-Font A, Molera J (2012) Composition, nanostructure, and optical properties of silver and silver/copper lusters. J Appl Phys 112: 054307-1–054307-103

Priven AI, Mazurin OV (2003) Comparison of methods used for the calculation of density, refractive index and thermal expansion of oxide glasses. Glass Technol 44(4):156–166

Quinten M, Kreibig U (1993) Absorption and elastic scattering of light by particle aggregates. Appl Optics 32(30):6173–6183

van de Hulst HC (1980a) Multiple light scattering; tables, formula and applications, vol 1. Academic Press, New York

van de Hulst HC (1980b) Multiple light scattering; tables, formula and applications, vol 2. Academic Press, New York

van de Hulst HC (1981) Light33333 scattering by small particles. Dover Publications, Inc, New York

Verita` M (1996) Composition, structure et mechanism de deterioration des grisailles in: Grisailles, jaune d'argent, sanguine, e´mail et peinture a` froid. Dossier de la Comission Royale des monuments, sites et fouilles, 3, Forum pour la Conservation et la Restauration des Vitraux, pp 117–121

Chapter 6

Conclusions

The coloured historical glasses and glazes studied in this thesis were obtained either by the presence of micro-pigment particles in the bulk glass or by the presence of metallic nano-particles forming thin surface layers.

The optical properties are in both cases determined by the scattering and the absorption of light by the particles causing the opacity and the colour of the glass respectively. The peculiar optical properties of metallic nanoparticles are also responsible of the high specular reflectance and of the dichroism shown by some of the decoration layers.

Pigment particles maybe either formed at high temperatures by the reaction of the components present in the initial glass mixture or during the cooling of the glass. The stabilization of the adequate pigment particles depends on the glass and pigment particles composition and on the temperature; consequently, the production methods must be adapted in each case.

Yellow glass in New Kingdom Egypt and during the Roman Empire

- Lead antimonate particles were used to produce yellow glass in New Kingdom Egypt and during the Roman Empire.

- A yellow cooked precursor was mixed with the molten transparent glass. However, in the Egyptian glass the precursor was a *pigment* obtained by firing a mixture of lead oxide and antimony oxide with excess lead; while in the Roman glass it was an *anime* (a glass with crystalline particles) obtained by firing a mixture of lead oxide, antimony oxide and silica with excess lead.

- The pigment particles are a lead antimonate oxide of the type $Pb_2Sb_2O_7$, with a cubic crystallographic structure (space group Fd-3m with a ≈ 10.40 Å) known as pyrochlore structure. Sb is partially substituted by iron and zinc in the Egyptian glass and by iron and tin in the Roman glass. Their presence may be related to the source of lead used, although it is also possible that tin was deliberately added in the Roman glass. The presence of these impurities modifies slightly the hue and increases the stability of the pyrochlore $Pb_2Sb_2O_7$ crystallites.

- The thermal stability of $Pb_2Sb_2O_7$ crystallites in the Egyptian glass is probably due to the higher viscosity of the Egyptian glass compared to the Roman glass. This also seems to be the reason for the use of a high lead *anime* instead of a high lead *pigment* the Roman glass.

- From the historical point of view although in both cases the pigment particles used are the lead antimoniate oxide, there is a change in the production process followed to obtain the colour glass. Consequently, at first sight we cannot talk about a direct relationship between both productions. However, the diverse composition of the transparent glass used by Egyptians and Romans seems to justify the change in the production process of the yellow glass. In fact the Romans most probably changed the composition of the transparent glass in order to obtain a more transparent glass. The high magnesium content of Egyptian glass is responsible for the precipitation of calcium-magnesium silicates –

pyroxenes, $(CaMg)Si_2O_6$- which are responsible for the cloudiness and sometimes opacity of Egyptian glasses.

Technology of production of lustre

The optical properties of thin layers of metallic nanoparticles depend on the nature and size of the nanoparticles, on their concentration in the layers and also on the thickness of the layers. The technology of production of such layers is known as the *lustre technique* which implies a precursor pigment which interacts with the glass surface resulting in ionic exchange and diffusion of the metal ions into the glass surface. This process depends not only on the nature of the precursor mixture but also on the composition of the glass and firing temperature. Furthermore, the reduction of the metal ions to the metallic state and the formation of the metallic nanoparticles are determined also by the reducing atmosphere.

We have studied three different lustre decorations: polychrome Iraqi lustre (9^{th} century AD), Syrian lustre-ware (12^{th} to the 14^{th} century AD) and yellow and red silver stain (16^{th} century).

Polychrome Iraqi lustre (9^{th} century AD)

- The samples studied combine red (produced by the presence of copper nanoparticles) and yellow, white or black (due to the presence of metallic silver nanoparticles).
- As had been previously observed the addition of lead oxide in the glass composition helps the development of the metallic like reflectivity shown by some of those layers, helping the formation of more concentrated layers of metallic nanoparticles.
- The colour of the silver lustres is essentially related to the size of the metallic silver nanoparticles (>100 nm for the white, <10 nm for the yellow, about 20nm for the green and the black) and also to their distribution in the layers; either forming separated (high reflectant yellow or green silver on red copper lustre layer) or mixed copper and silver nanoparticles in the lustre layer (black and white).

- We have demonstrated that the red lustre was first fired in a high reducing atmosphere while the silver lustre was applied subsequently and fired under a lighter reducing atmosphere.

Syrian lustre-ware (12th to the 14th century AD)

- Syrian lustre shows many innovations with respect to its precursor Fatimid lustre. A transparent glaze (without tin oxide particles) is used and also stonepaste (a ware made of quartz mixed with some clay and fluxes). The light colour of the ware made the use of a tin free glaze possible.
- There are three main productions and also lots of small workshops working:

  Tell Minis ware shows clear stylistic similarities with Fatimid productions. The lustres are silver-copper lustres

  Raqqa lustre ware is made on an iron richer alkaline glaze, the lustres are copper rich. The addition of iron (Fe^{2+}) may help the reduction of copper ions into metallic copper. This is clearly linked to the glass industry. The lustre is chocolate brown and does not show metallic shine.

  Later *Damascus* lustre wares are also studied, and in this case we have a variety of ceramic body, glaze and lustre compositions. More work has to be devoted to these materials.
- Although *Tell Minis* lustre decorations shows stylistic and similarities with the Fatimid lustre productions, and *Raqqa* lustre decorations with contemporary Iranian productions, the technology appears very different (transparent low lead and alkaline iron richer glazes) and in the last case with strong connections with the glass industry.

Yellow and red silver stain from Spain(15-16th century)

- Silver stain decorations from last quarter of the 15th century- first third of the 16th century glassiers is compared to those from the second half of the 16th century onwards. In particular the differences in the production technology between yellow and red silver stains.
- Small silver nanoparticles with sizes ranging between a few and 30 nm are found in the yellow silver stains. The absorption of the silver nanoparticles is responsible for the yellow colour shown both in transmission and in reflection.
- Small silver nanoparticles (≈ 20 nm) near the surface and large silver nanoparticles (≈ 90 nm) deeper in the layer are found. The scattering of the large nanoparticles is responsible for the red hue observed in transmission while the absorption of the small particles and scattering of the large particles is responsible for the yellow colour observed in reflection.
- The production of large silver nanoparticles is related to the addition of copper and also of lead in the precursor mixture which also show diffusion profiles on the glass surface. Both copper and lead are known to help copper reduction to the metallic state and growth of silver nanoparticles.
- The production of a range of colour varying from light yellow, deep-yellow, orange and red was of high interest to increase the colour range of glasses available. Higher temperatures, addition of copper in the precursor mixture and addition of other metal ions in the glass were the most common procedures used in the Renaissance. However, red silver yellows were not easy to produce. This is the first case in which the addition of lead in the precursor mixture is demonstrated.

Finally, with regard to the analytical techniques used, it is important to highlight the need of specific and complementary analytical techniques used for the study of each type of decoration. SEM with coupled EDS, μ-XRD and UV-Vis have been used to determine the global composition of the glasses, glazes, micro-particles, the distribution of the particles in the glass, to identify their nature and structure and to determine the hue, lightness and chroma of the decorations. RBS has been used to determine the chemical composition profiles of lustre layers and FIB polishing and secondary electron images to determine the size and distribution of the nanoparticles in the lustre layers and the thickness of the lustre layers. Replication of the

technology has been used to determine methods of production and stability of the yellow Egyptian and Roman glasses.

Appendix A

Publications of this thesis

T.Pradell, J. Molera, G. Molina and M.S.Tite (2013) "First analysis of Syrian lustre pottery (12th-14th centuries AD)", Applied Clay Science http://dx.doi.org/10.1016/j.clay.2013.05.018

Glòria Molina, Sonia Murcia, Judit Molera, Clodoaldo Roldan, Daniel Crespo and Trinitat Pradell; "Color and dichroism of silver stained glasses" Journal of Nanoparticle Research (2013) DOI 10.1007/s11051-013-1932-7

Glòria Molina; Gillian Odin; Trinitat Pradell; Andrew Shortland; Michael S. Tite, The production technology and replication of lead antimonate yellow glass from New Kingdom Egypt and the Roman Empire, Jounral of Archaeological Science http://dx.doi.org/10.1016/j.jas.2013.07.030

Glòria Molina, Michael S. Tite, Judit Molera, Aurelio Climent-Font and Trinitat Pradell. Technology of production of polychrome lustre, Journal of the European Ceramic Society. In revision

Appendix B

Glossary

Anime. It refers to a coloured semi-finished crystalline product used as opaque pigment in glass slabs, that after cooled and reduced to a powder, was added to transparent glass to produced colour glass. The term meaning 'soul' was used on the Venetian island of Murano.

.

Blow glass. Glass obtained by a forming technique that involves blowing up molten glass into a bubble (or *parison*), with the aid of a *blowpipe* (or blow tube).

Cameo glass: A luxury form of glass art produced by etching and carving through fused layers of differently coloured glass to produce designs, usually with white opaque glass figures and motifs on a dark-coloured background. The technique is first seen in ancient Roman art of about 30BC, where it was an alternative to the luxury engraved gem vessels in cameo style that used naturally layered semi-precious gemstones such as onyx and agate.

Ceramics. It is constituted by a body of mineral origin (natural clay or synthetic paste) which may be wet shaped and which is afterwards fired at high temperatures resulting in a *stone like synthetic* material.

Colorants. Metals that appear completely dissolved in the glass giving colour to it (mainly iron, copper, cobalt and manganese). The colour obtained depends on the metal colorant dissolved, its oxidation state and the glass composition. The presence of small amounts of other metals

(arsenic, zinc, nickel, titanium, chromium, tin or antimony), that may modify the oxidation state and the chemical coordination of the metals in the glass affects also the colour.

Enamel. A material made by fusing powdered glass to a substrate (metal, glass, glazed ceramic) by firing, usually between 750 and 850°C. The powder melts, flows, and then hardens to a smooth, durable vitreous coating. The term "enamel" is most often restricted to the application on metal. Enameled glass is also called "painted".

Faience. A mixture of quartz sand and a *flux* which may be wet shaped and which after firing acquires a stone-like consistency. During the drying of the object the flux salts migrate to the surface and produce a soda-rich glaze. It is considered the precursor of glass.

Float glass. A sheet of glass made by floating molten glass on a bed of molten metal, typically tin, although lead and various low melting point alloys were used in the past. This method produces a glass sheet of uniform thickness and very flat surfaces.

Fluxes. Substances added to reduce the melting temperature. Two different types of *fluxes* were used in the production of historical glasses and glazes, alkaline salts obtained either from plant ashes (*sodalite* plants whose ashes are rich in sodium carbonate, and wood ashes are rich in potassium) or natural salt deposits (*natron* a highly hydrated variety of sodium carbonate found in the valley of Wadi al Natrum in Egypt) and lead oxide. Both alkaline and lead glazes were also used in the production of glazes.

Glass. Glasses are disordered materials with a structure similar to those of liquids but that behave mechanically like solids. The most common way of making a glass is by cooling a viscous liquid fast enough to avoid crystallization. The glassy state is therefore a kinetically frustrated metaestable state of matter reached decreasing the mobility of the atoms so as the atomic order of the liquid is frozen into an amorphous (non-crystalline) solid. This transformation called glass transition is reversible.
Glasses are typically brittle and can be optically transparent. The most familiar type of glass is soda-lime glass, which is composed of about 75% silicon dioxide (SiO_2) plus 25% sodium oxide (Na_2O) and calcium oxide (CaO), and other several minor additives.

Glaze. Vitreous coating constituted by the same materials used to produce glass. During melting and solidification of the glaze dissolution of the ceramic in the melt, diffusion of chemicals from the ceramic into the glaze, and formation of new crystallites in the glaze-ceramic interface occur, giving adherence and stability to the glaze.

Grisaille. A brown-blackish decoration made of iron oxides and also copper, zinc, lead and/or manganese oxides with a lead glass or other glassy materials with a low melting temperature. The lead glass is known to have a lower melting temperature than the window glass which after firing fixes the grisaille to the glass surface.

Luster decorations. Extremely thin surface micro-layers made of exceptionally small metal silver and/or copper nano-particles inside the glaze matrix. The peculiar optical properties of lustre, including the golden and coppery shine, are directly related to the size and volume fraction of the metal particles.

Mosaic glass. The technique of stretching prior thin rods of glass of different colors which are sintered together in a multicolor thicker rod that is cut into slabs which are joined together at their edges, like the pieces of a mosaic, and heat sealed.

Opacifiers. Refer to those pigments formed by micro-crystallites with large scattering capability (lead and calcium antimony oxides, lead tin oxide and tin oxide), able to enhance the light reflected and reduce the light transmitted in the glaze. The use of opaque pigments is particularly interesting to hide the reddish colour of some ceramic pastes. A white background is so desirable to highlight the colour decorations and hide the colour of clay based ceramic pastes, than *tin glazes* became of general use in ceramics since the 8th century until the 19th century.

Pigments. Compounds appearing as minute crystallites in the glaze (cuprite, metallic copper and silver, mixed metal oxides, metal aluminates among others). Their composition, structure and range of stability are highly dependent not only on the composition but also on the procedures followed to obtain them. Frequently the pigments are mixed with a *flux* that decreases the melting temperature of the paint up to 100°C below that of the background glaze (*enamels*). In this way, the *overglaze* colours may be fired in a second firing without the risk of damaging the base glaze.

Plaque glass. Coloured glass obtained by the application of layers of colour glass onto the transparent glass.

Silver stain. A type of decoration applied to glass that was developed in early medieval times and consists of a surface layer (between 10 and 300 μm thick) of metallic silver nanoparticles of varying sizes (typically between 1 and 30 nm) dispersed in the glass.

Slips. Refined clays of various colours applied as a decoration which vitrify to a larger extend than the ceramic body.

Stained glass. Pieces of coloured glass assembled to produce large boards (windows) and objects (lamps, skylights, clocks, sculptures).

Stonepaste. A synthetic ceramic paste made of sand, clay and glass frit.

Historical decorated glass and glazed ceramics are studied with the object to determine the technology of production and to relate it with the optical properties (colour, shine, opacity). Four different case of study are investigated: production technology and replication of lead antimonate yellow glass from New Kingdom Egypt and the Roman Empire, technology of production of polychrome lustre, analysis of Syrian lustre pottery (12th–14th centuries AD) and study of color and dichroism of silver stained glasses. Chemical and microstructural analysis are performed using a selection of complementary Microscopic and Spectroscopic techniques that are the most adequate for the analysis of each decoration. The composition and structure of the different phases formed during the processing of the decorations in historical times is obtained with the object to learn about their stability and processing conditions and to relate them to their optical properties.